AEROSOL SCIENCE AND ENGINEERING RESEARCH FOR MITIGATING HUMAN EXPOSURE AND IMPROVING INDOOR AIR QUALITY

by

SUMIT SANKHYAN

B.Tech., Vellore Institute of Technology, 2017

M.S., University of Colorado Boulder, 2019

A thesis submitted to the

Faculty of the Graduate School of the

University of Colorado in partial fulfillment

of the requirement for the degree of

Doctor of Philosophy

Department of Mechanical Engineering

2022

Committee Members:

Dr. Marina E. Vance

Dr. Peter Ciesielski

Dr. Michael P. Hannigan

Dr. Daven Henze

Dr. Jana Milford

Sankhyan, Sumit (Ph.D., Paul M. Rady Department of Mechanical Engineering)

Aerosol Science and Engineering Research for Mitigating Human Exposure and Improving Indoor Air Quality

Thesis directed by Assistant Professor Marina E. Vance

ABSTRACT

Aerosol science and engineering research can serve important roles in studying and improving Indoor Air Quality (IAQ) in residential settings and in assessing mitigation strategies related to the associated particulate matter (PM) exposure. In this dissertation, I present the results from four studies related to these timely topics. The first study focused on the assessment of $PM_{2.5}$ concentrations and transport in indoor residential environments using commercially available air quality monitors (AQM). Consumer-grade, low-cost PM sensors are gaining popularity as a convenient tool for consumers to monitor indoor air quality in their homes, so we investigated five commercially available AQMs (IQAir AirVisual Pro, Foobot Home, PurpleAir PA-II-SD, and PA-I-Indoor) and compared their response to a research-grade optical particle counter (OPS 3330, TSI Inc.) by deploying them in four different houses over a period of 9-12 weeks each. Additional objectives of this study also included studying indoor PM transport between the kitchen and bedroom areas due to cooking in different homes and evaluating the reduction of $PM_{2.5}$ exposure in residential homes by using a portable air cleaner in kitchen and bedroom areas respectively. The second study investigated aerosol emissions, their volatility, and respiratory deposition characteristics associated with the use of different cooking oils at multiple cooking temperatures. Oils tested include canola, peanut, soybean, coconut, and lard. This study was aimed to bring indoor cooking measurements into perspective by isolating frying oil emissions from other

ingredients and understanding the fate of these emissions in an indoor setting. The third study compared filtration efficiencies of different face covering options widely available in the market and investigated the potential for reusability of cotton cloth masks by repeated machine washing and drying. The results from this study will facilitate a better understanding of the relative protection of different masks against respiratory disease transmission in addition to reducing $PM_{2.5}$ exposure during wildfire events. An extension of this study involved developing improved cloth filter materials using a coating of biodegradable cellulose nanofibril in order to promote sustainable face mask usage. Overall, these studies demonstrated the role experimental aerosol research can have in understanding and reducing different indoor sources of aerosols primarily due to cooking, thus leading to potential improvements to indoor air quality and, consequently, to human health.

ACKNOWLEDGEMENTS

First, I would like to thank Dr. Marina Vance for her continuous advice and support throughout the last 4 years. It was a great learning experience working under an advisor who has time and again shown a lot of patience and calmness while dealing with what I call “make-it-or-break it” moments I witnessed over the course of my Ph.D. and I certainly would try to inculcate those virtues in my life while facing similar situations in the future.

Many thanks to team members of Vance Lab who I worked with during last few years. It was a fun experience being a part of team with highly motivated individuals who I am sure will achieve a lot of recognition in their respective fields due to their excellent work ethic. Special thanks to all the contributing authors who I worked with during different projects throughout my graduate studies. It is only because of your continuous help and support that these manuscripts were successfully published in various high impact journals and are helping advance research in topics related to air quality and health.

I would also like to thank once again all the committee members for agreeing to chair on my dissertation committee. I believe all of you have shown that with hard work and great dedication towards learning new concepts, a doctorate can surely bring positive change to other people’s life through their research work. Lastly, I would like to acknowledge all my friends and family members for their emotional support throughout my studies. It was an awesome journey and I glad I was able to share that with you all.

CONTENTS

TABLES

Table

FIGURES

Figure

CHAPTER I

INTRODUCTION

1.1. Cooking and Indoor Air Quality in Residential Environments

Indoor air quality (IAQ) in built environments, especially residential homes, is an important parameter that affects human health.[1] Cooking is one of the most commonly undertaken activity in indoor environments and it has a major effect on IAQ levels because cooking emissions contain particulate matter (PM), volatile organic compounds (VOCs), carbon dioxide, and nitrogen oxides.[2] In areas where ambient PM levels are low, cooking can be one of the main contributors to indoor PM exposure, especially in non-smoking homes. Long-term exposure to PM emissions in the fine ($PM_{2.5}$) and ultrafine (<100 nm) range has been associated with a variety of health effects such as lung cancer and cardiovascular ailments.[3] There has been a concerted effort in the research community to characterize different aspects of indoor cooking emissions in order to put forth recommendations for optimizing this activity to ensure healthy IAQ levels in addition to the development of different control measures for reducing the associated human exposure from emissions; both of which serve as a motivation for this thesis.

Chapter II focuses on the use of low-cost air quality monitors (AQMs) in four different households for studying $PM_{2.5}$ concentrations and transport between the bedroom and kitchen areas in 4 different residential homes primarily due to indoor cooking. Nowadays, the use of portable air cleaners (PAC) has become an important

intervention strategy for reducing PM exposure in residential environments especially in scenarios where source control and increased ventilation are not practical or feasible methods in controlling PM levels.[4] Therefore, in this study we investigated the effects of using a PAC in the kitchen and bedroom areas to reduce $PM_{2.5}$ exposure levels and also looked into the ideal placement for a PAC in a typical residential home. In order to investigate the transport between the kitchen and bedroom areas of different homes, we used $PM_{2.5}$ concentrations reported by low-cost air quality monitors during various cooking activities and we quantified the transport phenomenon in terms of time difference between the peaks and a ratio between bedroom and kitchen concentrations.

1.2. Characterization of Cooking Oil Emissions

Cooking oils are widely used in the United States and the world, in the food processing industry (i.e., manufacturers of prepared food products), the foodservice industry (i.e., restaurants and catering services), and in residential settings. The United States consumed approximately 17 million metric tons of edible oils in the year of 2021, the majority of which (~11 million metric tons) was soybean oil.[5] While cooking oils can be used in the preparation or flavoring of foods not involving heat, typically cooking oils are used in cooking and frying food preparations.

Heated cooking oil emissions have been associated with fine and ultrafine PM in addition to the release of a variety of VOCs, including thermally degraded aldehydes, which may ultimately lead to various health concerns.[6,7] Chapter III of this dissertation focuses on the characterization of emissions from different cooking

oils as they were heated over wide ranges of temperatures including their smoke points. The cooking oils were heated over different temperatures inside a fume hood and the size distributions of the resulting oil emissions were compared using a scanning mobility particle sizer (SMPS) and an aerodynamic particle sizer instrument (APS).

In order to study the fate of these heated oil generated emissions, we also looked into the volatility parameters of the resulting aerosol volume distributions by observing the changes in their physical properties after being thermally conditioned via a thermodenuder (TD) system. For studying low volatile compounds released from the smoke of these oils, we performed the chemical characterization of smoke sample extracts using the Electrospray ionization Fourier Transform-Ion Cyclotron Mass Spectrometry (ESI FT-ICR MS) analysis and did a qualitative comparison between the soft ionization spectra for different frying oils.

1.3. Use of Face Masks as Personal Protection Devices

In recent years mask usage among general public has increased since it has been recommended as one of the mitigation strategies to curb COVID-19 spread among communities.[8] Masks serve as an important tool for preventing airborne transmission of COVID-19 via two ways- blocking outward spread of respiratory droplets from an infected person and filtering aerosols containing viruses from inhalation by the user.[9,10] Use of face masks as means to reduce fine and ultrafine PM exposure is also encouraged during wildfire events and during periods of high levels of ambient air pollution.[11,12] Chapter III of this dissertation focuses on the

assessment of filtration efficiencies of various face masks as personal filtration devices. The first phase of the study involved comparing size resolved filtration efficiencies in the 60 nm- 4 μm size range under perfect seal condition and inhalation resistances (breathability) for different type of face masks and their combinations. The second phase of the study involved studying filtration characteristics of cotton filter material as it was machine washed and dried from 0 to 52 cycles to test whether cloth masks made out of cotton material can be reused for long periods of time.

During mask mandates in the last few years, increased use of respirators and disposable surgical masks among general public has contributed to the ever increasing problem of improper waste disposal practices often leading to dumping of microplastics in oceans.[13] Chapter IV of this dissertation focuses on the work done on developing filter materials made up of biodegradable cellulose nanofibril (CNF) layer coated on cotton fabric in a bid to promote sustainable cloth mask usage. Different ways to obtain a stable layer of CNF coating on cotton fabric were investigated mainly oven drying and freeze drying. Size-resolved filtration efficiencies for CNF coated fabric samples were also compared with uncoated fabric to show the improvements in filtration efficiencies that can be achieved via this method.

1.4. Organization of this Document

The thesis is organized into five chapters. Chapter I gives a brief introduction about the three studies related to aerosol science and engineering that characterize

IAQ in residential settings and assess aerosol exposure mitigation strategies. Chapter II investigates the response of different low-cost air quality monitors for monitoring $PM_{2.5}$ concentrations and transport in indoor residential environments. This work also assesses the use of a portable air cleaner in different areas of a house to reduce personal exposure to aerosols emitted from indoor cooking activities. Chapter III quantifies the emissions as well as their volatility from the use of different oils heated at different temperatures including smoke point temperatures. Chapter IV assesses the use of face mask as one of the mitigation strategies for preventing aerosol transmission of COVID-19 virus via direct inhalation through respiratory droplets and reducing personal PM exposure during periods of severe ambient pollution. Chapter V includes preliminary results for the optimization of filtration characteristics of biodegradable cloth masks coated with cellulose nanofibril using two different drying methods. The final Chapter VI presents the concluding remarks detailing scientific contributions from different studies and future scope of this dissertation.

Chapter II has been published in the following peer-reviewed journal paper:

Sankhyan, Sumit, Julia K. Witteman, Steven Coyan, Sameer Patel, and Marina E. Vance. "Assessment of $PM_{2.5}$ concentrations, transport, and mitigation in indoor environments using low-cost air quality monitors and a portable air cleaner." *Environmental Science: Atmospheres* (2022)

Chapter III is currently under preparation for publication submission.

Chapter IV has been published in the following peer-reviewed journal paper:

Sankhyan, Sumit, Karen N. Heinselman, Peter N. Ciesielski, Teresa Barnes, Michael E. Himmel, Hannah Teed, Sameer Patel, and Marina E. Vance. "Filtration Performance of Layering Masks and Face Coverings and the Reusability of Cotton

Masks after Repeated Washing and Drying." *Aerosol and Air Quality Research*, 21, no. 11 (2021): 210117.

Chapter V presents preliminary findings that are not intended to be published in a peer-reviewed publication at this point.

CHAPTER II

ASSESSMENT OF $PM_{2.5}$ CONCENTRATIONS, TRANSPORT, AND MITIGATION IN INDOOR ENVIRONMENTS USING LOW-COST AIR QUALITY MONITORS AND A PORTABLE AIR CLEANER

Contributing authors: Sumit Sankhyan, Julia K. Witteman, Steven Coyan, Sameer Patel, Marina E. Vance

2.1. Abstract

In this study, we deployed multiple low-cost air quality monitors (AQMs) to investigate the transport of kitchen-generated fine particulate matter ($PM_{2.5}$) into the bedrooms of four homes of different sizes over a period of more than nine weeks at each home. We also estimated the human exposure to $PM_{2.5}$ associated with each microenvironment and evaluated the effects of using a portable air cleaner (PAC) to reduce those exposures. To select the best AQM for these analyses, we compared the field response of five commercially available models with that of a research-grade optical particle spectrometer. The AirVisual AQM showed the best correlation during collocation phases with R^2 values in the range of 0.5-0.9 during cooking and background periods for all locations. The bedroom monitors picked up cooking emissions from the kitchen area within 1-45 min depending on the layout of each home, and median $PM_{2.5}$ concentrations in the bedroom were up to 30% lower than those in the kitchen. Results from the exposure analysis suggest that PAC use is an important intervention strategy for reducing personal $PM_{2.5}$ exposure, especially in indoor environments where cooking is the main source of $PM_{2.5}$ concentrations. In three of the four homes using PAC consistently in the kitchen or bedroom area

during cooking intensive periods reduced overall exposure values by 30-90%. Moreover, during nighttime periods, PAC usage in the bedroom area yielded the lowest levels of $PM_{2.5}$ exposure for all the homes.

2.2. Environmental Significance Statement

This article describes a comprehensive study of the $PM_{2.5}$ response from a low-cost air quality monitor to study the transport between the kitchen and bedroom areas of four different houses and the resulting exposures at these fixed locations. We also quantified the benefits of using a portable air cleaner (PAC) in the kitchen and bedroom areas to reduce the resulting exposures due to indoor cooking and outdoor penetration. This study brings forth multiple results of interest to the science community as well as the general public, such as the effect of different control strategies such as window opening, extracting range hood use over the stove, and PAC use to reduce the overall PM exposure values in built environments.

2.3. Introduction

In recent years, significant attention has been placed on improving indoor air quality (IAQ) in built environments primarily by reducing the indoor concentrations of fine particulate matter ($PM_{2.5}$) attributed mainly to indoor sources or infiltration from outdoors.[14–17] This is because $PM_{2.5}$ exposure has been linked to several adverse health outcomes, such as increased cancer risk and premature mortality,[18–22] added to the fact that people spend approximately 90% of their time indoors.[23] Due to increased awareness of the health effects of $PM_{2.5}$ exposure, the general public is being encouraged to use low-cost air quality monitors (AQMs) to monitor

indoor pollutant levels.[24–26] AQMs offer a low-cost alternative to research-grade instruments for monitoring air quality enabling users to easily deploy them in home environments.[27–30] They can be integrated with different interfaces (website, mobile applications, computer software) so the data collected can be easily accessed by the user. Some AQMs also employ color scales or display windows for ease of viewing and understanding the air quality index data.[31]

For indoor environments, basic strategies adopted for improving IAQ (mainly by reducing $PM_{2.5}$ concentrations) include source control, increased ventilation, and pollutant removal.[4,32] Source control measures include using improved cookstoves for lower emissions, switching to cleaner fuels for residential heating and cooking purposes.[33,34] $PM_{2.5}$ levels indoors can also be managed by using a mechanical ventilation system or opening the windows to increase the ventilation rates. However, the latter is only applicable in areas with low levels of ambient pollutants.[35,36] In cases where source control and natural ventilation are not effective control strategies, using range hoods over the stove and portable air cleaners near the receptor can be a good alternative to reduce $PM_{2.5}$ exposure.[37–42] In terms of control strategies, AQMs provide an opportunity to alert consumers about degrading levels of air quality in their homes and enable them to perform some of these mitigation strategies. AQMs can also be deployed in different areas of a household, and their real-time data can be used to decide on the best placement of air cleaners for effective particle removal in multizone indoor environments.[43] In terms of occupant exposure, people spend about 70% of their time in a residence.[23]

Of the time spent at home, people are estimated to spend about 10% of it in the kitchen microenvironment and 53% in the bedroom microenvironment.[44] Although the time spent in the kitchen is significantly smaller than that in the bedroom, higher total $PM_{2.5}$ exposures may take place in the kitchen depending on cooking habits, control strategies used, and outdoor penetration of ambient $PM_{2.5}$.

Most AQMs measure particulate matter (PM) concentrations using a low-cost PM sensor which either uses an optical particle counter (OPC) to count particles in various size bins based on assumptions about particle shape and refractive index or use a nephelometer to measure the amount of light scattered by each particle which is in turn converted into a mass concentration using a conversion factor based on laboratory calibration.[45] Previous studies, focusing on determining correction factors for different types of aerosols and ambient locations, have reported that the sensors used in AQMs need to be calibrated according to the local conditions for better correlation with data reported by federal equivalent methods of measurement.[46–48] In recent studies, the hygroscopic growth of sampling aerosols in humid conditions (Relative Humidity >50%) has also been shown to affect the PM response of AQMs.[49,50] There are also concerns about their performance during periods of low concentrations or very high concentrations, especially in ambient environments where they tend to deviate from linear correlation with reference instruments.[51–53] Even with these challenges, the data reported by low-cost air quality monitors can provide reliable results for quantifying personal exposure, especially compared to exposure values estimated from outdoor fixed monitoring stations.[54] For consumers,

low-cost AQMs can be especially informative in educating occupants in real-time about their own activities that generate large amounts of $PM_{2.5}$ and, conversely, actions that are effective in lowering concentrations.

The main goal of this study was to assess the indoor transport of $PM_{2.5}$ and its mitigation in four households of different sizes and configurations for a total duration of nine months. Specific research objectives were to: (1) Compare the $PM_{2.5}$ concentration measurements from four different AQMs with a research-grade instrument to select the best AQM for subsequent research objectives. (2) Study the transport of $PM_{2.5}$ between the kitchen and a bedroom for each home during cooking activities by placing identical and inter-corrected AQMs in these two areas of the household. (3) Determine the effectiveness of deploying a filtering portable air cleaner (PAC) to reduce $PM_{2.5}$ exposure primarily due to indoor cooking. (4) Investigate the effects of PAC placement—in the kitchen or a bedroom—in reducing personal $PM_{2.5}$ exposure during different periods of the day.

2.4. Methods

Instrumentation

For this study, we used an Optical Particle Sizer (TSI OPS 3330, St Paul, MN) as a relatively portable comparison instrument for studying $PM_{2.5}$ concentrations in different indoor environments. $PM_{2.5}$ concentrations were calculated from mass distribution data assuming particle density of 1 g cm^{-3} which has been used in previous studies measuring indoor PM concentrations.[55–57] The OPS instrument had been recently purchased when deployed at the start of the

study, so it had been recently factory calibrated. Additionally, flow calibration checks were conducted, and new filters were also installed at the start of the study.

We chose the OPS as a comparison instrument for this study because it also operates on the principle of single particle counting using a laser and photodetector assembly.[58] It can measure particles in the size range of 0.3-10 μm (16 bins) with an inlet flow rate of 1 liter per minute. Its compact size and low pump noise make it suitable for indoor environments. Although the OPS is not a regulatory reference instrument, it has been widely used in previous studies and has shown good agreement with other research-grade instruments.[58,59] The four AQM models used in this study are also listed in Table 1. Two identical units were deployed for each AQM model.

Because all particle instruments used in this study are limited to particles > ~0.3 μm in diameter, their measurements are likely to underestimate actual $PM_{2.5}$ concentrations because they miss potential PM mass contributions from particles < 300 nm, which may be important indoors, especially during some indoor cooking activities. As such, all $PM_{2.5}$ concentrations reported in this work should be interpreted as $PM_{0.3\text{-}2.5}$.

Table 1. The four AQMs used for this study and their properties.

Product	**Foobot Home**	**IQAir AirVisual Pro**	**PurpleAir PA-II-SD**	**PurpleAir PA-I-Indoor**
Air quality measurements	$PM_{2.5}$, total volatile organic compounds (TVOCs)	$PM_{2.5}$, carbon dioxide	PM_1, $PM_{2.5}$, PM_{10}	PM_1, $PM_{2.5}$, PM_{10}

Time resolution	~300 s	10 s	80 s	80 s
PM sensor	Sharp GP2Y1010AU0F	AVPM25b	Plantower PMS5003	Plantower PMS1003
PM detection technique	Light scattering (0.3- 2.5 μm)	Light scattering (0.3- 2.5 μm)	OPC (6 size bins 0.3- 2.5 μm)	OPC (6 size bins 0.3- 2.5 μm)
Cost estimate	$240	$270	$230	$180
Example studies that used or evaluated these AQMs	[60–66]	[31,60,61,67,68]	[50,53,69–73]	[45,74]

The different AQMs chosen for this study had been extensively tested in previous studies and were readily available in the market. PM sensors used in the PurpleAir AQMs (Plantower) have been deployed on large scales in different studies for various applications, primarily in ambient environments.[53,69–71] Foobot AQMs have been used to quantify personal exposures in different indoor settings.[63–65] In recent studies, the AirVisual Pro has been shown to be a reliable AQM with ease of access and better accuracy in indoor environments.[60,67]

The PAC used in this study (EJ120, Oransi, Raleigh, US) uses a combination of an activated carbon filter and a MERV 17 (Minimum Efficiency Reporting Value) filter to provide a maximum air flow of 330 cubic feet per min (0.16 m^3 s^{-1}). It is recommended for rooms sizes up to 116 m^2 with 2 air changes per hour.[75] The manufacturer recommends changing the filter every 12 months, so we used the same filter for all the homes during the entire study period of nine months. Filter

loading effects were not quantified for this study and were assumed to be negligible due to the generally low background PM concentrations found in all four homes.

Data acquisition and processing

For this study, we used only the $PM_{2.5}$ sensor data from each AQM and compared those values with the corresponding OPS data. All AQMs were connected to local Wi-Fi networks for data acquisition. Foobot data were recorded using an IFTTT ("If This, Then That" automation tool) recipe and was exported in ~5 min time resolution to a Google Sheet output. The AirVisual data were exported to a computer using the local Wi-Fi network, at 10 s time resolution. PurpleAir data were exported through the PurpleAir website at 80 s time resolution. While the PurpleAir PA-II-SD monitors include two Plantower $PM_{2.5}$ sensors providing two sets of mass concentration readings, we only used data corresponding to the 'CF=1' channel, recommended for indoor monitoring.[50,73] For the PurpleAir Indoor monitors, data from the same channel (CF=1) were also used for intercomparison. The $PM_{2.5}$ data from all AQMs were synchronized in 60 s time resolution with the OPS data using the MATLAB synchronize function incorporating a linear interpolation method to obtain time series as shown in Figure A1 and Figure A2. Both Foobot AQMs consistently reported constant values for $PM_{2.5}$ concentrations without showing any response during cooking events in later stages of deployment in Home 2 and Home 3. Therefore, Foobot $PM_{2.5}$ data were not used for further analysis.

Description of the homes

This study was carried out in four different non-smoking households within Boulder County. The layout for each home is shown in Figure 1. Home 1 and Home 4 were located near the University of Colorado campus. Home 2 was located in the suburbs with the nearest state highway around 500 m from home. Home 3 was located on the city's outskirts, with no significant highways within a 500 m radius. Homes 1, 3, and 4 were apartments while Home 2 was a single-family detached home. Homes 3 and 4 were located on the first floor whereas Home 1 was located on the ground floor.

Figure 1. Layouts for all the locations used for this study. Note all the layouts are approximate to scale (1":16' for a printed page). The OPS and AQMs were placed on a wire shelf rack, at either 0.3 m or 0.6 m above the floor.

The study spanned nine months in 2019 and 2020, comprising fall, winter, spring, and summer seasons in Boulder, CO. The ambient daily average $PM_{2.5}$ data

provided by United States Environmental and Protection Agency (US EPA) for Boulder County location during these nine months is also shown in Figure A3. All the four homes used for this study were within a 10 km radius from the monitoring station. In Homes 1-3, the windows and doors were kept shut to maintain comfortable living conditions (T=~21-25°C, RH= 30-50%) inside the homes through mechanical HVAC systems. Home 4 did not have a cooling system, so the windows were kept open continuously throughout the deployment because that coincided with the peak summer season.

Homes 1 and 3 had recirculated microwave range hoods over the stove, whereas Home 2 had an extracting wall mounted range hood (Vent-a-hood dual blower 600 CFM). Extracting range hood usually have a higher capture performance.[76] Home 4 did not have any range hood over the stove. The bedroom areas in Homes 2 and 3 were mostly unoccupied throughout the day whereas in the case of other two homes, the bedroom areas were inhabited. The occupants also maintained a time log with information about the start and end times of all cooking activities. This study was exempted from Institutional Review Board review for lacking participant information or risk. Additional details regarding each location are also given in Table A1.

Phases of AQM deployment

Deployment in each home took place sequentially from Home 1 through Home 4. The data collection for each home was divided into three different phases (Table 2). Phase 0 was a two-day minimum collocation period at the start and at the

end of the deployment period for each home (Phases 0A and 0B, respectively). During Phase 0, all eight AQM units (two of each model) and an OPS were collocated in the kitchen area. In Phase 1 (2-4 weeks), one set of AQMs, including the four different models, were kept in the bedroom area, while the other set with matching models (and the OPS) were maintained in the kitchen area. This was followed by Phase 2 of a similar duration, during which a PAC was used in the kitchen area. The same PAC was moved from the kitchen area to the bedroom area for Phase 3. The PAC was operated at the lowest fan setting of 1 at all the times; however, the occupants were advised to increase the fan settings during cooking periods. The exact deployment dates for each phase of this study are also given in Table A2.

Table 2. Data collection process repeated for each of the four households.

Phase	**0A**	**1**	**2**	**3**	**0B**
Activity	Collocation (no PAC)	No PAC	PAC in kitchen	PAC in bedroom	Collocation (no PAC)
AQM location	Kitchen	Kitchen + Bedroom	Kitchen + Bedroom	Kitchen + Bedroom	Kitchen
Duration	2 days (min)	3 weeks	3 weeks	3 weeks	2 days (min)

2.5. Results and discussion

Intercomparison with OPS $PM_{2.5}$ measurements during collocation phases

An intercomparison of $PM_{2.5}$ measurements between AQMs and the OPS was first performed by taking the ratio of time-averaged concentrations for a given cooking period to calculate a C_{AQM}/C_{OPS} factor. These datasets were 90 min in duration and also included the decay period post cooking activities. 2-4 cooking

activities and background periods (also 90 min in duration) were selected for each collocation period, and the resulting values were plotted in Figure A4 to observe the overall trend of this factor between different homes. The resulting C_{AQM}/C_{OPS} values were in the range of 1-4 for most of the AQMs during both cooking and background periods for different collocation phases in all the homes and did not change over time. Therefore, we did not observe any significant sensor measurement drift within the timeframe of this study.

Next, we combined the collocation data from all the homes into two distinct periods— cooking and background. The resulting distributions of C_{AQM}/C_{OPS} values (in 1 min time resolution) are shown in Figure 2. All AQMs presented $PM_{2.5}$ concentrations that were higher—sometimes >10× higher—than that of the OPS. Both AirVisual AQMs had the highest coefficient of determination (R^2) values with the OPS $PM_{2.5}$ data as shown in Table A3 and Table A4.

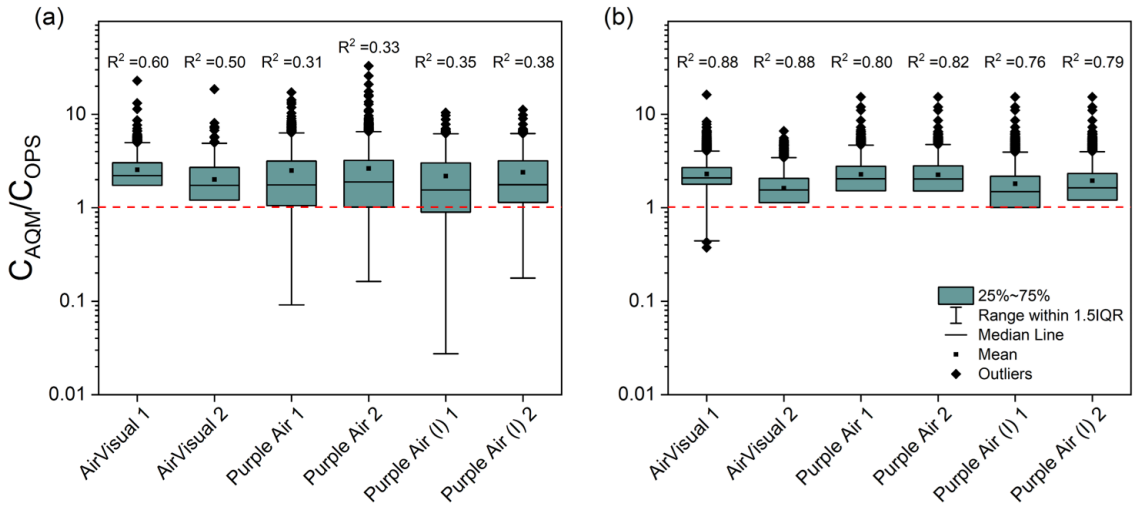

Figure 2. Boxplots showing the distribution of C_{AQM}/C_{OPS} values for different AQMs during two time periods: (a) cooking periods (n=1365 min) and (b) background periods (n=2618 min). The corresponding R^2 values for each AQM with OPS $PM_{2.5}$ concentrations are also shown above each box. Note that the y-axis is in log scale.

During cooking periods, the median C_{AQM}/C_{OPS} values for the two AirVisual sensors (AV1 and AV2) were 2.2 and 1.7. The corresponding values for the PurpleAir and PurpleAir (I) AQMs ranged from 1.6-1.9. These results agree well with previous studies that also reported overestimation of $PM_{2.5}$ concentrations within a factor of 2 by different low-cost AQMs compared to the mass-based measurements from different reference instruments.[45,61,63,70,77] Moreover, low-cost OPCs and nephelometers have been shown to exhibit greater amounts of error in mass loading values compared to the high end OPCs in these conditions.[78]

The R^2 values for all AQMs were higher during background periods than cooking periods. During background periods, particles are likely to have penetrated from outdoors and are more likely to match low-cost sensor calibration inputs. Infiltrated particles are also less unlikely to suffer strong temporal and spatial gradients. During cooking periods, particle concentration, size distribution, optical properties, and chemical composition are likely to change quickly, creating strong temporal and spatial gradients. Sudden changes in these parameters may have led to deviation of response linearity.

$PM_{2.5}$ measurements from the AirVisual units presented the highest values of R^2 in the range of 0.5-0.9 for both units, and the corresponding slope values ranged between 1.3-2.2. Moreover, the mean normalized bias (MNB) and the root mean squared error (RMSE) values were lowest for the AirVisual 2 unit as compared to other AQMs during both background and cooking periods (Table A3 and Table A4). Based on these results, the $PM_{2.5}$ concentrations reported by AirVisual had the best

agreement with OPS among the AQMs tested in this study. For this reason, we used AirVisual results for all subsequent analyses in this work. In order to get the results of the two AirVisual units in the kitchen and bedroom areas to agree, we applied a correction factor to the AV1 $PM_{2.5}$ values which was derived from a linear regression analysis obtained from Phase 0 (collocation) data as shown in Figure A5.

Indoor $PM_{2.5}$ transport between kitchen and bedroom among different homes

We studied the indoor $PM_{2.5}$ transport between the kitchen and bedroom areas using the $PM_{2.5}$ time series reported by the AirVisual AQMs located in the kitchen and the bedroom areas for each home during Phase 1 (no PAC use). A characteristic time series for a given cooking period during Phase 1 for each home is also shown in Figure A6. We also calculated the first-order decay rate associated with each cooking event to compare the effective particle loss rates (including deposition losses) in the kitchen areas for different homes, as shown in Figure A7. The median values for the first three homes were close to 1 h^{-1} whereas Home 4 had a higher median value (~2 h^{-1}), likely due to open windows.

A $C_{Bedrrom}/C_{Kitchen}$ factor was used to compare the concentrations in the kitchen and bedroom area for each home. This factor was calculated by taking the time-averaged concentrations over 90 min for both kitchen and bedroom $PM_{2.5}$ concentrations, considering a starting time (t=0) the concentration peak as reported by the bedroom monitor. Similar factor mentioned as L/K ratio in Wan et al.[79] has been used to compare PM levels due to indoor cooking in the living rooms and kitchens of 12 different homes. We also calculated the time difference (Δt) between

the peak as it occurred in the kitchen and in the bedroom for a given cooking activity during Phase 1. A boxplot showing the distributions of Δt and $C_{Bedroom}/C_{Kitchen}$ factors for all four homes is shown in Figure 3.

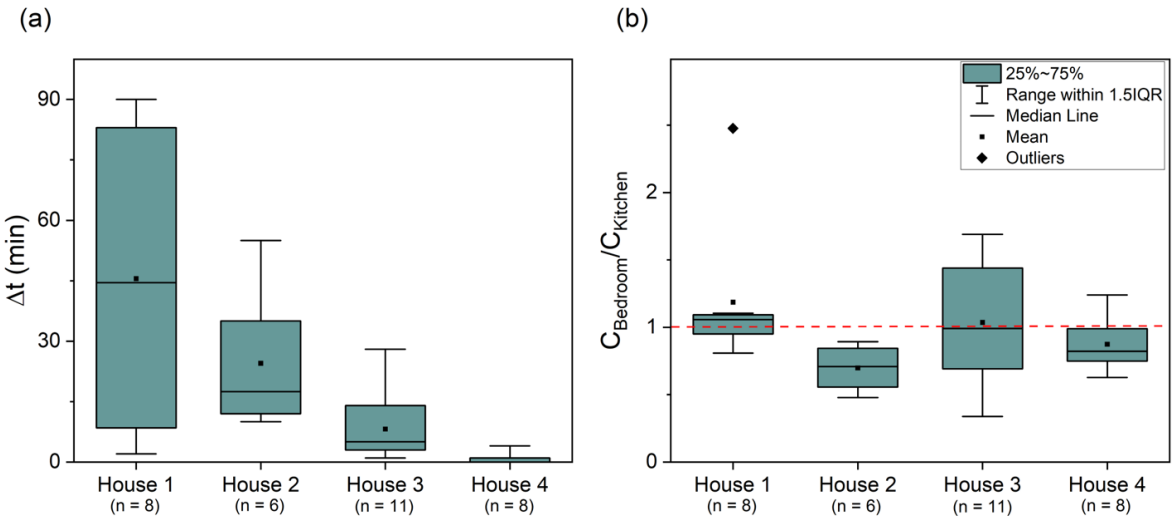

Figure 3. Panel (a) represents the distribution of the time elapsed between the kitchen and bedroom peak $PM_{2.5}$ concentrations for a given cooking period during Phase 1. Panel (b) represents the distribution of $C_{Bedroom}/C_{Kitchen}$ factors for different homes.

For Home 1, the median values of Δt were highest among all the homes (45 min). This could be because the bedroom door was usually kept closed. The corresponding median value of $C_{Bedroom}/C_{Kitchen}$ value was close to 1 since the kitchen area was adjacent to the bedroom area in this home, so $PM_{2.5}$ concentrations equalized between the two spaces whenever the bedroom door was opened. A similar median value of $C_{Bedroom}/C_{Kitchen}$ factor was also calculated for Home 3. In this home, the bedroom was located directly across the hallway from the kitchen area. For this home, the median value of Δt was ~5 min, which is much lower than in Home 1, probably because in Home 3 the bedroom door was always open.

The distance between the stove and bedroom AQMs was largest for Home 2 (~10 m around two corners) and, therefore, the median value of $C_{Bedroom}/C_{Kitchen}$ (0.7) was lowest among all the homes studied. The corresponding median value of Δt for this home was 17.5 min and the bedroom door was always open. In Home 4, due to open windows in the bedroom and kitchen area, and due to the absence of interior walls between the two units (Home 4 being a studio apartment), the bedroom AQMs picked up the concentrations from the kitchen area within a minute for each cooking activity and the median $C_{Bedroom}/C_{Kitchen}$ was 0.8.

Overall, the most important factors governing $PM_{2.5}$ transport from the kitchen to the bedroom of these four homes were the presence of physical barriers between these spaces (e.g., interior walls and whether doors were kept open or shut), different layouts of kitchen and bedroom areas in each home, distance from the stove to the kitchen and bedroom AQMs in addition to the ventilation conditions (e.g., open windows). It is also interesting to note that the median values of $C_{Bedroom}/C_{Kitchen}$ for homes which had an extracting fume hood (Home 2) and open windows in the kitchen area during cooking periods (Home 4) were lower than that value for the other homes. This could be due to the fact that these control measures prevented the majority of the kitchen concentrations from reaching the bedroom area, thereby lowering the time-averaged concentrations (calculated for 90 min post peak). These results indicate the effectiveness of such control measures in reducing PM exposure due to indoor cooking in both the kitchen and bedroom areas. This is expanded in greater detail in the next section.

Understanding the role of PAC location in reducing indoor $PM_{2.5}$ exposure

Time-averaged $PM_{2.5}$ concentrations were used to estimate an occupant's exposure with the assumption that the individual was present in the kitchen or bedroom area for the entire duration of the analysis. Although this approach is limited due to the monitor's fixed location, this has been applied in previous studies to quantify black carbon and PM exposure due to indoor cooking in controlled indoor environments.[80,81] A time series showing the median $PM_{2.5}$ concentrations in the kitchen area of each home is shown in Figure 4. As observed by median peaks, each home showed consistent daily cooking trends in the kitchen area, especially for Home 1 and Home 3.

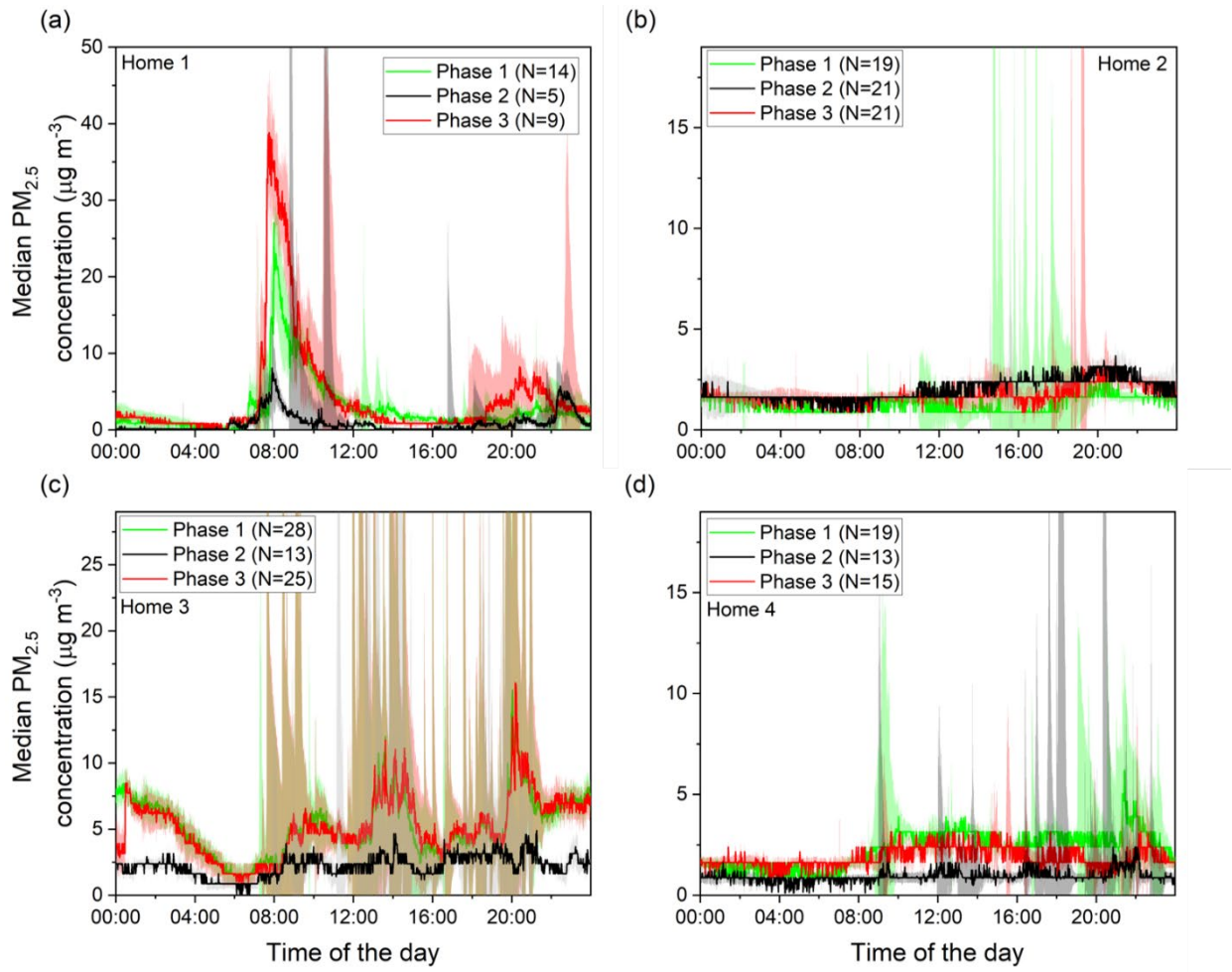

Figure 4. Median $PM_{2.5}$ concentrations in the kitchen area during the day for different phases in Homes 1-4 are shown in panels a, b, c, and d, respectively. The shaded region represents standard error. The brown shaded region represents the overlap between Phase 1 and Phase 3. Note that the y axis is different for each panel.

For Homes 1 and 3, median concentrations during Phase 2 (PAC in kitchen) were significantly lower than that of the other two phases indicating the effectiveness of PAC use for reducing $PM_{2.5}$ exposure. The median concentrations for Phase 1 and Phase 3 in all the homes also exhibit the same diurnal pattern and an overlap to a certain extent. This shows that PAC deployment in the bedroom (Phase 3) did not affect concentrations in the kitchen in a significant manner. Homes 2 and

4 had significantly lower $PM_{2.5}$ concentrations in the kitchen area, due to an efficient extracting range hood in Home 2 and open windows in Home 4, as explained in the previous section. According to the inhabitants of Home 3, the high $PM_{2.5}$ concentrations observed overnight in kitchen of Home 3 during could be attributed to the infiltration of tobacco and marijuana smoke from the downstairs unit. Smoke transported into the apartment through the kitchen sink drainpipes.

Next, we present the $PM_{2.5}$ exposure analysis in the kitchen and bedroom areas for two distinct periods: a daytime analysis using time intervals between 6:00 am to 10:00 pm and a nighttime analysis using the remainder of the day (10:00 pm to 6:00 am).

Daytime exposure analysis

Daytime exposure values for different phases in all four homes are shown below in Figure 5. When no PAC was used, the average (± standard error) daytime $PM_{2.5}$ concentration in all four homes was 10.3 ± 0.2 μg m^{-3} in the kitchen and 6.3 ± 0.1 μg m^{-3} in the bedroom. During nighttime, concentrations were ~3-4× lower. The average $PM_{2.5}$ concentrations were 2.8 ± 0.1 μg m^{-3} in the kitchen and 2.5 ± 0.1 μg m^{-3} in the bedroom.

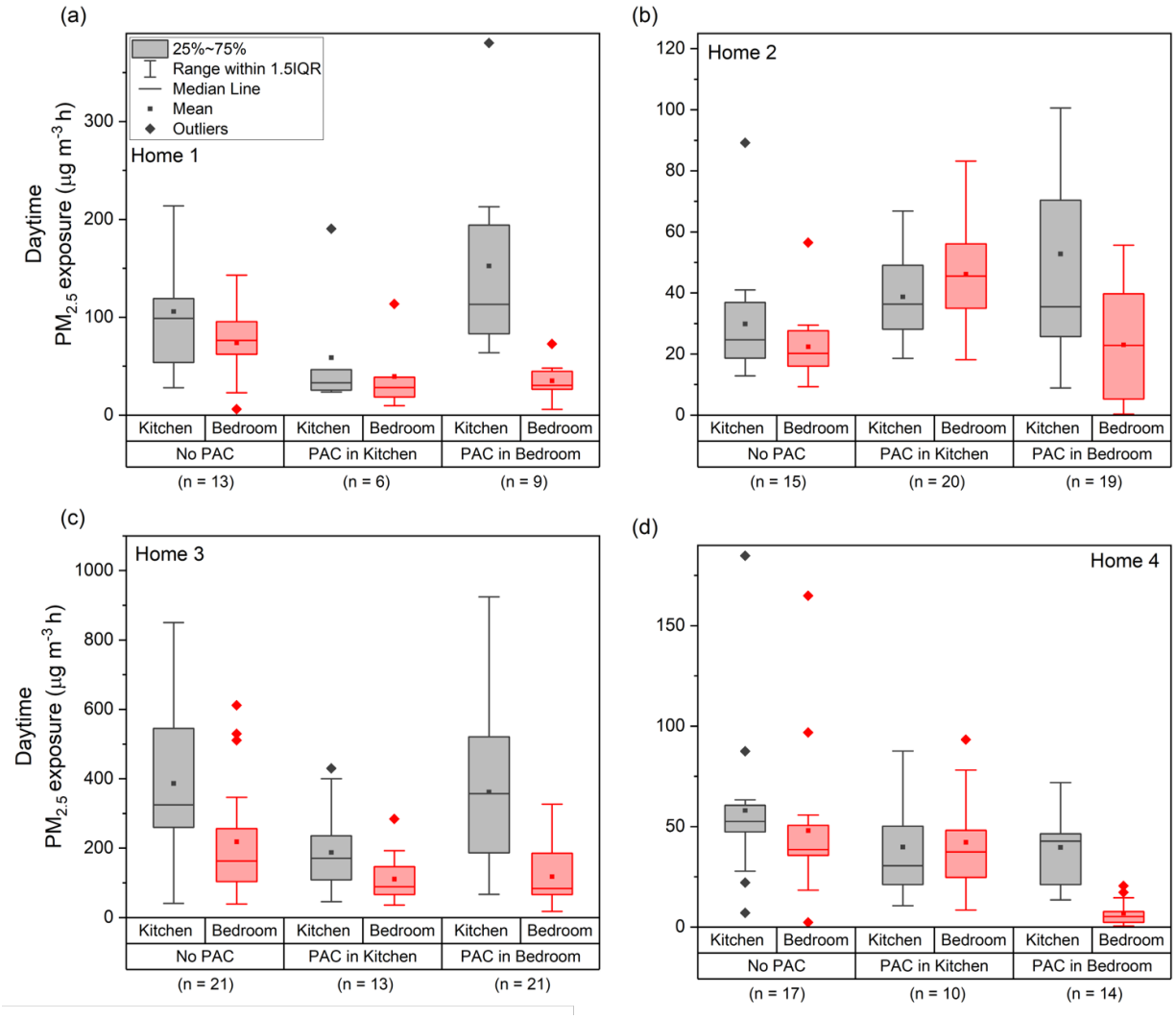

Figure 5. Boxplot of daily $PM_{2.5}$ exposure values during time periods between 6:00 am to 10:00 pm for Homes 1-4 is shown in panels (a), (b), (c), and (d), respectively. The number of datasets for each phase is also represented by n. Note that the y-axis in each panel has a different scale.

During Phase 1 (no PAC use), daytime $PM_{2.5}$ exposure values were on average 17-43% lower in the bedroom compared to the kitchen of the four homes. This is likely due to $PM_{2.5}$ emissions during cooking activities increasing concentrations in the kitchen, which are then diluted and lost to surface deposition and exfiltration during transport to the bedroom.[82,83] During the nighttime (Figure

6), this difference dropped to 0-23%, which further confirms the hypothesis that the differential is driven by cooking activities.

Using a PAC in the kitchen (Phase 2) or bedroom (Phase 3) reduced the mean exposure values by 30-90% in that respective area when compared to the corresponding values from Phase 1 (no PAC use) in three of the four homes. When the PAC was used in the kitchen (Phase 2), the average mean exposure values in the kitchen area dropped by 30-70% for all homes except Home 2. For Home 2, an increase in exposure was observed during PAC use compared to Phase 1. However, this phase also coincided with the holiday season, with additional guests and significantly more cooking being performed in the home. A similar comparison between the mean exposure values of the bedroom area during Phase 3 (PAC in bedroom) with Phase 1 values also yielded similar reductions in mean values: 53% for Home 1, 46% for Home 3, and 85% for Home 4.

Also noteworthy is that for both Homes 2 and 4, the mean exposure values were slightly higher in the bedroom area compared to the kitchen area during Phase 2. This could be because Home 2 had an extracting range hood and Home 4 occupants opened windows during cooking periods. These strategies may have played larger roles in governing $PM_{2.5}$ exposures than the use of a PAC in the kitchen. Therefore, the exposure values calculated for the bedroom areas may be from other sources, such as outdoor infiltration.

The use of a PAC in the bedroom (Phase 3) was also very effective in reducing daytime $PM_{2.5}$ exposure in that room. The mean values in the bedroom area were

53-85% lower than in the kitchen area for all four homes. This difference is much more pronounced than during Phase 1 (no PAC use), when bedroom exposures were 17-43% lower than in the kitchen. Between Phase 2 and Phase 3, the bedroom exposure values were either in the same range (Home 1 and Home 2) or slightly lower for the latter phase in the case of remaining homes. Therefore, PAC use in the kitchen area during the daytime can be an effective option for reducing personal $PM_{2.5}$ exposure levels due to indoor cooking for occupants who will be spending majority of their time indoors in the kitchen and bedroom areas combined during that period. Moreover, after the period of active cooking when the occupant moves out of the kitchen to other areas, pollutants could homogenize spatially over the entire home, therefore, maximizing personal exposure which again supports this intervention strategy of reducing emissions at the source.

Overnight exposure analysis

In order to examine the role of ambient PM penetration into the homes, we performed an analysis of overnight periods, when cooking activities are less likely to occur. Overnight $PM_{2.5}$ exposure trends for different phases among the four homes are shown in Figure 6. The mean exposure values in the bedroom area for all the homes were lowest for Phase 3 when the PAC was used in the bedroom area.

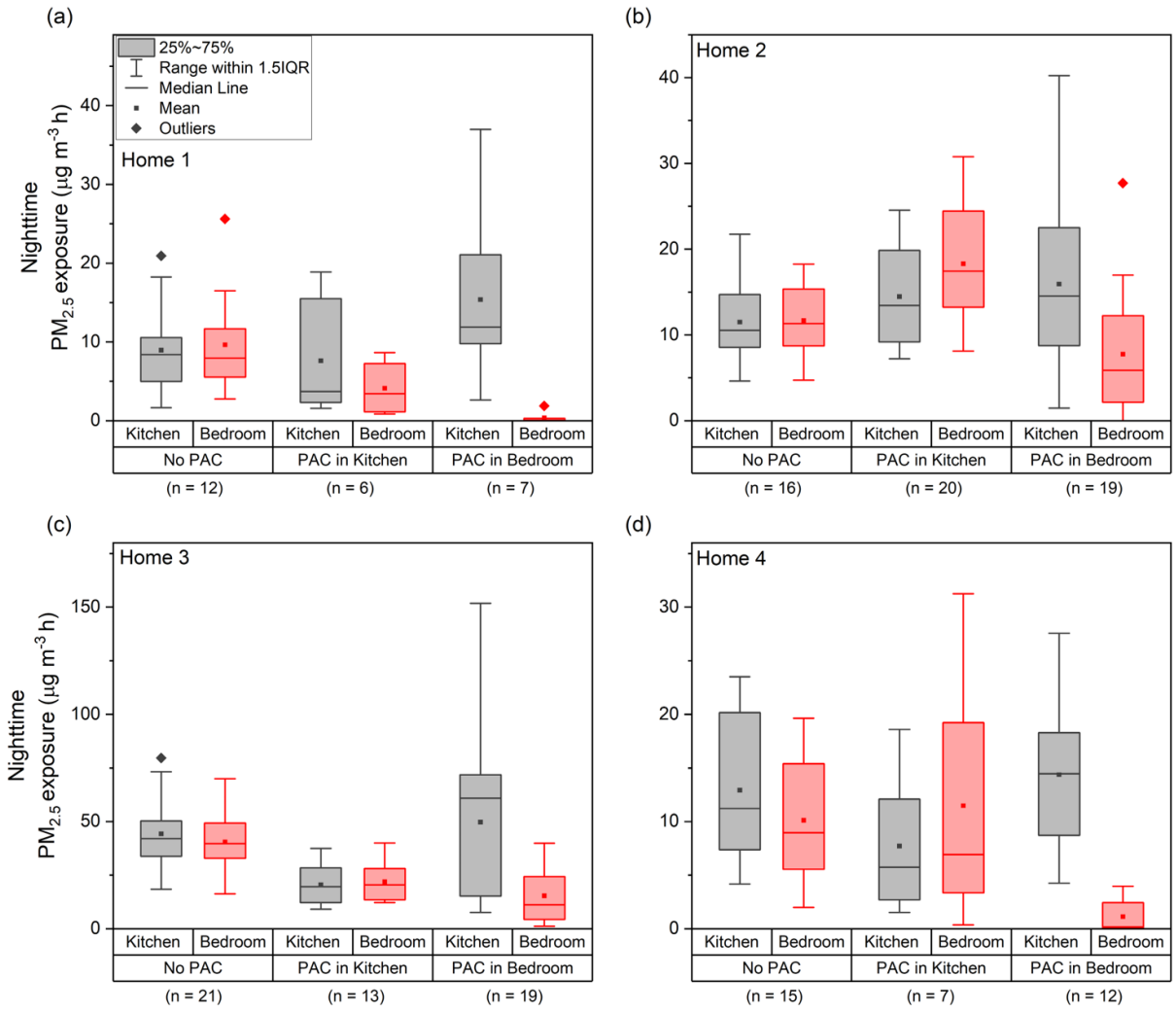

Figure 6. Boxplot of $PM_{2.5}$ exposure values for time periods between 10:00 pm to 6:00 am the following day for Homes 1-4 is shown in panels (a), (b), (c), and (d) respectively. Note that the y-axis in each panel has a different scale.

The overnight $PM_{2.5}$ exposure values during Phase 1 were one order of magnitude lower compared to daytime periods, thereby suggesting the role of outdoor infiltration in $PM_{2.5}$ on exposure levels indoors, even though its contribution is much lower than indoor cooking. This is likely due to low ambient $PM_{2.5}$ levels during this study. However, it is important to mention that the time period for daytime exposure was twice that of nighttime periods (16 h vs 8 h). During Phase 2, the mean overnight exposure values for the kitchen area of Home 3 were ~50%

lower than those of the corresponding mean values for Phase 1 (21 μg m^{-3} h). A moderate reduction in mean exposure (~35%) was also observed for Home 4 where the average exposure value during nighttime periods was calculated to be 8 μg m^{-3} h . Similarly, when the PAC was placed in the bedroom area (Phase 3), the mean exposure values in the bedroom area were 30-90% lower than the corresponding Phase 1 values for all the homes combined. Overall, the mean bedroom exposure values during Phase 3 were lowest among all the phases for all homes. The corresponding mean exposure values were calculated to be: Home 1 (1 μg m^{-3} h), Home 2 (8 μg m^{-3} h), Home 3 (15 μg m^{-3} h), and Home 4 (1 μg m^{-3} h).

In summary, using a PAC in the kitchen and bedroom areas reduced $PM_{2.5}$ exposure between 10-90% during daytime and overnight periods in most of the homes, with only a few exceptions as shown in Table A5 and Table A6. For homes that did not have an effective control strategy (Home 3 and Home 1), the reductions in mean exposure values were usually greater as compared to the other two homes with extracting range hood and open windows for higher air exchange rates, especially during Phase 2 of deployment. Moreover, the absolute values for the reduction in mean exposure compared to no PAC phase were greater in the kitchen area than the bedroom area during the daytime periods in both Homes 1 and 3, suggesting PAC placement in the kitchen areas during daytime periods. For overnight periods when people usually spend majority of the time in the bedroom area, the $PM_{2.5}$ exposure values in the bedroom area during Phase 3 were lowest as compared to the other phases in all the homes.

2.6. Conclusion

During Phase 1, when no PAC was employed, the overall mean (± standard error) daytime $PM_{2.5}$ concentration for all four homes was 10.2 ± 0.2 μg m^{-3} in the kitchen and 6.3 ± 0.1 μg m^{-3} in the bedroom. During the nighttime period, $PM_{2.5}$ concentrations were ~3x lower, with overall means of 2.8 ± 0.1 μg m^{-3} in the kitchen and 2.5 ± 0.1 μg m^{-3} in the bedroom. These concentration ranges are relatively low, likely due to low ambient $PM_{2.5}$ concentrations during the study period. The highest concentrations observed in all four homes occurred due to indoor cooking activities in the kitchen.

In terms of indoor $PM_{2.5}$ transport between the kitchen and bedroom areas of different homes, concentrations in the bedroom were 70 – 100% of those in the kitchen. The kitchen emissions peaked in the bedrooms after 1-45 minutes were elapsed from the start of a cooking event. The fastest transport was observed in Home 4 (no internal walls) and the slowest in Home 1, where the bedroom door was kept closed. Overall, both parameters varied depending upon the layout and relative location of the AQMs in the kitchen and bedroom area with regards to the stove. Baseline conditions were investigated during Phase 1, when no PAC was employed.

The exposure analysis performed in this study suggests that PAC use is an important intervention strategy for reducing personal $PM_{2.5}$ exposure, especially in indoor environments where cooking is the main source of $PM_{2.5}$. The bedroom exposure values were also comparable to the exposure at the kitchen location in all

the homes. During daytime (6:00 am- 10:00 pm), PAC use in the bedroom or kitchen area yielded 30-90% reductions in $PM_{2.5}$ exposure in three of the four homes. Daytime exposure results also suggest that using a PAC in the kitchen results in lower exposure values in both the bedroom and kitchen areas. During overnight periods, PAC use resulted in the lowest exposure values in all homes, with a reduction in mean exposure values by 30-90% or 4-25 $\mu g\ m^{-3}$ h as compared to not using a PAC in the bedroom.

This study is limited to four homes located in one city during a 9-month period when ambient $PM_{2.5}$ concentrations were relatively low. As such, our exposure analysis showed greater importance of cooking activities compared to outdoor $PM_{2.5}$ infiltration in driving the $PM_{2.5}$ exposure values indoors. Another important caveat for this study is the fact that people on average spend much less time in their kitchen areas as compared to the bedroom areas during an entire day. However, the concentrations in the kitchen are usually higher during active cooking periods so the resulting exposure values in the kitchen area could still be comparable to the bedroom area values especially in areas where outdoor infiltration doesn't play a major role in driving the indoor $PM_{2.5}$ exposure. A study like this should be performed in a more polluted period or city and in homes with varying air-tightness levels to study the importance of outdoor infiltration that might become a greater contributor to indoor $PM_{2.5}$ exposure than cooking emissions.

Finally, we did not observe any drift in $PM_{2.5}$ concentrations as reported by various AQMs as they were moved from one home to the other. Overall, $PM_{2.5}$ data reported by AirVisual AQM showed the best correlation with the corresponding OPS data during colocation phases with R^2 values in the range of 0.5-0.9 for cooking and background periods.

2.7. Acknowledgments

This work was supported by the Dean's Innovation Research Assistantship through the Paul M. Rady Department of Mechanical Engineering at the University of Colorado Boulder. We also acknowledge the Alfred P. Sloan Foundation (G-2017-9944) for funding this study.

CHAPTER III

AEROSOL EMISSIONS AND THEIR VOLATILITY FROM HEATING DIFFERENT COOKING OILS AT MULTIPLE TEMPERATURES

Contributing authors: Sumit Sankhyan, Kayley Zabinski, Rachel E. O'Brien, Steven Coyan, Sameer Patel, Marina E. Vance

3.1 Abstract

Using cooking oils at high temperatures emit aerosols in the fine and ultrafine size ranges as well as a variety of volatile organic compounds. Exposure to these cooking emissions has been associated with various respiratory and cardiovascular ailments. In this study, we characterized aerosol emissions from various popular frying oils using an electric heat source at various temperatures (below and above their individual smoke points). At 180 °C, a common deep-frying temperature, oils with lower smoke points (olive oil and lard) were associated with the highest aerosol mass concentrations among all oils tested. The volatility characteristics of these oil-generated aerosols were also studied by analyzing their volume distributions after thermal conditioning through a thermodenuder. For most of the oils, thermal conditioning beyond temperatures of 75 °C resulted in the near removal of volatiles leaving behind non-volatile cores in the 60-100 nm range. Results from the Fourier Transform-Ion Cyclotron Mass Spectrometry analysis suggest that sample extracts obtained from smoking different oils exhibited large chemical similarity with average molecular mass in the range of 620-640 atomic mass units and low oxygen-to-carbon ratios (~0.16). Lastly, we estimated the

respiratory deposition values of different oils for a 30-minute frying period, and the results show that lard had the highest average deposition values for three regions of the respiratory system (1-10 μg) whereas peanut oil reported the lowest values of aerosol mass deposited (~1 μg).

3.2. Introduction

Cooking is a major source of indoor air pollution. Cooking emissions usually contain ultrafine and fine particulate matter (PM) as well as a variety of volatile organic compounds (VOCs) such as alkanes, formaldehyde, benzene, toluene and xylene, and polycyclic aromatic hydrocarbons (PAHs).[2,84–86] Exposure to cooking emissions has been linked with various respiratory and cardiovascular ailments and cancer-related risks[87–89]. In recent years, various studies characterizing different aspects of cooking activities included type of stove and fuel used, cooking ingredients and methods, and evaluating measures for reducing cooking emissions and mitigating associated occupant exposures.[2,33,80,81,90] These works have highlighted the need for continuously optimizing indoor cooking practices to reduce occupant exposure. Indoor cooking—especially in commercial settings—has also been shown to impact ambient air quality and global climate due to the release of PM and VOCs.[91–93] As such, it is also important to investigate their fate to optimize control strategies that also reduce emissions to the outdoor environment while minimizing indoor occupant exposure.[81,83,94–97]

Since most of the cooking activities undertaken indoors include a heat source, there have been concerted efforts to promote the switch to cleaner fuels and

improved cookstoves, especially in developing countries to reduce PM exposure associated with fuel burning. These studies have also led to a proliferation of different models of improved cook stoves, which have shown to work well for their intended purpose.[33,98] In the developed world, the focus has shifted primarily towards the use of different control strategies and optimizing cooking practices due to the mass availability of cleaner fuels. Significant progress has been made towards diverting the attention of the general public towards the use of control measures such as extracting range hoods and portable air cleaners, as well as increased ventilation in cooking areas to reduce exposure.[99–101] In terms of optimizing cooking activities, past research has focused largely on characterizing the effects of cooking temperature, combination of ingredients, and cooking methods such as frying versus grilling on the release of PM and VOCs in different indoor settings.[6,102–105]

Frying in particular has been associated with higher PM emissions, especially in the ultrafine range, compared to other cooking practices utilizing oil.[86,103,106] It has been well documented that keeping the cooking temperature below the oil's smoke point results in lower emission rates.[103,107] At temperatures near the smoke point, fat breakdown occurs, leading to the formation of glycerol and free fatty acids. These products can then decompose further into VOCs and can further act as precursors to secondary organic aerosol (SOA) formation, which may explain the increased particle emission rates.[7,102,108] Therefore, cooking temperature control may be useful in not only reducing human exposure to cooking aerosols but

also preventing the release of organic compounds into ambient air—especially for oils with lower smoke points.[109] Moreover, due to considerably larger quantities of oil being used in the frying process, it becomes important to study the relevance of smoke point and compare aerosol emissions relative to frying temperature.

In terms of health effects, the VOCs emitted during deep-frying present greater carcinogenic risk—primarily due to aldehydes—compared to other cooking methods using oil.[105] This is in addition to the release of fine and ultrafine particulate matter further aggravates the health risk associated with cooking oil emissions.[109–111] Moreover, previous studies on the volatility of cooking emissions have reiterated that cooking aerosols can also contribute to SOA formation in ambient environments due to different aging processes making cooking emissions a pollutant of outdoor concern.[97,108,112–114] The lower volatility compounds in cooking emissions could also feature in indoor surface organic films, thereby driving various gas-phase partitioning mechanisms and further affecting the indoor chemistry of aerosols.[115–117]

The main objectives of this study were to characterize emissions from different cooking oils as they were heated over a range of temperatures, including 180 °C, a common deep-frying temperature, as well as each oil's individual smoke point and 20 °C above it. We also investigated the volatility characteristics of different cooking oils using a thermodenuder. We further characterized the lower volatility compounds in terms of their chemical composition and double bond equivalencies. Lastly, we compared the particle deposition values in different

regions of the respiratory system associated with heating different cooking oils to relate these results to the potential health effects associated with their use in indoor settings.

3.3. Methods

Oils Tested

In this study we tested five different types of cooking oils with a wide range of smoke points. These oils were selected because of their market popularity as cooking oils and due to their wide ranges in smoke point and fat composition. All the oils used for this study were purchased directly from a local store and were stored in a lab shelf at room temperature, away from direct sunlight, during the course of the experiment. The physical and chemical characteristics for each oil are given in the table below.

Table 3. Physical and chemical characteristics of the oils tested, including the smoke point and weight percentages of saturated and unsaturated fats.

Oil		**Lard**	**Coconut (Refined)**	**Olive**	**Peanut**	**Soybean**	**Canola**
Smoke point (°C)		190	204	208	227	234	238
Fatty acid (%)	**Saturated**	39%	82.5%	14.3%	20.3%	15.6%	7.4%
	Monounsaturated	45%	6.3%	70%	48.1%	22.8%	63.3%
	Polyunsaturated	11%	1.7%	10.7%	31.5%	57.7%	28.1%

Lard has the lowest smoke point (~190 °C), whereas both canola and soybean oils have the smoke points in the higher range (232-238 °C). In terms of fat

composition, canola oil has the lowest saturated fat content (7.4%) and highest unsaturated fat content (91.4%), while coconut oil is the opposite, with the highest saturated fat content (82.5%) and lowest unsaturated fat content (8%). The olive oil used for this study was advertised by the manufacturer as "ideal for frying" and, according to the product label, contained a mixture of refined olive oil and virgin olive oil. Another thing to mention here is that the soybean oil was marketed as vegetable oil on the product label by the particular brand we opted to use for this study.

Experimental Setup

The schematic for the setup that was used to compare aerosol size distributions for different cooking oils heated over a range of temperatures is shown in Figure 7. Briefly, 200 ml of oil was heated in a shallow frying pan, kept on an electric hot plate inside a fume hood. Similar setups have been used previously in other cooking oil characterization studies.[102,118] The power supply of the hot plate (kept at medium heat setting) was controlled according to the oil temperature feedback from a k-type thermocouple to the proportional-integral-derivative (PID) controller.

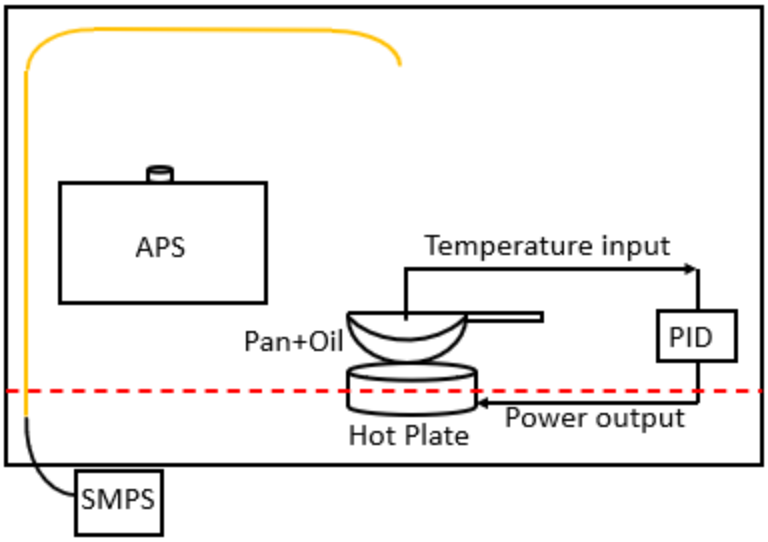

Figure 7. Schematic of the setup used for characterizing aerosol emissions from the use of different cooking oils. The red line represents the fume hood sash opening. The metal and silicone tubing are shown in orange and black colors respectively.

The fume hood sash was kept slightly open (13 cm from a fully closed position), pulling ambient air at a flow rate of ~0.6 m^3 sec^{-1} towards the back panel of the fume hood. The pan was kept at the center of the fume hood, 2 cm away from the sash opening. We measured an air velocity of 0.24 m sec^{-1} for up to 7 cm above the pan surface and zero air velocity for the remainder of the height of the fume hood. The lab space was usually unoccupied while the experiments were being conducted, thereby reducing the chances of any background sources interfering with the fume hood measurements.

The pan was washed with dish soap before each experiment and preheated for ~15 min on the electric hot plate to remove any oil residue from the previous experiment and from any deposition taking place during storage. Afterwards, a given oil sample was poured onto the heated pan, and the resulting emissions were sampled. The temperature of the PID-controlled hot plate was set to 100 °C, 150 °C,

180 °C (the most commonly used deep-frying temperature), each oil's smoke point, and 20 °C above the smoke point. Each of these temperature setpoints was held for 15 - 20 min. We also recorded the real time oil temperature values from the controller display panel in 1-5 minute intervals and the average of the percentage difference between the actual temperature and the set temperature (180 °C) values ranged between 4-6 % for different oils.

An aerodynamic particle sizer (APS 3330, TSI, Shoreview MN) and a scanning mobility particle sizer (SMPS 3936, TSI), composed of a long differential mobility analyzer (DMA 3080L, TSI) and a water-based condensation particle counter (CPC 3788, TSI), were used for sampling aerosol size distributions. The APS was kept on an elevated platform (30 cm above the fume hood floor surface) next to the heat plate inside the fume hood whereas the SMPS sampled emissions through a copper inlet (0.64 cm ID) installed at the top of the fume hood. The last remaining section of the tubing was connected to conductive silicone tubing for connection with the SMPS inlet. We assumed a particle density of 1 g cm^{-3} throughout our analysis based on recommendations from previous studies.[80,119]

For studying the aerosol volatility characteristics, a thermodenuder (TD) was connected between the sampling inlet and the SMPS. During the experiment, the cooking oil was kept at 180 °C and the temperature of the heated section was ramped up in 25 °C increments till it reached 150 °C. The fraction of volatized material lost due to heating for different oils was qualitatively compared by observing the trends in averaged geometric mean diameter (GMD) of the volume

distribution for a given TD temperature and volume fraction remaining (VFR). The VFR was calculated by taking the ratio of the averaged total volume concentration at a given TD heated section temperature to the averaged total volume concentration at ambient temperature.[120] The TD system was derived from the design proposed and characterized in Huffman et al.[121] A schematic of the TD used in this study is shown in Figure 8.

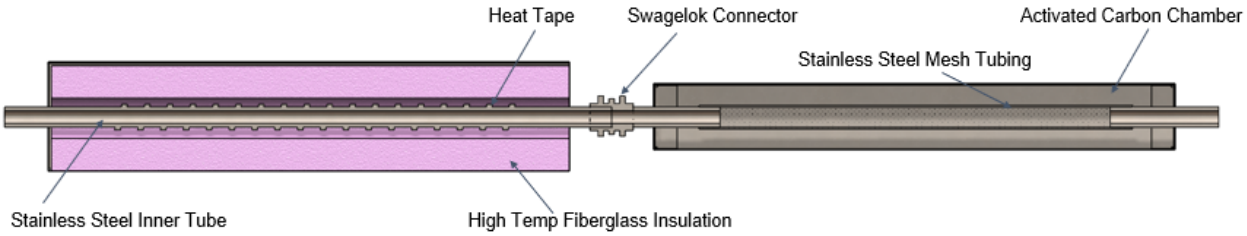

Figure 8. Cross section view of the thermodenuder used in the study, highlighting its different components. The temperature of the heating section was monitored via a K-type thermocouple placed at the surface of the sampling tube, providing feedback to an external temperature controller unit.

The TD consisted of two sections a heating section and a denuding section. The heating section was made up of stainless-steel tubing (1-inch OD) with heating tape wrapped around it encased in a stainless-steel chamber with rectangular cross-section, filled with fiberglass insulation material. The temperature of the heating section was monitored using a surface K-type thermocouple (attached to the outer surface of the heating tube) connected to a temperature controller. This measurement was previously calibrated using a different thermocouple at the center of the airstream. A temperature characterization of the heating section is described in greater detail in section B1 of the SI file.

The denuder section consisted of a stainless steel-mesh tube (1-inch OD) inside a 4-inch aluminum pipe and its annular space was filled with granular

activated carbon for VOC adsorption. Both sections were connected using a Swagelok connector and a Swagelok reducing union was also used at the ends of the assembly so that the entire assembly could be connected to quarter-inch conductive silicone tubing. Information on the particle loss calculations for the sampling line and the TD setup is given in SI file section B2.

FT-ICR MS of smoke generated from heated cooking oils

For chemical characterization of oil-generated smoke, a comparable heating set-up was used in a hood at William & Mary to minimize the time between collection of particles and extraction for further analysis. For these studies, the oils were heated to around the smoke point or up to ~ 20 °C above it. Smoke particles were collected through a small denuder at ~4-5 lpm onto a Teflon filter for ~1 hour. Samples were extracted with acetonitrile and concentrated under a gentle flow of ultra-pure nitrogen. For analysis, these samples were shipped over-night on ice to Old Dominion University for analysis in a Fourier Transform-Ion Cyclotron Resonance (FT-ICR) Mass Spectrometer. This data was collected at the COSMIC lab on a Burker Daltonics 12 Tesla Apex Qe FT-ICR MS using methanol as the solvent, positive ion mode, and an Apollo II electrospray ionization (ESI) source. Mass Spectra were picked using DeCON 2LS (https://pnnl-comp-mass-spec.github.io/DeconTools/) with a peak to background ratio of 5 and a signal to noise threshold of 3. Peaks were picked in the range of $C_{0\text{-}100}$ $H_{0\text{-}200}N_{0\text{-}3}O_{0\text{-}50}$ within a ±1 ppm window using the Molecular Formula Calculator ((https://nationalmaglab.org/user-facilities/icr/icrsoftware).

For peak assignments, 2D and 1D kendrick mass series were used (CH_2, H_2, and O) and all peaks were removed that overlapped within ±2 ppm of peaks measured using solvent blanks run on the same day. The double bond equivalence (DBE) was calculated using Eq. (1):

$$DBE = 1 + \frac{1}{2}(2C - H + N) \quad (1)$$

Where C, H, and N represent the number of carbon, hydrogen, and nitrogen atoms in the molecular formula. The data were converted to neutral mass (subtracting the mass of Na^+ or H^+ as needed). For this detailed characterization, a subset of the four cooking oils were selected based on the availability of the same products in Williamsburg (lard, peanut, soybean, and canola oil).

Respiratory Deposition

We compared the PM mass deposited in different regions of the respiratory system associated with an arbitrary 30 minutes of heating time for each type of oil. We used the deposition model developed by the used International Commission on Radiological Protection (ICRP)[122]. The model uses empirical equations to estimate deposition in three main regions of the human respiratory system- head airways (HA), tracheobronchial (TB) and alveolar (AL) using aerosol number size distribution data. The model input parameters were set to a particle density of 1 g cm^{-3} and a volumetric inhalation rate of 7.8 l min^{-1}, that corresponds to the breathing rate for adults engaged in sitting activity.[123]

Results And Discussion

Aerosol size distributions from heating different cooking oils

In this section we present particle size distributions in terms of number and mass concentrations for different cooking oils heated at the common 180 °C deep-frying temperature. The distributions varied greatly between different oils with clear differences in modes and peak number concentrations observed distinctly for each oil as shown in Figure 9. A table showing the mode, total particle number and mass concentrations for each oil is also presented in Table B1 of the SI file.

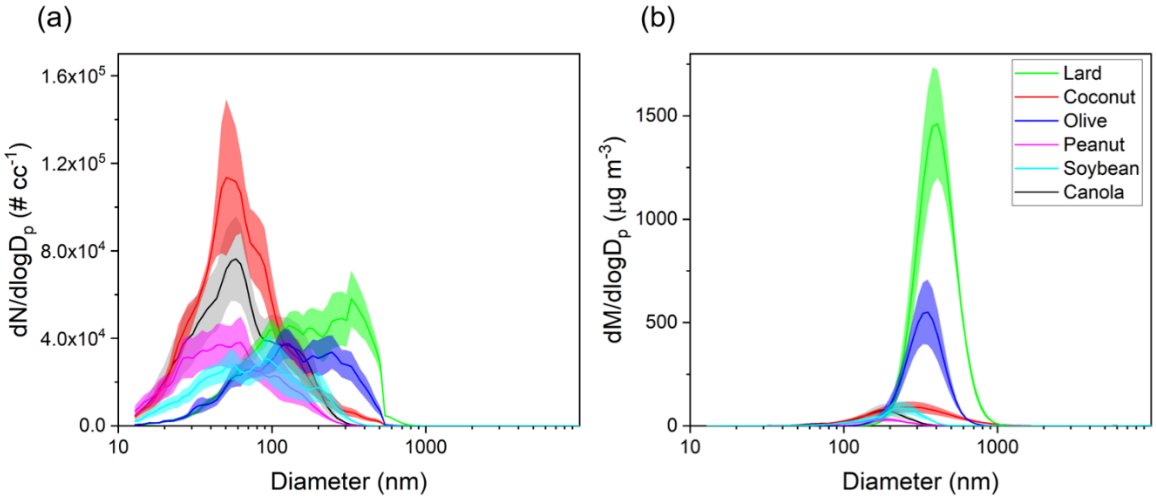

Figure 9. Aerosol size distributions in terms of number and mass concentrations for different oils heated at 180 °C is shown in panels a and b, respectively. The lines represent average values, and the shaded region represents standard error (n = 4). The particle mass distributions for lard, coconut oil, and olive oil were merged between the SMPS and APS measurements using the TSI DataMerge software.

In terms of the particle number size distributions for different oils, the total number concentration values ranged between 2.5×10^4 - 6.5×10^4 # cm^{-3} with the highest concentration attributed to coconut oil whereas the lowest concentration was measured for soybean oil. The modes for the particle size distributions for coconut, canola, peanut, and soybean oil were calculated to be in the ultrafine range

(50-90 nm) whereas for olive oil and lard the mode of the distribution was in the accumulation mode range. These results agree well with those from Torkmahalleh et al.[109] (with the exception of olive oil) in which the particle number mode diameters in the 130-197 °C cooking temperature range for different plant-based oils ranged between 16-82 nm.

In terms of mass distributions, the particle modes were in the 200-400 nm range for all oils. Particles in the size range of 100 nm - 1 μm constituted most of the total mass concentrations as was observed in previous studies characterizing cooking oil emissions.[6,124] Heating lard (smoke point of 190 °C) resulted in the highest total mass concentration value of 450 μg m^{-3} followed by olive oil (163 μg m^{-3}, smoke point of 210 °C), whereas the lowest value of 14 μg m^{-3} was measured for peanut oil (smoke point of 232 °C). Among plant-based oils, olive oil has been shown to emit higher PM mass at a fixed temperature due to the presence of increased triolein content; triolein has high molecular weight as compared to other triglycerides found in the oils.[103] In general, oils with higher smoke points (>227 °C) had lower values of total mass concentrations when compared to low smoke point (190-210 °C range) cooking oils as shown in Figure B3. However, although soybean and canola oil have the highest smoke points (234 °C and 238 °C), their total particle mass concentrations were over 2× higher than that from peanut oil (227 °C).

Next, we present size distributions for two oils commonly used for deep frying, peanut oil and lard, over different cooking temperatures to observe

differences in their behavior based on smoke points and their source (peanut being plant-based and lard being animal-based), as shown in Figure 10. The corresponding aerosol mass distributions are also shown in Figure B4.

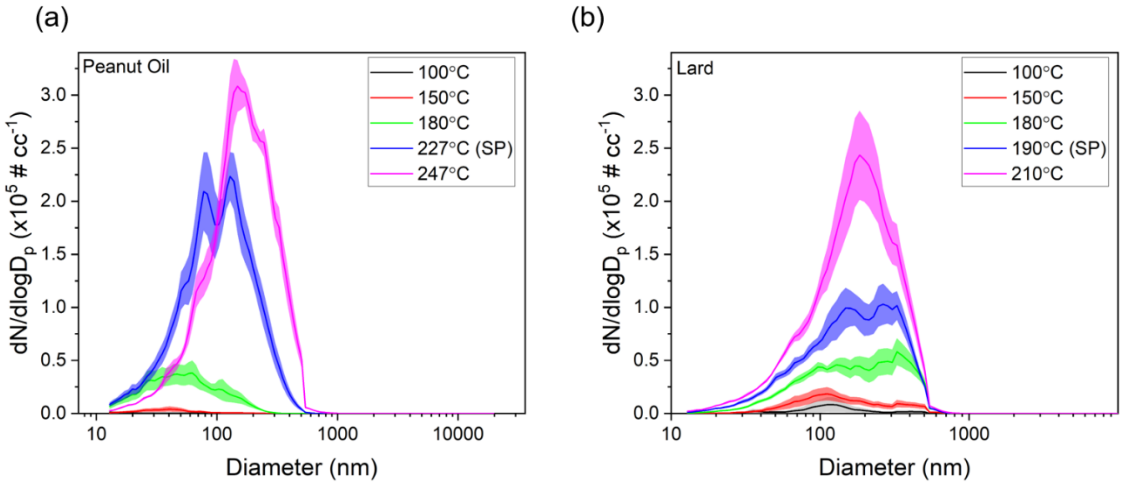

Figure 10. Particle number size distributions for peanut oil and lard over different cooking temperatures are shown in panels a and b respectively. The lines represent average values, and the shaded region represents standard error (n = 4).

For lower cooking temperatures of 100 and 150 °C, the mode of the distributions was in the ultrafine range for both oils. However, as soon as the temperature went above 180 °C, the mode started to shift into the accumulation mode range (100 nm -1 µm) for both oils. If we compare the total number concentrations for 180 °C and SP + 20 °C for both oils, the increase was around 600% and 300% for peanut oil and lard, respectively. This could be due to thermal oxidation of oils resulting in increased SVOC emissions which can be sorbed onto the particle cores emitted by heat plate or by coagulation. These results also agree with previous studies wherein increased cooking temperatures were shown to exhibit bimodal distributions with higher concentrations in the accumulation mode.[96] Overall, these findings present strong evidence for ensuring cooking

temperatures below the smoke point and, if possible, employing the use of a strict temperature control, especially in commercial settings such as restaurants and in situations in which a high efficiency extracting range hood is not available.

Volatility characterization of emissions from heated cooking oils

The GMD of the aerosol volume distributions and the resulting VFR after thermal conditioning over a range of temperatures for different cooking oils (heated at 180 °C) are shown in Figure 11. The GMD profile shows an approximately linear decrease in particle volume followed by a plateauing trend demonstrating that the heated cooking oil aerosols started exhibiting non-volatile distributions at elevated heated section temperatures (except for olive oil, where GMD still shows a linear decrease till 150 ° C thermal conditioning temperature).

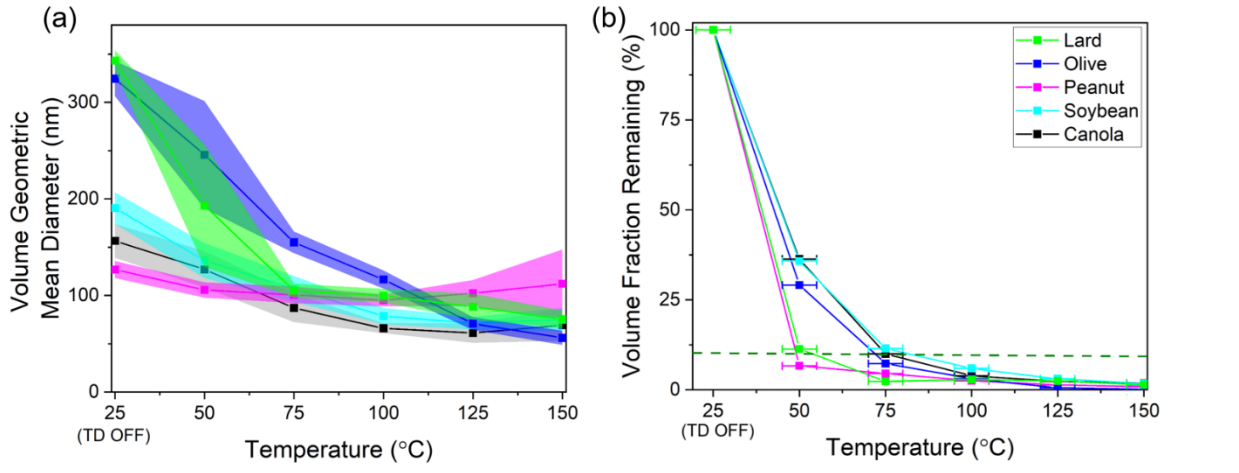

Figure 11. Plot showing the trends in GMD for volume aerosol distributions and VFR for different oils being heated at 180 °C after being thermally conditioned over a wide range of temperatures. The shaded region in panel a, and whiskers in panel b represent the standard deviation. The dotted green line corresponds to the VFR value of 10%. Note also data for coconut oil is missing due to market unavailability of that particular brand for this volatility experiments.

When the heating section of the TD was off (room temperature of ~25 °C), the GMD for different oils ranged between 130 - 350 nm with the lowest GMD

associated with peanut oil and the highest value attributed to lard and olive oil. The bi-modal volume distributions (TD switched off) for most of the oils as shown in Figure B5 also hints towards presence of a mixed state between the volatile and non-volatile particles. However, as soon as the temperature of heated section was raised, the distributions started exhibiting a single mode towards smaller diameters suggesting removal of volatiles with varying rates depending upon the chemical composition of these aerosols.

The sharpest decrease in the GMD values between the temperatures of 25 - 75 °C was also observed for the lard and olive oil, where the diameter reduced by more than 200 nm, almost double than the GMD decrease for the remaining oils. For temperatures beyond 75 °C, the GMD trends for all the oil distributions (except olive oil) start to level off in the 60-100 nm range suggesting that the remaining aerosols comprised mostly of non-volatile core as seen in previous studies on volatility characterization of aerosols of outdoor origin at similar conditioning temepratures.[120,125] The GMD profile for olive oil on the other hand shows a decreasing trend even at higher TD temperatures which could mean that the volatiles hadn't completely evaporated for this oil.

Next, we compared the $T_{0.1}$ temperatures (aerosol heating temperature corresponding to a 10% aerosol VFR value) between different oils by linearly interpolating results between the measured heating temperatures. Peanut oil had the lowest $T_{0.1}$ value of 49 °C, followed by lard at 54 °C, whereas the remaining oils showed higher temperatures in the range of 72-83 °C. In addition, the VFR values

started to overlap among the different oils around the heating temperature range of 75-100 °C. Similar VFR values for this temperature range has been reported on similar studies focusing on SOA volatility measurements.[126,127] Overall, these results suggest that peanut oil and lard generated higher volatility aerosols compared to the remaining oils, which has potential implications for fate and transport indoors and outdoors. Using large quantities of these oils in a poorly ventilated indoor space could accelerate various gas-particle phase transformation processes indoors, and these compounds can also act as a precursor to ambient SOA formation. For further chemical characterization of these aerosols, we will now focus on the high molecular mass compounds that might remain in particle phase via organic films as described in the next section.

FT-ICR analysis

The soft ionization mass spectra for the smoke samples of different oils show that there is a pretty high amount of chemical similarity in terms of intensity values for carbon, hydrogen, and oxygen compounds (Figure 12). The average molecular formula for each sample and the resulting oxygen to carbon (O/C) and hydrogen to carbon ratios (H/C) for each cooking oil sample is also given in Table B2.

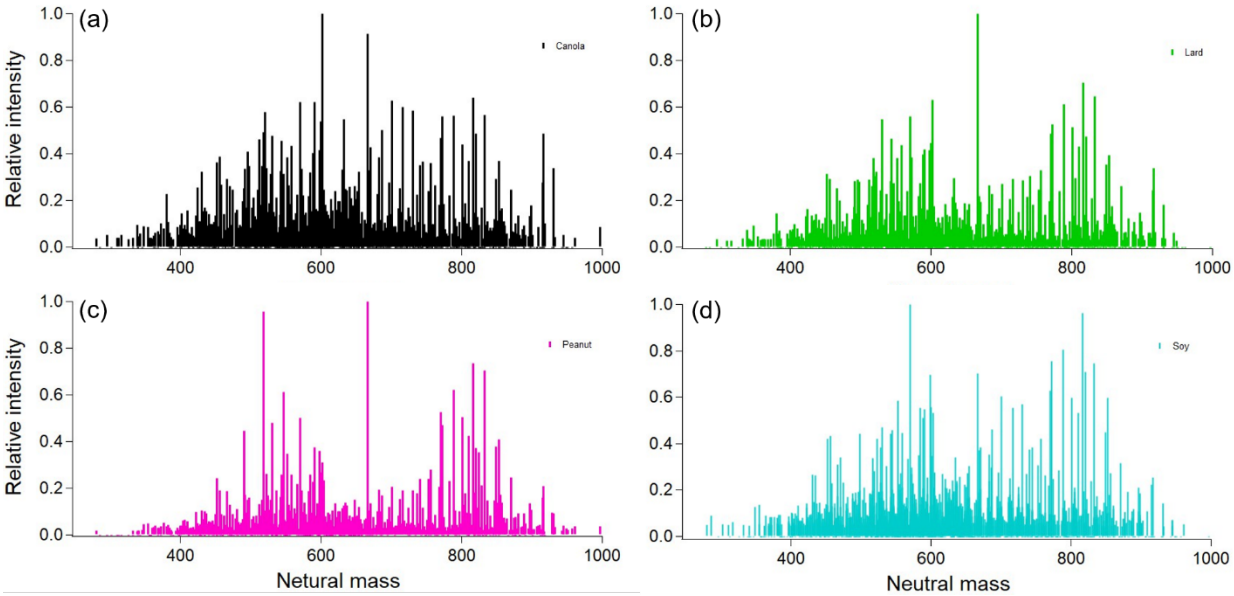

Figure 12. Plot showing the soft ionization mass spectra for the C, H, and O containing ions in the extract obtained during the smoking of different oils. Panels a-d represent canola, lard, peanut, and soybean oil respectively.

Overall, there were 1484 total identified ions and of these, 751 were common for all four samples. The O/C ratios for different oils ranged between 0.15-0.17 consistent with values obtained for cooking organic aerosol in both indoor and ambient environments.[115,128] The canola oil sample was pretty uniform in terms of intensity with two groups centered around 560 and 800 amu (atomic mass units). These values are slightly lower than the expected averages for di- (~600 amu) and tri-glycerides (~900 amu), consistent with thermal degradation of those precursors. Lard was similar to peanut oil, with a little more intensity in a third group around 700 amu. Soy oil seems to have three main groups with a larger signal in the 700 amu range than the others. A summary about the number of similar compounds in the smoke sample extracts from different oils is also given in Table B3.

An interesting point to mention here is that we did find CHON signals in the soft ionization spectra for all the oils (Figure B6). The source for these is unknown,

as there were no proteins or other food items in the heated oils. Possible sources include additives in the raw oil or reactions with gas-phase ammonia or amines. No gas-phase concentrations are available, but William & Mary is located very close to Colonial Williamsburg with commercial sheep farms, and ammonia from ambient air might have ended in the smoke samples. Future work will investigate possible reaction pathways for the formation of CHON compounds, here we focus on the CHO compounds measured in the oil samples. Next, if we compare the DBE values and the resulting Van Krevelen diagram, then the results also show similar trends as shown in Figure 13.

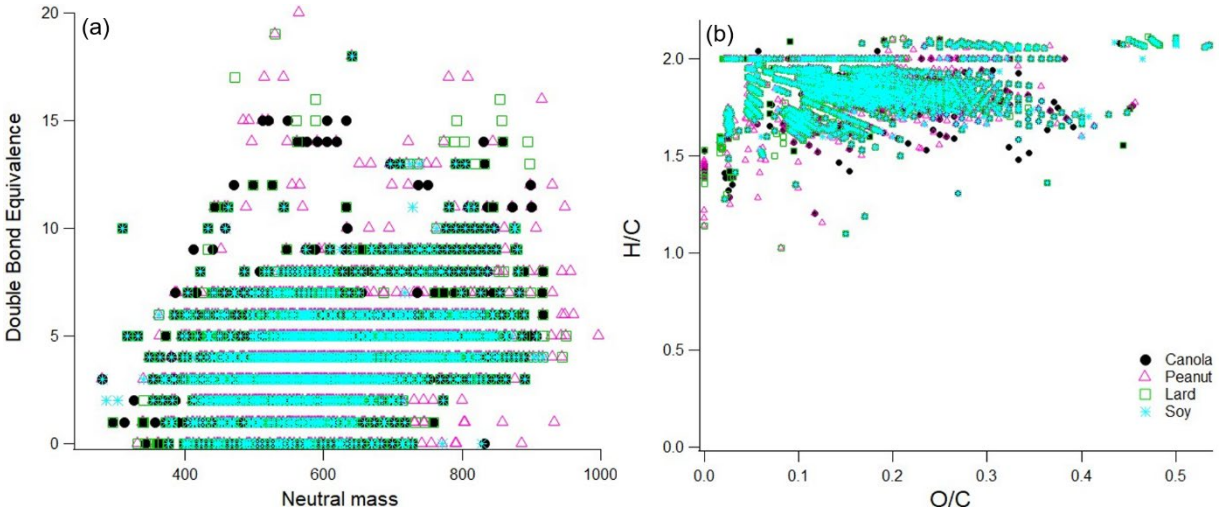

Figure 13. Panel a and Panel b represent the DBE values and the resulting H/C and O/C ratios for the smoke sample extracts of different cooking oils respectively.

The DBE values for all the oil samples show a great degree of overlap mainly due to the chemical similarity in the smoke samples due to the breakdown of diglycerides and triglycerides at smoke points. The higher DBE values does however suggest the presence of aromatics, esters, and aldehyde precursors such as oleic acid and linoleic acid.[102,115] For peanut oil, there appears to be some proportion

of compounds in the higher mass (800-1000 amu range) containing double bond equivalents suggesting a higher degree of unsaturation as compared to the rest of the oils. Therefore, these compounds may participate in further chemical breakdown reactions affecting indoor chemistry processes on an even larger time scale.

Overall, this analysis provides insights into the chemical properties of the lower volatility chemicals that are collected in aerosol particles formed from oils at or just above their smoke point. These results also provide a good qualitative comparative analysis into the lower volatility portion of the mixture which is the fraction that would be expected to remain in the particles during dilution, or remain on surfaces after particles deposit. However, we would also like to acknowledge that cooking emissions usually contain low molecular mass decomposition compounds. Some of these will be lost due to volatilization during collection, some to volatilization during the sample preparation (concentrating). Others may have lower intensity due to lower ionization efficiencies and the tuning in the FT-ICR.[107,129]

Respiratory deposition analysis

In this section we present results from the ICRP model to compare aerosol mass deposited in different regions of the respiratory system upon exposure to different cooking oils heated at 180 °C for a total duration of 30 minutes (Figure 14). Since these results were calculated using a fixed-point sampling method, the deposition values are meant for a qualitative comparison between different oils. In

general, exposure to aerosol emissions from heating lard was associated with the largest PM mass deposited in the respiratory system while those from peanut oil led to the lowest PM mass deposited.

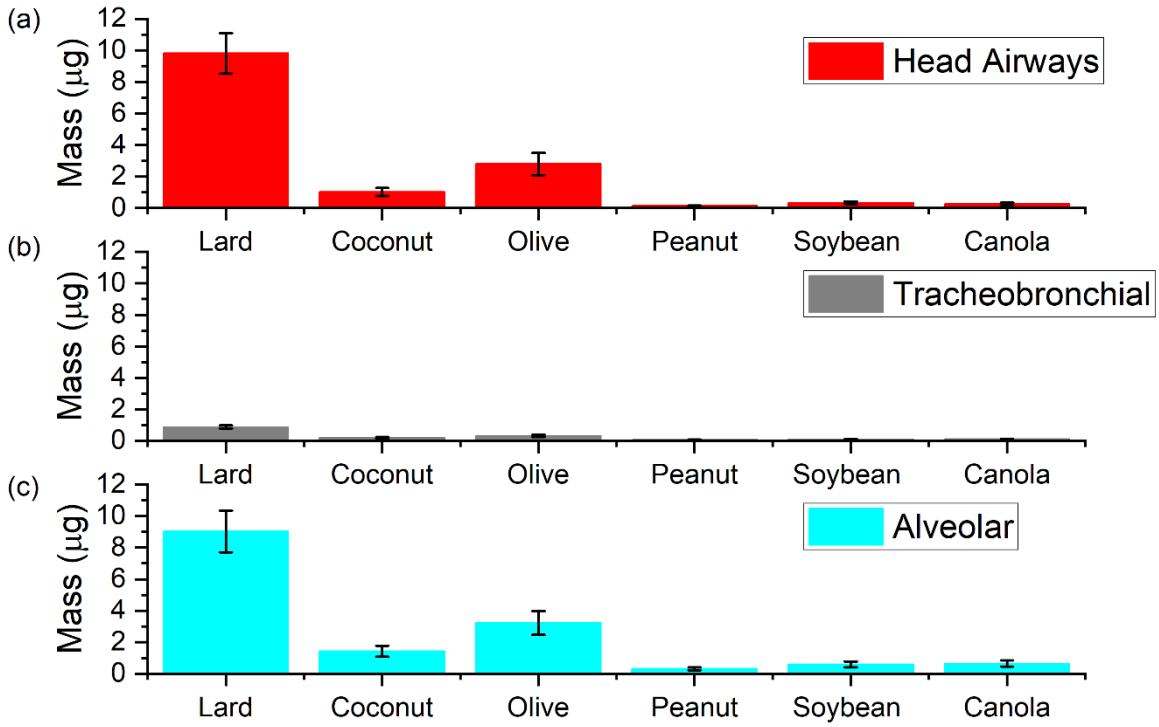

Figure 14. Average aerosol mass deposited in the head airways, tracheobronchial, and alveolar regions of the respiratory system for different oils heated at 180 °C for 30 minutes in panels a-c respectively. The whiskers represent the standard error for n = 6.

At the 180 °C cooking temperature, the deposition results emphasize the importance of heating cooking oils below their smoke points. The smoke point for lard being closest to the cooking temperature resulted in deposition values up to one order of magnitude higher than the other oils. The corresponding average values of mass deposited in the head airways (HA), tracheobronchial (TB), and alveolar (AL) region were calculated to be 9.8, 0.9 and 9.0 µg, respectively for lard. For canola, soybean, and peanut oil, the three most commonly used oils other than lard for deep

frying, total average mass deposited in these three regions was less than 1 μg respectively. Coconut and olive oil both reported higher values for mass deposited when compared to other plant-based oils; with average values corresponding to HA, TB, and AL regions for olive oil (2.8, 0.3 and 3.2 μg) being almost double than that of coconut oil. It is also important to mention here is that between the deposition values corresponding to AL and TB regions in all the oils, the values for AL were an order of magnitude higher. Therefore, emissions from these oils at 180 °C have the potential to reach the deepest parts of the respiratory system in larger numbers which reiterates the need for effective control measures especially when using large quantities of such oils.

Next, we compared the deposition values for two different source-based oils (lard and Peanut oil) over a wide range of cooking temperatures to observe the overall trends in these values with increasing cooking temperatures (Figure 15).

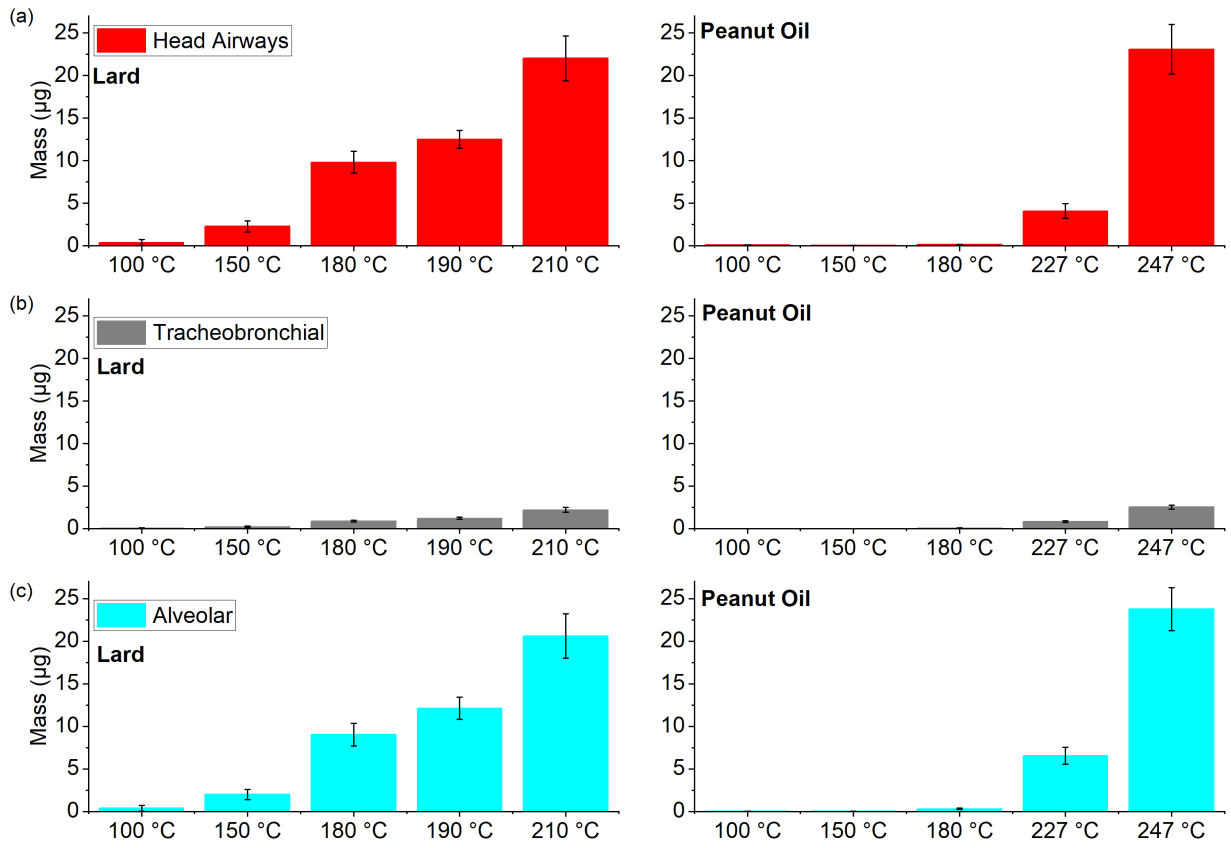

Figure 15. Average aerosol mass deposited in the head airways, tracheobronchial, and alveolar regions of the respiratory system for lard and peanut oil over a range of cooking temperatures in panels a-c, respectively. The whiskers represent the standard error for n = 6.

Peanut oil (smoke point of 227 °C) was associated with very low deposition values in the three regions (average <1 µg) until the smoke point was surpassed. On the other hand, the deposition values for lard even in the 150-180 °C temperature range were comparable to the corresponding peanut oil values at smoke point. However, for cooking temperatures at or above smoke points, the average deposition values in all the three regions were in the range of 0.8-23 µg for both the oils despite a 30 °C difference in their respective smoke points. As mentioned in the previous section, the soft mass spectra from smoking different cooking oils were found to be

quite similar and the deposition values also suggest that once the cooking temperature approaches the smoke point for a given oil, the physical and chemical characteristics of these emissions start to exhibit a degree of similarity to a certain extent. Therefore, future research efforts should focus on isolating chemical compounds on a molecular scale to help understand the indoor chemistry related process that may transform these organic compounds into pollutants of both outdoor and indoor concern.

3.5. Conclusions

In this study, we characterized aerosols emissions from the use of different cooking oils with distinct smoke points over a range of cooking temperatures. First, we observed the differences in the aerosol size distributions for different cooking oils when heated at the usual frying temperature of 180 °C. The mode of the number distributions for lard and olive oil (lower smoke points) was observed to be in the 100-300 nm range, whereas for the rest of the oils the mode was in the ultrafine range. Similarly, the total mass concentrations associated with these two oils were much higher (>100 μg m^{-3}) than the other oils. We also compared the size distributions for two different source-based oils (lard and peanut oil) and found that in both the cases, the total number concentrations increased by more than threefold between the cooking temperature of 180 °C and SP+20 °C, thereby suggesting the need for temperature control while using such oils in larger quantities for reducing the associated exposure with their use.

The geometric mean diameter of the volume distributions associated with heating cooking oils at 180 °C ranged between 130-350 nm when the heating section was switched off and these values dropped down by ~30% as the temperature of the heated section was ramped up to 100 °C (indicative of removal of volatiles from non-volatile cores). In terms of VFR, lard and peanut oil had the lowest $T_{0.1}$ temperature around 50 °C whereas the rest of the oils had $T_{0.1}$ values in the 75-80 °C range suggesting increased number of volatiles in the aerosols generated from using these two oils as compared to the rest. The soft ionization spectra from smoke samples of different cooking oils showed a high degree of chemical similarity between the samples due to similar breakdown products from the diglycerides and triglycerides. The smoke samples also showed an abundance of carbon double-bond equivalents and low O/C ratios for lower volatile carbon, hydrogen, and oxygen containing compounds further implying the potential of these compounds to form organic pollutants of outdoor concern through oxidation of the carbon-carbon double bonds.

The deposition values calculated using the ICRP model for different parts of the respiratory system when a given cooking oil was used for 30 minutes and showed that heating an oil close to its smoke point (lard) led to much higher PM deposition than other oils. Similar comparison between peanut oil and lard over different cooking temperatures showed that the latter with lower smoke points had higher total deposition values for cooking temperatures in the range of 100-180 °C but as soon as the cooking temperature exceeds the smoke point, the total deposition values were calculated to be in the same range. Therefore, care should be

taken in controlling cooking temperatures and avoiding using cooking oils at or above their smoke points to reduce the associated exposure and related health risks.

3.6. Acknowledgements

We acknowledge the contributions of Cole Nielsen, Kwasi Kyeremeh-Dapaah, and Paul Yanowich for building the thermal denuder and providing all schematics of the working model. This work was supported in part by the Alfred P. Sloan Foundation (G-2017-9944, G-2020-13953) and a CU Boulder Dean's Innovation Research Assistantship.

CHAPTER IV

FILTRATION PERFORMANCE OF LAYERING MASKS AND FACE COVERINGS AND THE REUSABILITY OF COTTON CLOTH MASKS AFTER REPEATED WASHING AND DRYING

Contributing authors: Sumit Sankhyan, Karen N. Heinselman, Peter N. Ciesielski, Teresa Barnes, Michael E. Himmel, Hannah Teed, Sameer Patel, Marina E. Vance

4.1. Abstract

In this study, filtration efficiency of different respirators, face masks, and a 2-ply cotton handkerchief bandana was compared for particles in the size range of 60 nm–4 μm under a "perfect fit" condition. The filtration efficiency at the most penetrating particle size of 0.3 μm on average ranged from 83–99% for N95 and KN95 respirators, 42–88% for surgical masks, 16–23% for cloth masks, and 9% for bandana. We also investigated the effects of using double surgical masks or layering a cloth mask over various surgical masks in terms of their filtration characteristics. In most of these combinations, the filtration efficiency improved by ~25% for particles 0.3–1 μm in diameter without any substantial change in the filter quality factor when compared to the highest of the individual mask results. To investigate the reusability of cotton cloth masks, 2-layer cotton fabric sample coupons were machine washed and dried for 52 cycles leading to an increase in inhalation resistance (~20 Pa) without affecting size-resolved filtration efficiency. Scanning electron microscopy revealed that washing and drying led to the gradual deconstruction of cotton fibers at the scale of several micrometers to hundreds of nanometers in the form of delamination of the fiber wall and fibrillation of the

nanofiber constituents. Results indicate that cloth masks may be layered over surgical masks for additional benefits, and that cloth masks made out of cotton fabric can be washed and reused numerous times without a significant loss in filtration efficiency.

4.2. Introduction

The coronavirus disease (COVID-19) worldwide pandemic, caused by the severe acute respiratory syndrome coronavirus 2 (SARS-CoV-2), led to a widespread healthcare supply and personal protective equipment (PPE) shortage, especially in terms of N95 respirators and surgical masks, for healthcare workers and the broad community [130]. This severe shortage led essential workers to reuse disposable PPE and for the public to turn to new suppliers and products, such as bandana and cloth masks, surgical masks, and KN95 respirators for everyday use.

Face coverings are now required or encouraged in many locations around the world [131,132]. This stems from the important role that airborne transmission plays in the spread of COVID-19, as shown by empirical evidence in recent studies describing "super spreader events". A chorale rehearsal in which 53 of 61 members contracted COVID-19 demonstrated that the air was the most likely route of transmission [133]. The investigation of an outbreak in a large German meat processing complex showed that transmission likely occurred via airborne route, over long distances (~8 m) in a poorly ventilated space [134]. Additionally, the ventilation system was shown to play a key role in an outbreak in a restaurant in China [135].

There are several important aspects associated with the use of face coverings in the context of reducing respiratory disease transmission, namely: (1) inward filtration efficiency, providing protection to the wearer, (2) outward filtration efficiency, preventing the exhaled virus spread from the wearer, (3) inhalation resistance, or pressure drop across the material, and (4) how well the mask or face covering fits the wearer, preventing air shortcuts along the sides of the material.

Recent studies have demonstrated that the use of face masks reduces respiratory aerosol/droplet emissions and respiratory virus shedding [136–138]. Face masks, if worn consistently and correctly can also reduce the risk of respiratory virus transmission by acting as personal protection devices that filter out infectious respiratory droplets containing the virus [139,140]. However, the filtration performance of face masks depends on a variety of factors including number of filter material layers and their overall filtration efficiency, conditions in which they are being worn, and the fit or air seal that can be achieved on the wearer's face [141].

Face masks and respirators can also be useful for reducing $PM_{2.5}$ exposure in regions affected by wildfires. Face masks with higher filtration efficiencies in the fine and ultrafine size ranges would be preferred in this scenario. Also since the aerosol transmission of SARS-CoV-2 virus is likely to take place via respiratory droplets in the 1-4 μm size range, it is important to study the filtration performance of different face coverings over a large size range for their usage in the context of protection against fine PM exposure in addition to reducing COVID transmission [142–144].

Disposable surgical masks are more effective in reducing fine particulate matter ($PM_{2.5}$) exposure than cloth masks [145]. Previous studies demonstrated that face masks made out of layered fabrics are 35-45% efficient in removing submicron PM and in some cases, material combinations had higher filtration efficiencies than N95 respirators and surgical masks, albeit the substantially lower breathability of such combinations makes them an unsuitable option [146]. A similar study tested the penetrations levels of cloth masks and other filters against 20-1000 nm sized polydisperse Sodium Chloride (NaCl) aerosols and reported filtration efficiencies in the 40-90% range [147].

Although cloth masks may only provide marginal protection against submicron PM exposure, they are a reusable and potentially more sustainable approach than disposable masks and have been used widely by the public during the COVID-19 pandemic. The filtration efficiency of cloth masks can be optimized by layering different filter materials while maintaining similar breathability levels as commercially available masks. A study tested four cloth masks made using different combinations of Cotton, Lycra, and PTFE membrane layers and reported filtration efficiency for particles in the 0.1-1 μm size range in the 23-88% range [148]. Cloth masks made out of polyester, nylon, polypropylene or silk fabrics can even be triboelectrically charged to enhance their filtration efficiency [149]. Moreover, layering multiple masks, i.e., double-masking, has become popular in the later months of the COVID-19 pandemic and is suggested to improve fit and filtration efficiency,

although quantitative assessments of filtration efficiency and breathability lack in the current literature [150].

The sustainability, reusability, and end-of-life of face coverings are important aspects of increased mask usage during the COVID pandemic. The increase in demand for disposable surgical masks (containing polymer nanofibers as filters) contributes to the already existing issue of microplastic pollution in terrestrial and aquatic environments [13]. Cloth masks made out of cotton on the other hand can be reused by washing, are cheaper to make, can be produced locally in the absence of manufacturing facilities, and are biodegradable in the natural environment[151,152]. Regular washing of cloth masks also serves an important role in reducing the risk of infection due to increased moisture retention in case of their prolonged and repeated use [136,153].

In this work, we compare the filtration performance of different classes of respirators, face masks, and a 2-ply cotton handkerchief bandana in terms of PM-number based concentrations, PM-mass based filtration efficiency at the 300 nm particle diameter, and the resulting filter quality factor (QF). We also quantify the benefits of using double surgical masks or a combination of surgical mask and cloth mask compared to the filtration performance of a single mask. In order to investigate the potential for long-term reusability of cloth masks made out of cotton fabric, we characterize the effects of washing and drying these masks regularly on their filtration characteristics.

4.3. Methods

Materials Tested

In this study we investigated N95 and KN95 respirators, surgical mask samples from 4 different manufacturers, 3 different types of commercially available cloth masks (one made entirely of cotton, and two that included a top layer made of polyester), a 2-ply cotton handkerchief bandana, as well as separate 2-layer cotton coupons prepared specifically to investigate wash/dry cycles (Figure C1). We also investigated the use of double masks as a measure to achieve better filtration characteristics as compared to wearing a single mask. Surgical mask samples from three different manufacturers were mounted on the testing apparatus in duplicates. Additionally, identical cloth mask was also layered over these three different surgical mask brands to evaluate the improvement in filtration efficiency from this combination strategy. All samples were pre-conditioned in a chamber at 85±5% relative humidity and 38±2.5 °C for 25±1 hours before testing, according to the testing conditions and requirements of the NIOSH N95 filtration efficiency procedure [154]. After conditioning, samples were either tested immediately or sealed in an air-tight container and tested within 10 hours.

Wash/Dry Sample Coupons

The wash/dry sample coupons were made of 2 layers of Kona cotton broadcloth, a 120-thread count, 100% cotton fabric commonly used for quilting. The reported fabric weight is 147.5 g m^{-2}. The fabric underwent one hot wash and hot dry cycle before cutting, to pre-shrink the cotton. The fabric was then cut into 20 × 20 cm squares, and 2 squares (1 light and 1 dark side) were placed right sides

together and sewn around the edges with a ¼" seam, leaving a 5 cm gap to flip the raw edge to the inside. Before flipping the coupon right side out, the corners were clipped to reduce bulk. The coupon was then flipped right side out, pressed into shape, and finally top-stitched to seal up the hole left for flipping the raw edge in and reinforce the seams (Figure C2).

Wash/Dry Procedure

Washing and drying was performed using a washer and dryer system (High-Efficiency Duet Steam, Whirlpool Corp., Benton Harbor, MI). For the wash cycle, the normal/casual setting was used, with the temperature adjusted to the hot wash/cold rinse option, to maximum temperature of around ~ 50 °C. The laundry detergent used was a non-enzymatic (non-cellulase) detergent that contains biodegradable anionic and nonionic surfactants (Xtra Lasting ScentSations, Church & Dwight Co., Inc.). For the dryer cycle, the heavy-duty setting was used, which automatically set the dry cycle temperature to Hot.

Experimental Design

Two experimental setups (Setup 1 and Setup 2) were used to investigate the filtration performance of the different masks and respirators over a wide range of particle sizes.

Setup 1

Setup 1 was used to characterize filtration efficiencies for particles in the size range of 60 nm - 450 nm. Tests were performed in a 37.8 m^3 test room (Figure C3) and the testing conditions were adapted from the NIOSH N95 filtration efficiency

procedure [154]. A fan was kept inside the room to ensure well-mixed conditions. The testing chamber was maintained at ~22 °C and ~37% relative humidity. All instruments, the aerosol generation system and accessories, and pumps were kept outside the room. Copper (ID: 3 mm) sample lines of equal length and diameter, but one with and one without a mask, ran in parallel to ensure that particle losses were equal in both the lines. A solution of 10% by weight of ammonium sulfate [$(NH_4)_2SO_4$] in deionized water was prepared and placed in a Collison-type atomizer, operated at ~32 psi to generate an aerosol with a median diameter of 75±20 nm. We used ammonium sulphate instead of sodium chloride, which is recommended by NIOSH (NIOSH, 2019a), to avoid the risk of corrosion in stainless steel parts of the test setup. The aerosol stream passed through a diffusion dryer to remove water and an X-ray neutralizer to neutralize electrical surface charge before being injected into the testing chamber. Measurements in this setup were performed by a Scanning Mobility Particle Sizer (SMPS 3080, TSI Inc., MN, USA) outfitted with a water-based Condensation Particle Counter (CPC 3788, TSI Inc., MN, USA) and an Aerosol Particle Sizer Spectrometer (APS 3321, TSI Inc., MN, USA). The measurements from SMPS and APS were both exported at a resolution of 32 channels/decade for better agreement.

For each test run, which lasted 60 minutes, the atomizer operated for the first 15 minutes followed by 45 minutes of filtration efficiency test leading to ~0.1 mg particle loading on mask. During this period, particle concentrations in the test room and downstream of the sampling material were measured multiple times by

switching between the blank line and the mask line with the help of a 3-way valve to generate a filtration efficiency over time with four replicates.

Setup 2

Setup 2 (Figure C4) was used to characterize the filtration efficiencies of larger particles, in the 542 nm – 4 µm particle size range, using the same APS instrument as in Setup 1. In this setup, a 1.7 m^3 acrylic chamber containing a small fan to aid in aerosol mixing was used. This chamber was kept at ~22 °C and ~30-40% relative humidity. A mixture of 5% by weight of $(NH_4)_2SO_4$ and 3-µm and 7-µm polystyrene latex spheres (PSL, Sigma-Aldrich, MO, USA) in deionized water was used to generate particles using a medical-grade nebulizer (Sigma-Aldrich, MO, USA). The aerosol stream passed through a diffusion dryer to remove water before entering the testing chamber. Since previous studies have reported similar filtration efficiencies with and without using a neutralizer, we did not use an X-ray neutralizer in this setup to avoid sampling losses for larger particles [143,155]. Example particle concentrations inside the chambers during the testing duration for both Setup 1 and Setup 2 are shown in Figure C5 and Figure C6, respectively.

For both testing setups, respirators were mounted on a mannequin head, a Leland Legacy pump (SKC Ltd., DT, UK) was used to maintain a sampling rate of 15 L min^{-1} in both mask and blank line. This flow rate is comparable to human breathing rate at a light intensity activity level for most of the age groups [156]. Assuming the surface area of a standard N95 respirator to be 175 cm^2 [157], the corresponding face velocity through the respirator was calculated to be 1.4 cm s^{-1}.

The face velocity used in our study lies in the range of 0.5-25 cm s^{-1} based on the filtration efficiency test standards used by the American Society for Testing and Materials and the U.S. Food and Drug Administration.[146,158,159] All the face masks, bandana, and washing study coupon samples were mounted on a 4-inch (~10 cm) diameter stainless steel funnel instead of mannequin head to achieve an air tight seal. For funnel-mounted samples, a sampling flow rate of 6.7 L min^{-1} was maintained to achieve the same flow velocity of 1.4 cm s^{-1} through the filter cross-section.

For both testing setups, the filtration efficiency corresponding to a given particle size Dp was calculated using Eq. (2):

$$FE(D_p) = \frac{C_{blank} - C_{mask}}{C_{mask}} \quad (2)$$

where C_{blank} is the average concentration of the blank line measured before and after the mask line concentration (C_{mask}). This method of estimation accounts for temporal variations in chamber concentrations and has been used by several studies in the past [143,160,161].

For double mask combinations, we compared the experimental results with the results from a simple model based on the classical filtration theory for filters to check whether these mask combinations can be treated as series of filters connected in series. The filtration efficiency of a given mask combination was calculated using the Eq. (3) [123]:

$$T_c = T_{m_1} \times T_{m_2} \quad (3)$$

where T_c is the particle transmission through a given double mask combination, T_{m_1} and T_{m_2} are particle transmission through mask 1 and mask 2 respectively.

Particle transmission T is further related to the filtration efficiency (FE) by the following equation:

$$T = 1 - \frac{FE(\%)}{100} \quad (4)$$

Inhalation Resistance

The test for the determination of inhalation resistance was performed according to NIOSH procedure TEB-APR-STP-0007-508 [162], which lists a 35 mm water-column height limit for N95 respirators. Each sample was affixed to a funnel (4.5 cm diameter) in the case of masks and flat filter samples, or taped to a mannequin head in the case respirators. A flow rate corresponding to an 8 cm s-1 face velocity (corresponding to 85 LPM flow rate through an N95 respirator) was pulled through the material and the pressure drop was measured using a digital manometer (Datum 2239-1, Setra Systems Inc., Boxborough, MA).

Filter Quality Factor

The filter quality factor (QF) which relates the pressure drop of the material with the PM mass-based filtration efficiency was calculated using Eq. (4) [123,163]:

$$QF(D_p) = -\frac{(ln(1-FE(D_p)))}{\Delta P} \quad (4)$$

Where QF (D_p) is the filtration efficiency at particle size D_p and ΔP is the pressure drop across the material. The value of QF (0.3 μm) has been used in previous studies to compare filtration performance among different filters so we will use the same values in our study for comparison. High values of QF for a given filter imply that the filter can give better filtration performance with greater breathability.

Scanning Electron Microscopy Analyses

In order to characterize morphological changes on the cotton fabric due to repeated washing and drying, we visualized those samples through scanning electron microscopy (SEM) using a FEI Quanta 400 FEG instrument (FEI, Hillsboro, OR). Single layer fabric samples of ~0.5 cm^2 were cut from larger fabric samples after 0, 24, and 52 wash/dry cycles. The specimens were mounted on aluminum stubs with double-sided conductive carbon tape and sputter-coated with 12 nm of iridium. Imaging was performed with beam accelerating voltage of 5 keV at magnifications below 1000×, accelerating voltage of 10 keV was used at higher magnifications.

4.4. Results And Discussion

Size-resolved Filtration Efficiencies

The results for the size-resolved filtration efficiency of different samples are shown in Figure 16. N95 and KN95 respirators presented highest filtration efficiencies (>95%) throughout the size range investigated (60 nm to 4 μm), as expected. The filtration efficiency curve for rest of the masks and bandana samples

exhibited the traditional "u" shape with minima in the accumulation mode size range (0.1-1 μm), except for surgical mask A, which presented high filtration efficiencies (>85%) through the entire size range. For most double mask combinations, the average filtration efficiency increased by ~25% for particles in the accumulation mode size range for a given mask combination when compared to the highest of the individual mask results. The results for overall filtration efficiency in terms of total $PM_{2.5}$ number and mass, and in terms of PM mass at 300 nm for all the samples collected using Setup 1 are presented in supplemental Table C1.

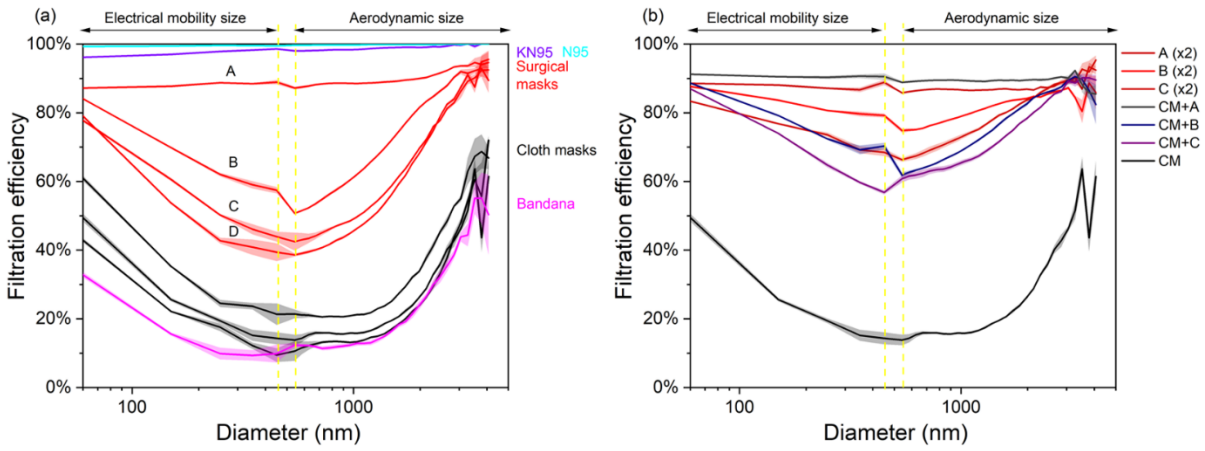

Figure 16. Panel (a) Size-resolved filtration efficiency measured using particle number-based concentrations for different respirators, masks, and bandana. Panel (b) Size-resolved filtration efficiency for different mask combinations, where A, B, and C are the same surgical masks as shown in panel (a) and CM is a cloth mask used for layering. The shaded region represents standard errors (n = 4).

While the filtration efficiency curve for the N95 respirators remained constant at ~99% for the entire size range, the KN95 respirators presented slightly lower filtration efficiencies (from 96% to 98%) for particles 60-400 nm, and remained constant at 98% for larger particles. Filtration efficiency results for N95 and KN95 respirators were used to verify the testing setup adapted for this study,

and they also agree well with results from similar studies based on NIOSH respirator testing [147,148,161,164].

The cloth masks and 2-layer bandana presented similar average filtration efficiencies, between 30-60% for particles smaller than 100 nm size, 10-25% for particles sized between 300 nm and 1µm, and 12-68% for particles sized 1-4 µm. The cloth mask that was made of all-cotton layers had a slightly lower filtration efficiency compared to the other two cloth masks, which both included a polyester top layer. For surgical masks, the average filtration efficiency for mask A ranged between 87-95% showing a slight overall linear increase for particle sizes in the range of 60 nm - 4 µm, whereas the filtration efficiency of samples B-D was 70-85% for particles smaller than 100 nm size, dropped to 40-60% for particles between 300 nm - 1µm, and increased to 45-94% particles in the size range of 1-4 µm. These results agree well with previous studies reporting filtration efficiencies in the 50-80% range for submicron particles for surgical masks, although these studies employed higher test flow rates, commonly used for NIOSH test method of N95 certification [143,164].

The overall higher filtration efficiency measured for surgical mask A could be attributed to the presence of a "submicron filtration layer for dust protection" middle layer (as labeled on the packaging box), whereas no such layer was mentioned on the packaging of the other three samples. Since all 4 mask samples had no discernible features based on visual inspection, surgical mask A could have an electrically-charged filter in the middle which would lead to higher filtration

efficiency in the accumulation mode size range when compared to non-charged filter materials [165].

For double-mask combinations (Figure 16(b)), our results showed that doubling surgical masks led to an overall improvement in the filtration efficiencies of masks B and C whereas no such improvement was seen in the case of mask A, which could imply that mask A is at the upper limit of filtration performance which couldn't be improved further by doubling. Layering a cloth mask (CM) over each of these surgical masks led to higher filtration efficiency curves particularly in the accumulation size range when compared to the individual cloth and surgical masks. These results suggest that the combination of a cloth mask over a surgical mask is likely to be a better alternative than wearing just a single mask.

These experimental results agreed with theoretical calculations for particle transmission through most double-mask combinations based on classical filtration theory. Filtration efficiency curves showing good overall agreement in combinations can be observed in Figure C7. A better overall agreement was observed for cloth + surgical mask combinations (RMSE = 4-6%) compared to the double surgical mask combinations (RMSE = 5-11%). The higher values of RMSE in case of double surgical mask combinations could be attributed to the inference between individual filter layers resulting in lower filtration efficiencies than predicted [155].

It is important to bring these results under perspective because these tests are valid only for a "perfect fit" condition, i.e., assuming that there are no gaps between the mask and the face of the wearer, so it would be essential that the

surgical mask is properly sealed and that the additional cloth mask or surgical mask does not affect that fit in any way. Previous studies have reported that a drop of >50% in filtration efficiency can occur in the presence of minor leaks when compared with a perfect seal condition [155,160].

Filtration Efficiency, Inhalation Resistance and Resulting Filter Quality Factors

Figure 17 shows the PM-mass based filtration efficiency for particles 300 nm in diameter as a function of their inhalation resistance or pressure drop, and the resulting filter QF value.

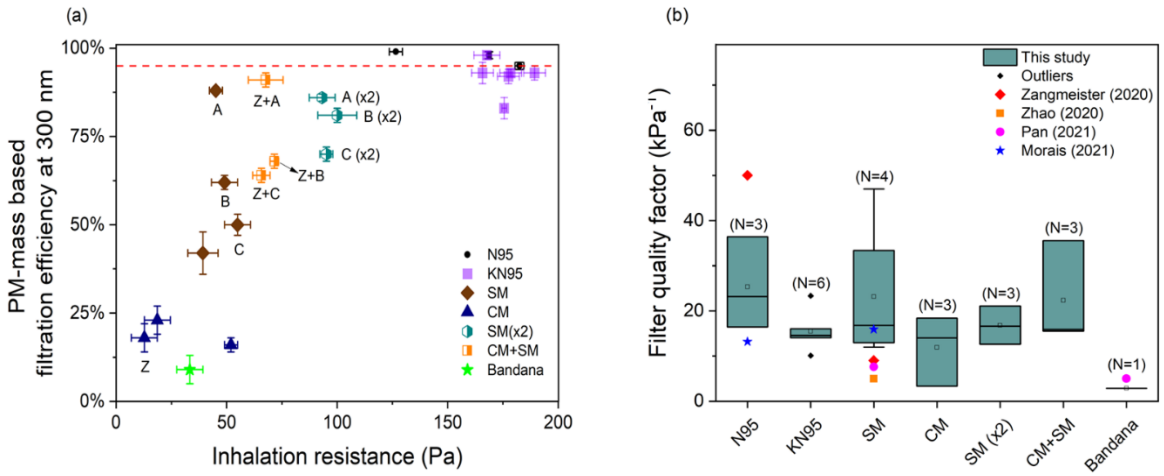

Figure 17. PM-mass based filtration efficiency at 300 nm as a function of the inhalation resistance of different respirators, masks, and bandana is shown in panel (a). The whiskers represent standard deviations (n=4 for filtration efficiency tests and n=3 for pressure drop tests). The cloth mask and the surgical mask samples along with their different combinations have been labeled for ease of viewing. Panel (b) shows the filter quality factors calculated for different sample categories. The squares represent the mean values whereas the median is represented by a horizontal line. The corresponding filter quality factor results from previous studies are also included in panel (b) for comparison.

The inhalation resistance of N95 and KN95 respirators was in the 125 – 200 Pa range, below the NIOSH limit of 343 Pa for N95 respirators [162] and the corresponding average PM based filtration efficiency at 300 nm size was in the 83-

99 % range. The inhalation resistance for surgical masks was much lower, in the 35-55 Pa range and the corresponding PM-mass based filtration efficiency at 300 nm size was calculated to be 88% on average for surgical mask A and 42-62% for the remaining surgical mask samples. As discussed in the previous section, the presence of a "submicron dust filtration layer" in surgical mask A may have led to a higher filtration efficiency without increasing the pressure drop considerably when compared to other surgical masks investigated. The lowest results for filtration efficiency at 300 nm (< 25%) were measured for cloth masks and the bandana and the average pressure drop was measured in the range of 10-50 Pa. In general, a trend can be observed in Figure 17(a), with lower pressure drop values associated with lower filtration efficiencies.

In the case of double surgical masks and the combination of cloth + surgical masks, the inhalation resistance increases were also accompanied by improvements in the filtration behavior relative to individual cloth mask and surgical mask results. There is one exception, in the case of surgical mask A, where doubling didn't improve the filtration efficiency at 300 nm (88% for the single mask versus 86±1% for the double mask) but increased the inhalation resistance, from 45±3 Pa for a single mask to 93±6 Pa for a double mask. As expected, doubling up surgical masks roughly doubled the inhalation resistance. Layered masks, either cloth + surgical or double surgical mask combinations, demonstrated lower inhalation resistance values and lower filtration efficiencies than those for N95 or KN95 respirators.

In terms of the mean QF, N95 respirators (25 kPa^{-1}) performed better than KN95 respirators (15 kPa^{-1}). Among face masks and coverings, surgical masks had the highest mean QF value (23 kPa^{-1}) followed by cloth masks (12 kPa^{-1}) and the bandana (3 kPa^{-1}). The surgical masks investigated in this study exhibited higher QF than KN95 respirators due to their relatively low inhalation resistance (~48 Pa compared to ~180 Pa for KN95 respirators).

In the case of mask combinations, the QF value for doubling surgical mask A (21 kPa^{-1}) and layering it with a cloth mask (36 kPa^{-1}) decreased when compared to wearing surgical mask A on its own (47 kPa^{-1}) but these QF values were still higher than that of the cloth mask (18 kPa^{-1}). A much smaller decrease (~3 kPa^{-1}) was observed for both doubling surgical mask B and for layering it with a cloth mask, compared to the corresponding QF value for the single surgical mask B (20 kPa^{-1}). On the other hand, the QF values for a single and double surgical mask C were similar (~12 kPa^{-1}) and the QF value increased by 4 kPa^{-1} while layering this mask with a cloth mask. These results indicate that doubling or layering can be a better option than single masks, especially when surgical masks with lower filtration efficiencies are available.

Effects of washing and drying on cloth masks

The effect of repeated washing and drying on the filtration behavior and inhalation resistance of cotton fabric is shown in Figure 18. An overall increase in inhalation resistance was observed as the fabric sample underwent 52 hot wash/dry

cycles, but overall filtration efficiency did not change significantly with wash/dry cycles.

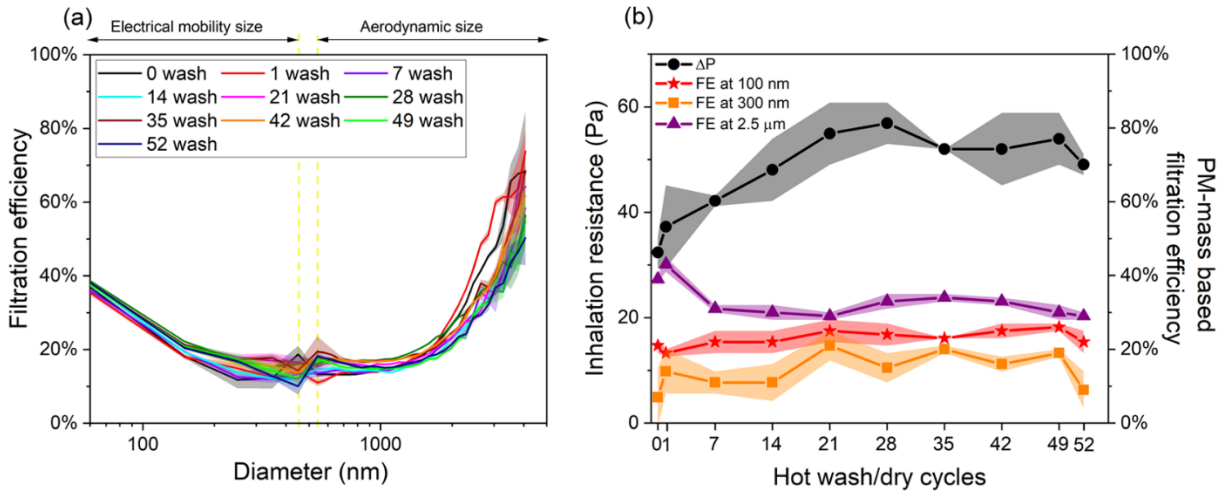

Figure 18. Size-resolved filtration efficiency calculated as a function of particle number distribution is shown in panel (a). The shaded region represents standard error (n=4). Panel (b) shows the inhalation resistance (black, left-hand y-axis) and PM-mass based filtration efficiency at 3 different particle sizes (plotted on the right-hand y-axis) of fabric material as a function of number of hot wash/dry cycles. The shaded region represents standard deviation values.

Except for a ~10% decrease ($p < 0.01$) in filtration efficiency at 2.5 μm from 1 to 7 wash/dry cycle, the PM-mass based filtration efficiency results didn't show any major fluctuations as the number of washing and drying cycles were incrementally increased to 52 cycles (Figure 18(b)). A previous study on the reusability of self-developed cloth masks made up of cotton, Lycra, and polypropylene fabric also reported insignificant changes ($p > 0.05$) in average filtration efficiency between an unwashed sample one that was washed and air-dried 30 times for accumulation mode particles [148].

In terms of the effect of wash/dry cycles on breathability, the inhalation resistance increased on average by ~17 Pa between zero and 52 wash/dry cycles (p =

0.002). The inhalation resistance for the unwashed sample coupon was measured to be 32±2 Pa and increased to a maximum inhalation resistance of 57±5 Pa for the 28-hot wash/dry cycle sample coupon. Afterwards, the curve somewhat plateaus at 53±5 Pa.

The resulting QF calculated for the cotton fabric samples as a function of wash/dry cycles remained below 5 kPa^{-1} and didn't change significantly between the unwashed and the sample that underwent 52 wash/dry cycles (Figure C8). This is likely because the QF value is more sensitive to changes in FE than in ΔP and, although a trend was observed for ΔP throughout the repeated wash/dry cycles, the same did not occur for the FE at 300 nm. Based on these results, we conclude that repeated washing and drying of cloth masks made of cotton fabric did not alter their filtration characteristics in a major way, thus indicating a favorable potential for the reusability of these products.

SEM analyses of wash/dry sample coupons

Scanning electron microscopy (SEM) was used to investigate changes in micro- and nanoscale morphology of the cotton fabric. Representative micrographs of cotton fabric subjected to 0, 28, and 52 washing cycles are presented in Figure 19.

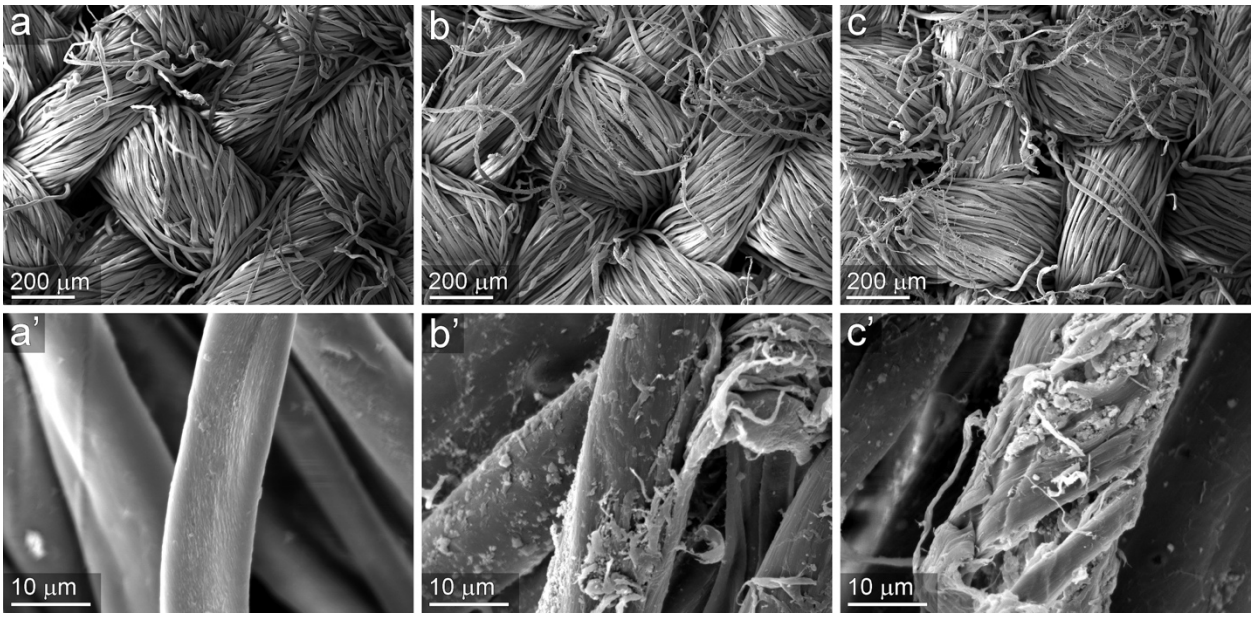

Figure 19. Scanning electron micrographs of cotton fabric subjected to varying numbers of wash/dry cycles: as received (a, a'), 28 cycles (b, b'), and 52 cycles (c, c'). Some cotton fibers displayed evidence of micro- and nanoscale deconstruction after 28 wash cycles. Both the population of deconstructed fibers and the extent of deconstruction increased further after 52 cycles.

The as-received cotton fabric exhibited largely intact bundles of cotton fibers (Figure 19(a)) with relatively smooth surface texture (Figure 19(a')). After 28 wash/dry cycles, the fiber bundles display a larger population of partially liberated fibers. Higher magnification images reveal deconstruction of individual fibers at the scale of hundreds of nanometers to several micrometers in the form of delamination of the fiber wall and fibrillation of the nanofiber constituents (Figure 19(b')). This pattern of deconstruction results from the hierarchical ordering of cellulose composing cotton cell walls and is similar to the morphology observed when fibers from other herbaceous species such as maize and switchgrass are subjected to thermochemical treatments [166,167]. Fabric samples that had experienced 52 wash/dry cycles showed an even greater population of partially liberated fibers

(Figure 19(c)) and more extreme degrees of nanoscale delamination and fibrillation (Figure 19(c')). These modes of deconstruction increase porosity of the macrofibers and liberate nanoscale cellulose bundles which may be subjected to bending stress in a convective flow field and likely contribute to the increased pressure drop observed as wash-dry cycles progress [168,169].

4.5. Conclusions

Recent medical and environmental events across the globe have dramatically increased the demand for use of face coverings as personal filtration devices. This work brings forth results of interest to the science community as well as the general public, such as the reusability of cloth masks after repeated washing and drying and the effects of overlaying multiple masks on their performance. In this study, size-resolved filtration efficiencies in the size range of 60 nm - 4 μm were investigated under perfect seal condition for different face covering options available in the market. The filtration efficiency at the most penetrating particle size of 0.3 μm on average ranged from 83-99% for N95 and KN95 respirators, 42-88% for surgical masks, 16-23% for cloth masks, and 9% for bandana. The study also presents a positive argument for using a surgical mask with an electrically charged middle layer due to its superior filtration performance as compared to other samples, especially in the accumulation mode particle size range. This work has also shown that doubling surgical masks or layering a cloth mask over surgical mask can be a better option than single masks, especially when only surgical masks with lower filtration efficiencies are available. Results from the washing study show

that filtration characteristics of cloth fabric did not change significantly despite the delamination of the fiber wall and fibrillation of the nanofiber constituents observed during SEM analysis. Since cotton masks offer a biodegradable and washable alternative to commonly used disposable surgical masks, the results of this work points towards an a more sustainable path to mask wearing.

4.6. Acknowledgements

Research was supported by the DOE Office of Science through the National Virtual Biotechnology Laboratory, a consortium of DOE national laboratories focused on response to COVID-19, with funding provided by the Coronavirus CARES Act. The authors also thank numerous service clients who agreed to share their samples and corresponding results anonymously.

CHAPTER V

USE OF CELLULOSE NANOBFIBRIL AS COATING MATERIAL FOR IMPROVING FILTRATION EFFICIENCY OF COTTON FABRIC

Contributing authors: Sumit Sankhyan, Peter N. Ciesielski, Karen N. Heinselman, Marina E. Vance

5.1. Abstract

In this study we explored the use of cellulose nanofibril (CNF) coating over cotton fabric as means to improve the filtration efficiency of existing cloth masks. Cotton fabric samples were soaked in different concentrations of CNF suspensions overnight and then a couple of different drying methods (oven drying and freeze drying) were explored to obtain a stable layer of CNF coating on cloth fabric. CNF coatings obtained using oven drying were uniformly depositing over the cloth fabric however cracks were appearing after mounting these samples over funnel for filtration efficiency testing. On the other hand, freeze dried samples had specks of coating distributed over the cloth fabric due to agglomeration however, the filtration efficiency results still show an improvement in filtration efficiency of around 10% for particles in the size ranges of 60 nm-4 μm for cloth fabrics coated with 0.05 and 0.1 wt.% CNF suspension. The corresponding inhalation resistance increase for these samples as compared to the uncoated sample was less than 20 Pa and these values were well below the NIOSH limit of 120 Pa for respirators. These results suggest that freeze dried CNF coatings on cloth fabric can be used to improve the filtration characteristics of existing cloth masks thereby offering a more sustainable way of using masks during the pandemic.

5.2. Introduction

CNF is a biomaterial containing a strong network of entangled nanofibrils with diameter of 5-50 nm and length of few micrometers.[170] In recent years the use of cellulose nanofibrils in various applications such as composites, transparent films and barrier coatings has increased due to their high surface area with low density and high mechanical strength.[171] CNF suspensions when dried form stable films which are resistant to organic solvents and retain majority of their structure even when immersed in water.[170]

New research studies in past few months have raised concerns regarding increased usage of masks made out of plastic material during pandemic leading to littering and other problems related to their improper disposal.[172–174] In terms of life cycle assessment washable cloth masks were seen as a better option as compared to surgical masks in terms of their sustainable use.[172,175] However existing cloth mask options have been shown to have lower filtration efficiency values as compared to surgical masks so there is an urgent need to improve the filtration characteristics of current cloth masks while still ensuring their sustainable use.[143,161]

One of the main objectives of this study was to incorporate the use of CNF coating onto cotton fabric in order to optimize the filtration characteristics of the resulting filter material. We looked into two different methods of drying to obtain CNF films from suspension over cloth fabric- oven drying and freeze drying. The results from this study can be useful for development of biodegradable cloth masks with improved filtration characteristics. Such cloth masks promise a more

sustainable alternative to disposable surgical masks without creating any additional environmental concern with their increased usage.

5.3. Methods

Sample Preparation

First, we prepared 0.01 wt.%, 0.05 wt% and 0.1 wt% CNF suspensions with 10 w/w% citric acid (mass citric acid per mass of CNF) as a crosslinking agent and 10 w/w% of Glycerol as a plasticizer. Sodium hydroxide solution was also used to maintain pH of the final solution in the 6-7 range. The fabric samples were soaked overnight in different CNF suspensions overnight as shown in the figure below.

Figure 20. Fabric samples soaked in CNF suspension before drying.

Oven Drying

For oven drying, the samples were kept inside an industrial oven maintained at 70°C for 6-8 hours until all the water dries out leaving a CNF film on cotton fabric as shown in Figure 21.

Figure 21. Oven dried CNF coated sample fabric.

Freeze Drying

For freeze drying, the samples were freeze dried overnight using a four chamber Millrock Technology manifold freeze dryer. The fabric samples after freeze drying are shown in Figure 22.

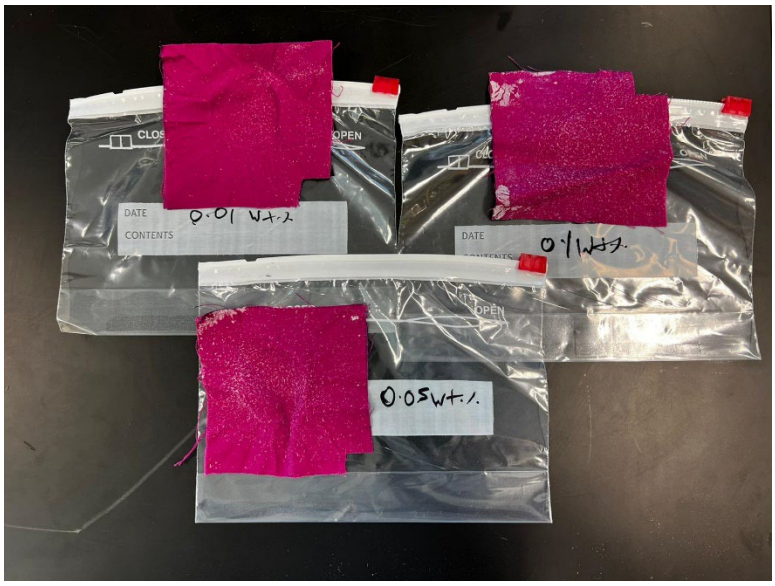

Figure 22. Freeze dried CNF coated sample fabrics.

5.4. Results and Discussion

Filtration characteristics of CNF coated cotton fabric

The oven dried CNF coated samples were tested first for size resolved filtration efficiency and inhalation resistance and the preliminary results looked promising as shown in Figure D1. The filtration efficiency of cotton fabric samples coated with different concentrations of CNF suspension were greater than that of the blank sample. The highest value of the inhalation resistance obtained for cotton fabric sample coated with 0.01 wt% CNF suspension was still lower than the NIOSH limit of 120 Pa. However, the CNF coatings were cracking (in some areas the cracking separated from cloth fabric as shown in Figure 23) as soon as they were mounted on the funnel making them unsuitable for use as such in cloth masks.

Figure 23. CNF coated sample fabric with visible cracks after it was removed from the funnel.

Freeze dried CNF coated samples

The freeze-dried CNF coated samples also showed similar results as oven dries samples but due to agglomeration of CNF coatings into tiny specks, the CNF coating didn't chip off as was the case previously. The corresponding results from the filtration efficiency and inhalation resistance tests are shown in Figure 24.

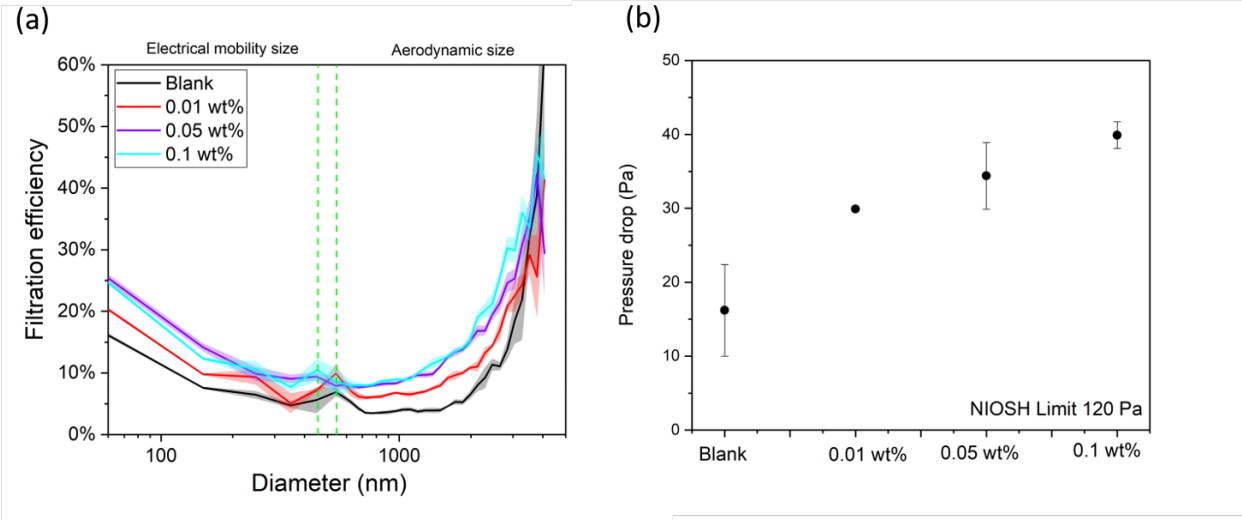

Figure 24. Size-resolved filtration efficiency results for different CNF coated fabric samples are shown in panel (a). The corresponding inhalation resistance trends are shown in panel (b).

When compared to the blank sample, the filtration efficiency of the 0.05 wt% and 0.1 wt.% CNF coated fabric sample had a filtration efficiency increase by 10% throughout the size range being studied. The inhalation resistance results show a linear trend with the concentration of CNF in the suspension used for coating the fabric with maximum value obtained for 0.1 wt.% to be around 40 Pa which was well below the NIOSH limit of 120 Pa. Therefore, CNF coated cloth fabrics can also be used in series which will further increase the filtration efficiency values making them a possible alternative for higher efficiency surgical masks.

SEM analyses of CNF coated cotton fabric

SEM analyses was performed on CNF coated cotton fabric obtained through oven drying and freeze drying to study the morphological differences between the samples as shown in Figure 25.

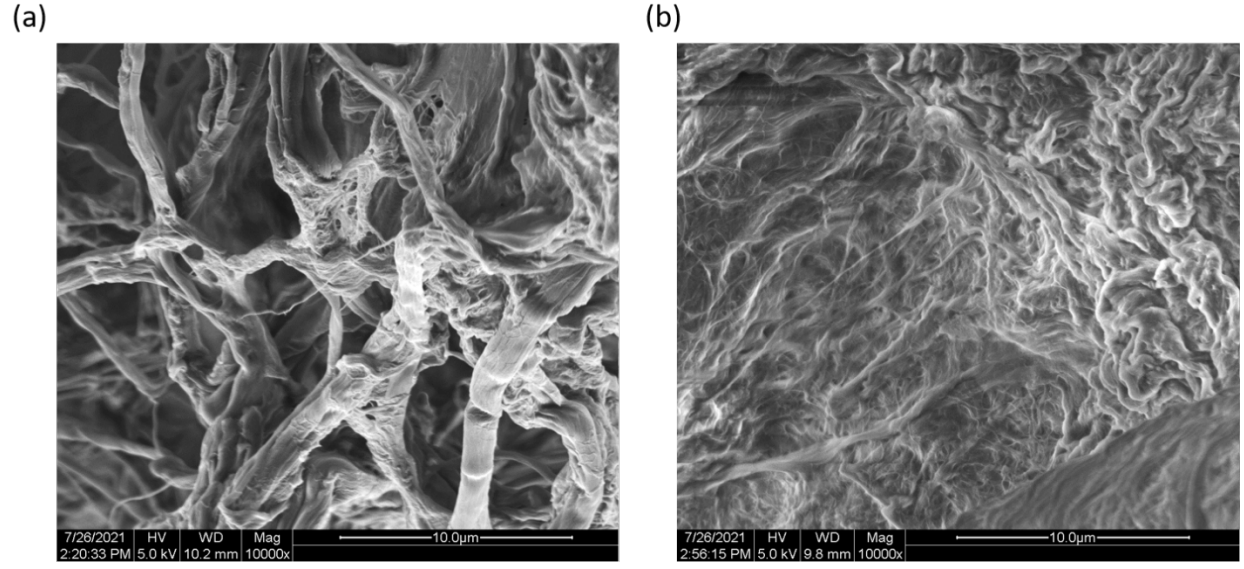

Figure 25. Scanning electron micrographs of CNF coatings on cotton fabric obtained through freeze drying and oven drying process are shown in panels a and b respectively.

The CNF coating obtained through freeze drying process had a porous structure whereas the oven dried CNF coatings had greater interlocking among fibrils which could explain the uniformity of the CNF layer in the latter case. However as mentioned earlier in case of CNF coatings obtained through oven drying process, the coatings began developing major cracks as soon as they were mounted on the funnel for testing.

Overall, these results suggest that CNF coated on cloth fabric through freeze-drying method can be a good alternative to surgical cloth mask. The filtration efficiency tests also hint at the possibility of using multiple layers of CNF coated cloth fabric to optimize the filtration efficiency values while maintaining the NIOSH limit of inhalation resistance. However, a considerable amount of research is still required to test such masks in different conditions which were well beyond the scope of this study.

CHAPTER VI

CONCLUSIONS

6.1. Scientific Contributions

This work offers new insights into indoor exposure to aerosols of a variety of sources, ranging from cooking oils, other everyday cooking emissions, outdoor infiltration, and human-exhaled respiratory droplets. The findings presented in this dissertation also offer practical recommendations for different mitigation strategies that can be adopted for reducing the resulting exposure from these aerosols.

The findings from Chapter II provides multiple results of interest to the science community as well as the general public, such as the effect of different control strategies such as window opening, using an extracting range hood over the stove, as well as the effect of home layout and ventilation on PM transport between residential kitchen and bedroom areas. These results also provide insights on the effective use of a portable air cleaner to reduce indoor exposure to PM of indoor and outdoor origin. In most of the studied homes, having a control measure near the kitchen stove (e.g., an extracting range hood, increased ventilation due to open windows, and PAC use) greatly reduced the overall PM exposure both in the kitchen and the bedroom areas. The study also highlights a need for awareness among general public in regard to low-cost sensor use indoors in combination with practical mitigation measures.

The investigation on aerosols emissions from heating frying oils demonstrates that a good mitigation strategy for indoor aerosol exposure from

cooking might be selecting oils based on their individual smoke points. The sudden increase in concentrations beyond the smoke point threshold yielding higher aerosol mass deposition values in the respiratory system suggests the need for temperature control to maintain cooking temperatures below respective smoke points, especially when using large quantities of oils in indoor environments. The results from volatility characterization part of this study highlighted that the volatiles in the cooking oil generated emissions could act as precursors to organic pollutant formation in different settings. Therefore, using a control mechanism to effectively capture these emissions will not only be relevant for reducing human exposure but also could prevent different pollutant transformation processes from transpiring at both indoor as well as regional scale.

Chapter IV and Chapter V emphasized the need for carefully balancing the demand for additional mask usage with sustainable alternatives. While it is important to choose the best available option for personal protection from various pollutants during different scenarios, it is equally important to ensure that the increased mask demand doesn't contribute to the already existing problem of environmental pollution. While the results suggested that commercially certified respirators such as N95 and KN95, and double surgical masks outperform cloth mask options in terms of inward protection against aerosols, one has to consider their mass availability in developing regions of the world in addition to their proper disposal practices after usage, further escalating the issues of marine and land pollution. Chapter V of this thesis was an attempt to promote research towards

improved filter materials that are comparatively less inexpensive, more easily accessible, and, most importantly, biodegradable in nature. The method of freeze drying of cellulose nanofibril-coated cotton fabrics did show some promising results, however additional research is needed before we can propose this method as a sustainable alternative.

6.2. Future Directions

Due to the lack of any specific air quality standards for residential environments and the fact that a majority of our daily lives are spent indoors, I have always been curious about understanding various processes related to aerosol science in indoor environments and about how to reduce the human occupant exposure to the different pollutants generated indoors. I hope the future generations interested in aerosol research will also share this same motivation and will continue finding new developments that have the potential to make a positive impact on all of our lives. The findings from these three studies have only highlighted a few of the different avenues a researcher can pursue in context of improving indoor air quality and there is still a long way to go. The first study has shown the importance of having some control measures in the kitchen area in reducing overall indoor PM exposure in residential environments. These findings will also help contribute to the growing scientific literature on the use of low-cost AQMs to better characterize indoor air quality and making progress towards integration of low-cost sensors along with a portable air cleaner to optimize low levels of PM exposure values for occupants inside a house.

In developing countries, a large fraction of the population cannot afford any control devices and—due to living in highly polluted ambient environments—do not have the option to open the kitchen windows for increased ventilation. Therefore, I hope future research targeted on developing cost-effective control measures for such scenarios will continue evolving with aims to save millions of people from PM exposure-related illnesses. Similarly, one has to acknowledge the need for continuously optimizing cooking methods for reducing indoor pollutant levels given that cooking is still the most prominent contributor to indoor air pollution in many residential environments. The results from the second study have shown a positive outlook on how even a small intervention step such as using frying oils with higher smoke points and temperature control could yield great dividends in controlling PM emissions and reducing the respiratory deposition values upon direct exposure but there is still a long way to go in further optimizing indoor cooking practices to maintain healthy IAQ levels.

As mentioned previously, the increased mask usage during the times of the COVID-19 pandemic has demonstrated the need for balancing high filtration performance demands of a material with increased reusability and biodegradability. While one might argue that the pandemic will only end up temporarily increasing the mask usage throughout the world based on the fact that nowadays the mask mandates are being lifted around the world, we still have to acknowledge that in the future, people in different pockets of the world will still have to protect themselves from seasonal episodes of wildfires, high ambient pollutant levels, and

high viral loads in different settings. Therefore, in context of reducing pressures on waste management systems and reducing global pollution in near future, it is imperative that we start developing these improved filter materials for general public usage in order to reduce the pressures on global waste mitigation practices and to promote environmental sustainability in our response towards similar future scenarios.

BIBLIOGRAPHY

1 J. Sundell, On the history of indoor air quality and health, *Indoor Air*, 2004, **14**, 51–58.

2 D. K. Farmer, M. E. Vance, J. P. D. Abbatt, A. Abeleira, M. R. Alves, C. Arata, E. Boedicker, S. Bourne, F. Cardoso-Saldaña, R. Corsi, P. F. DeCarlo, A. H. Goldstein, V. H. Grassian, L. H. Ruiz, J. L. Jimenez, T. F. Kahan, E. F. Katz, J. M. Mattila, W. W. Nazaroff, A. Novoselac, R. E. O'Brien, V. W. Or, S. Patel, S. Sankhyan, P. S. Stevens, Y. Tian, M. Wade, C. Wang, S. Zhou and Y. Zhou, Overview of HOMEChem: House Observations of Microbial and Environmental Chemistry, *Environ. Sci.: Processes Impacts*, 2019, **21**, 1280–1300.

3 G. Buonanno, G. Johnson, L. Morawska and L. Stabile, Volatility Characterization of Cooking-Generated Aerosol Particles, *Aerosol Science and Technology*, 2011, **45**, 1069–1077.

4 J. Pei, C. Dong and J. Liu, Operating behavior and corresponding performance of portable air cleaners in residential buildings, China, *Building and Environment*, 2019, **147**, 473–481.

5 M. Shahbandeh, U.S. consumption of edible oils by type, 2021, https://www.statista.com/statistics/301044/edible-oils-consumption-united-states-by-type/, (accessed 2 June 2022).

6 G. Buonanno, L. Morawska and L. Stabile, Particle emission factors during cooking activities, *Atmospheric Environment*, 2009, **43**, 3235–3242.

7 H. R. Katragadda, A. Fullana, S. Sidhu and Á. A. Carbonell-Barrachina, Emissions of volatile aldehydes from heated cooking oils, *Food Chemistry*, 2010, **120**, 59–65.

8 C. J. Worby and H.-H. Chang, Face mask use in the general population and optimal resource allocation during the COVID-19 pandemic, *Nat Commun*, 2020, **11**, 4049.

9 V. C.-C. Cheng, S.-C. Wong, V. W.-M. Chuang, S. Y.-C. So, J. H.-K. Chen, S. Sridhar, K. K.-W. To, J. F.-W. Chan, I. F.-N. Hung, P.-L. Ho and K.-Y. Yuen, The role of community-wide wearing of face mask for control of coronavirus disease 2019 (COVID-19) epidemic due to SARS-CoV-2, *Journal of Infection*, 2020, **81**, 107–114.

10 A. Catching, S. Capponi, M. T. Yeh, S. Bianco and R. Andino, Examining the interplay between face mask usage, asymptomatic transmission, and social distancing on the spread of COVID-19, *Sci Rep*, 2021, **11**, 15998.

11 J. K. Kodros, K. O'Dell, J. M. Samet, C. L'Orange, J. R. Pierce and J. Volckens, Quantifying the Health Benefits of Face Masks and Respirators to Mitigate Exposure to Severe Air Pollution, *GeoHealth*, 2021, **5**, e2021GH000482.

12 A. Pacitto, F. Amato, A. Salmatonidis, T. Moreno, A. Alastuey, C. Reche, G. Buonanno, C. Benito and X. Querol, Effectiveness of commercial face masks to reduce personal PM exposure, *Science of The Total Environment*, 2019, **650**, 1582–1590.

13 T. A. Aragaw, Surgical face masks as a potential source for microplastic pollution in the COVID-19 scenario, *Marine Pollution Bulletin*, 2020, **159**, 111517.
14 F. J. Kelly and J. C. Fussell, Improving indoor air quality, health and performance within environments where people live, travel, learn and work, *Atmospheric Environment*, 2019, **200**, 90–109.
15 P. M. Bluyssen, Towards an integrative approach of improving indoor air quality, *Building and Environment*, 2009, **44**, 1980–1989.
16 M. Hamilton, A. Rackes, P. L. Gurian and M. S. Waring, Perceptions in the U.S. building industry of the benefits and costs of improving indoor air quality, *Indoor Air*, 2016, **26**, 318–330.
17 P. Kumar, A. N. Skouloudis, M. Bell, M. Viana, M. C. Carotta, G. Biskos and L. Morawska, Real-time sensors for indoor air monitoring and challenges ahead in deploying them to urban buildings, *Science of The Total Environment*, 2016, **560–561**, 150–159.
18 N. Fann, A. D. Lamson, S. C. Anenberg, K. Wesson, D. Risley and B. J. Hubbell, Estimating the National Public Health Burden Associated with Exposure to Ambient $PM_{2.5}$ and Ozone, *Risk Analysis*, 2012, **32**, 81–95.
19 C. M. Wong, H. Tsang, H. K. Lai, G. N. Thomas, K. B. Lam, K. P. Chan, Q. Zheng, J. G. Ayres, S. Y. Lee, T. H. Lam and T. Q. Thach, Cancer Mortality Risks from Long-term Exposure to Ambient Fine Particle, *Cancer Epidemiol Biomarkers Prev*, 2016, **25**, 839–845.
20 A. Vodonos, Y. A. Awad and J. Schwartz, The concentration-response between long-term $PM_{2.5}$ exposure and mortality; A meta-regression approach, *Environmental Research*, 2018, **166**, 677–689.
21 V. C. Pun, F. Kazemiparkouhi, J. Manjourides and H. H. Suh, Long-Term PM2.5 Exposure and Respiratory, Cancer, and Cardiovascular Mortality in Older US Adults, *American Journal of Epidemiology*, 2017, **186**, 961–969.
22 S. E. Alexeeff, N. S. Liao, X. Liu, S. K. Van Den Eeden and S. Sidney, Long-Term $PM_{2.5}$ Exposure and Risks of Ischemic Heart Disease and Stroke Events: Review and Meta-Analysis, *Journal of the American Heart Association*, 2021, **10**, e016890.
23 N. E. Klepeis, W. C. Nelson, W. R. Ott, J. P. Robinson, A. M. Tsang, P. Switzer, J. V. Behar, S. C. Hern and W. H. Engelmann, The National Human Activity Pattern Survey (NHAPS): a resource for assessing exposure to environmental pollutants, *J Expo Anal Environ Epidemiol*, 2001, **11**, 231–252.
24 H. Chojer, P. T. B. S. Branco, F. G. Martins, M. C. M. Alvim-Ferraz and S. I. V. Sousa, Development of low-cost indoor air quality monitoring devices: Recent advancements, *Science of The Total Environment*, 2020, **727**, 138385.
25 A. L. Clements, W. G. Griswold, A. Rs, J. E. Johnston, M. M. Herting, J. Thorson, A. Collier-Oxandale and M. Hannigan, Low-Cost Air Quality Monitoring Tools: From Research to Practice (A Workshop Summary), *Sensors*, 2017, **17**, 2478.
26 S. Patel, J. Li, A. Pandey, S. Pervez, R. K. Chakrabarty and P. Biswas, Spatio-temporal measurement of indoor particulate matter concentrations using a wireless network of low-cost sensors in households using solid fuels, *Environmental Research*, 2017, **152**, 59–65.

27 F. Borghi, A. Spinazzè, S. Rovelli, D. Campagnolo, L. Del Buono, A. Cattaneo and D. M. Cavallo, Miniaturized Monitors for Assessment of Exposure to Air Pollutants: A Review, *Int J Environ Res Public Health*, 2017, **14**, E909.
28 E. G. Snyder, T. H. Watkins, P. A. Solomon, E. D. Thoma, R. W. Williams, G. S. W. Hagler, D. Shelow, D. A. Hindin, V. J. Kilaru and P. W. Preuss, The Changing Paradigm of Air Pollution Monitoring, *Environ. Sci. Technol.*, 2013, **47**, 11369–11377.
29 Y. Wang, J. Li, H. Jing, Q. Zhang, J. Jiang and P. Biswas, Laboratory Evaluation and Calibration of Three Low-Cost Particle Sensors for Particulate Matter Measurement, *Aerosol Science and Technology*, 2015, **49**, 1063–1077.
30 R. E. Connolly, Q. Yu, Z. Wang, Y.-H. Chen, J. Z. Liu, A. Collier-Oxandale, V. Papapostolou, A. Polidori and Y. Zhu, Long-term evaluation of a low-cost air sensor network for monitoring indoor and outdoor air quality at the community scale, *Science of The Total Environment*, 2022, **807**, 150797.
31 J. Li, S. K. Mattewal, S. Patel and P. Biswas, Evaluation of Nine Low-cost-sensor-based Particulate Matter Monitors, *Aerosol Air Qual. Res.*, 2020, **20**, 254–270.
32 O. US EPA, Improving Indoor Air Quality, https://www.epa.gov/indoor-air-quality-iaq/improving-indoor-air-quality, (accessed 19 November 2021).
33 M. L. Clark, J. L. Peel, J. B. Burch, T. L. Nelson, M. M. Robinson, S. Conway, A. M. Bachand and S. J. Reynolds, Impact of improved cookstoves on indoor air pollution and adverse health effects among Honduran women, *International Journal of Environmental Health Research*, 2009, **19**, 357–368.
34 X. Zhang, Y. Jin, H. Dai, Y. Xie and S. Zhang, Health and economic benefits of cleaner residential heating in the Beijing–Tianjin–Hebei region in China, *Energy Policy*, 2019, **127**, 165–178.
35 P. Wargocki, The Effects of Ventilation in Homes on Health, *International Journal of Ventilation*, 2013, **12**, 101–118.
36 C. Dimitroulopoulou, Ventilation in European dwellings: A review, *Building and Environment*, 2012, **47**, 109–125.
37 P. Fermo, B. Artíñano, G. De Gennaro, A. M. Pantaleo, A. Parente, F. Battaglia, E. Colicino, G. Di Tanna, A. Goncalves da Silva Junior, I. G. Pereira, G. S. Garcia, L. M. Garcia Goncalves, V. Comite and A. Miani, Improving indoor air quality through an air purifier able to reduce aerosol particulate matter (PM) and volatile organic compounds (VOCs): Experimental results, *Environmental Research*, 2021, **197**, 111131.
38 J. Pei, W. Dai, H. Li and J. Liu, Laboratory and field investigation of portable air cleaners' long-term performance for particle removal to be published in: Building and environment, *Building and Environment*, 2020, **181**, 107100.
39 P. K. Barn, C. T. Elliott, R. W. Allen, T. Kosatsky, K. Rideout and S. B. Henderson, Portable air cleaners should be at the forefront of the public health response to landscape fire smoke, *Environ Health*, 2016, **15**, 116.
40 K. K. Barkjohn, C. Norris, X. Cui, L. Fang, T. Zheng, J. J. Schauer, Z. Li, Y. Zhang, M. Black, J. (Jim) Zhang and M. H. Bergin, Real-time measurements of PM2.5

and ozone to assess the effectiveness of residential indoor air filtration in Shanghai homes, *Indoor Air*, 2021, **31**, 74–87.
41 L. Sun, L. A. Wallace, N. A. Dobbin, H. You, R. Kulka, T. Shin, M. St-Jean, D. Aubin and B. C. Singer, Effect of venting range hood flow rate on size-resolved ultrafine particle concentrations from gas stove cooking, *Aerosol Science and Technology*, 2018, **52**, 1370–1381.
42 M. M. Lunden, W. W. Delp and B. C. Singer, Capture efficiency of cooking-related fine and ultrafine particles by residential exhaust hoods, *Indoor Air*, 2015, **25**, 45–58.
43 A. Novoselac and J. A. Siegel, Impact of placement of portable air cleaning devices in multizone residential environments, *Building and Environment*, 2009, **44**, 2348–2356.
44 J. P. Robinson and J. Thomas, *Time spent in activities, locations, and microenvironments: A California-national comparison. Project report*, General Sciences Corp., Laurel, MD (United States), 1991.
45 Z. Wang, W. W. Delp and B. C. Singer, Performance of low-cost indoor air quality monitors for $PM_{2.5}$ and PM_{10} from residential sources, *Building and Environment*, 2020, **171**, 106654.
46 B. I. Magi, C. Cupini, J. Francis, M. Green and C. Hauser, Evaluation of $PM_{2.5}$ measured in an urban setting using a low-cost optical particle counter and a Federal Equivalent Method Beta Attenuation Monitor, *Aerosol Science and Technology*, 2020, **54**, 147–159.
47 C. Malings, R. Tanzer, A. Hauryliuk, P. K. Saha, A. L. Robinson, A. A. Presto and R. Subramanian, Fine particle mass monitoring with low-cost sensors: Corrections and long-term performance evaluation, *Aerosol Science and Technology*.
48 R. Jayaratne, X. Liu, K.-H. Ahn, A. Asumadu-Sakyi, G. Fisher, J. Gao, A. Mabon, M. Mazaheri, B. Mullins, M. Nyaku, Z. Ristovski, Y. Scorgie, P. Thai, M. Dunbabin and L. Morawska, Low-cost $PM_{2.5}$ Sensors: An Assessment of their Suitability for Various Applications, *Aerosol Air Qual. Res.*, 2020, **20**, 520–532.
49 P. Wang, F. Xu, H. Gui, H. Wang and D.-R. Chen, Effect of relative humidity on the performance of five cost-effective PM sensors, *Aerosol Science and Technology*, 2021, **55**, 957–974.
50 J. Tryner, C. L'Orange, J. Mehaffy, D. Miller-Lionberg, J. C. Hofstetter, A. Wilson and J. Volckens, Laboratory evaluation of low-cost PurpleAir PM monitors and in-field correction using co-located portable filter samplers, *Atmospheric Environment*, 2020, **220**, 117067.
51 M. R. Giordano, C. Malings, S. N. Pandis, A. A. Presto, V. F. McNeill, D. M. Westervelt, M. Beekmann and R. Subramanian, From low-cost sensors to high-quality data: A summary of challenges and best practices for effectively calibrating low-cost particulate matter mass sensors, *Journal of Aerosol Science*, 2021, **158**, 105833.

52 A. L. Holder, A. K. Mebust, L. A. Maghran, M. R. McGown, K. E. Stewart, D. M. Vallano, R. A. Elleman and K. R. Baker, Field Evaluation of Low-Cost Particulate Matter Sensors for Measuring Wildfire Smoke, *Sensors*, 2020, **20**, 4796.
53 K. K. Johnson, M. H. Bergin, A. G. Russell and G. S. W. Hagler, Field Test of Several Low-Cost Particulate Matter Sensors in High and Low Concentration Urban Environments, *Aerosol Air Qual. Res.*, 2018, **18**, 565–578.
54 L. Chatzidiakou, A. Krause, O. A. M. Popoola, A. Di Antonio, M. Kellaway, Y. Han, F. A. Squires, T. Wang, H. Zhang, Q. Wang, Y. Fan, S. Chen, M. Hu, J. K. Quint, B. Barratt, F. J. Kelly, T. Zhu and R. L. Jones, Characterising low-cost sensors in highly portable platforms to quantify personal exposure in diverse environments, *Atmospheric Measurement Techniques*, 2019, **12**, 4643–4657.
55 A. Chen, Q. Cao, J. Zhou, B. Yang, V. W. C. Chang and W. W. Nazaroff, Indoor and outdoor particles in an air-conditioned building during and after the 2013 haze in Singapore, *Build. Environ.*, 2016, **99**, 73-81.
56 S. Patel, S. Sankhyan, E. K. Boedicker, P. F. DeCarlo, D. K. Farmer, A. H. Goldstein, E. F. Katz, W. W. Nazaroff, Y. Tian, J. Vanhanen and M. E. Vance, Indoor Particulate Matter during HOMEChem: Concentrations, Size Distributions, and Exposures, *Environ. Sci. Technol.*, 2020, **54**, 7107–7116.
57 D. Licina, Y. Tian and W. W. Nazaroff, Inhalation intake fraction of particulate matter from localized indoor emissions, *Building and Environment*, 2017, **123**, 14–22.
58 K. Vasilatou, C. Wälchli, S. Koust, S. Horender, K. Iida, H. Sakurai, F. Schneider, J. Spielvogel, T. Y. Wu and K. Auderset, Calibration of optical particle size spectrometers against a primary standard: Counting efficiency profile of the TSI Model 3330 OPS and Grimm 11-D monitor in the particle size range from 300 nm to 10 µm, *Journal of Aerosol Science*, 2021, **157**, 105818.
59 S. S. Patra, R. Ramsisaria, R. Du, T. Wu and B. E. Boor, A machine learning field calibration method for improving the performance of low-cost particle sensors, *Building and Environment*, 2021, **190**, 107457.
60 R. He, T. Han, D. Bachman, D. J. Carluccio, R. Jaeger, J. Zhang, S. Thirumurugesan, C. Andrews and G. Mainelis, Evaluation of two low-cost PM monitors under different laboratory and indoor conditions, *Aerosol Science and Technology*, 2021, **55**, 316–331.
61 B. C. Singer and W. W. Delp, Response of consumer and research grade indoor air quality monitors to residential sources of fine particles, *Indoor Air*, 2018, **28**, 624–639.
62 I. Demanega, I. Mujan, B. C. Singer, A. S. Anđelković, F. Babich and D. Licina, Performance assessment of low-cost environmental monitors and single sensors under variable indoor air quality and thermal conditions, *Building and Environment*, 2021, **187**, 107415.
63 A. Moreno-Rangel, T. Sharpe, F. Musau and G. McGill, Field evaluation of a low-cost indoor air quality monitor to quantify exposure to pollutants in residential environments, *Journal of Sensors and Sensor Systems*, 2018, **7**, 373–388.

64 S. Manibusan and G. Mainelis, Performance of Four Consumer-grade Air Pollution Measurement Devices in Different Residences, *Aerosol Air Qual. Res.*, 2020, **20**, 217–230.
65 E. Zagatti, M. Russo and M. C. Pietrogrande, On-Site Monitoring Indoor Air Quality in Schools: A Real-World Investigation to Engage High School Science Students, *J. Chem. Educ.*, 2020, **97**, 4069–4072.
66 South Coast Air Quality Management District, Foobot Sensor Detail, https://www.aqmd.gov/aq-spec/sensordetail/foobot, (accessed 19 November 2021).
67 M. L. Zamora, J. Rice and K. Koehler, One year evaluation of three low-cost PM2.5 monitors, *Atmospheric Environment*, 2020, **235**, 117615.
68 South Coast Air Quality Management District, IQAir - AirVisual Pro Sensor Detail, https://www.aqmd.gov/aq-spec/sensordetail/iqair---airvisual-pro, (accessed 19 November 2021).
69 I. Stavroulas, G. Grivas, P. Michalopoulos, E. Liakakou, A. Bougiatioti, P. Kalkavouras, K. M. Fameli, N. Hatzianastassiou, N. Mihalopoulos and E. Gerasopoulos, Field Evaluation of Low-Cost PM Sensors (Purple Air PA-II) Under Variable Urban Air Quality Conditions, in Greece, *Atmosphere*, 2020, **11**, 926.
70 K. E. Kelly, J. Whitaker, A. Petty, C. Widmer, A. Dybwad, D. Sleeth, R. Martin and A. Butterfield, Ambient and laboratory evaluation of a low-cost particulate matter sensor, *Environmental Pollution*, 2017, **221**, 491–500.
71 A. Mousavi and J. Wu, Indoor-Generated $PM_{2.5}$ During COVID-19 Shutdowns Across California: Application of the PurpleAir Indoor–Outdoor Low-Cost Sensor Network, *Environ. Sci. Technol.*, 2021, **55**, 5648–5656.
72 South Coast Air Quality Management District, PurpleAir PA-II Sensor Detail, https://www.aqmd.gov/aq-spec/sensordetail/purpleair-pa-ii, (accessed 19 November 2021).
73 J. Bi, L. A. Wallace, J. A. Sarnat and Y. Liu, Characterizing outdoor infiltration and indoor contribution of $PM_{2.5}$ with citizen-based low-cost monitoring data, *Environmental Pollution*, 2021, **276**, 116763.
74 South Coast Air Quality Management District, PurpleAir PA-I-Indoor Sensor Detail, https://www.aqmd.gov/aq-spec/sensordetail/purpleair-pa-i-indoor, (accessed 19 November 2021).
75 EJ120 Air Purifier, https://oransi.com/products/oransi-ej-air-purifier, (accessed 1 November 2021).
76 I. S. Walker, G. Rojas and B. Singer, Comparing extracting and recirculating residential kitchen range hoods for the use in high energy efficient housing, *Proc. AIVC Conference*, 2017, **117**, 28.
77 T. Sayahi, A. Butterfield and K. E. Kelly, Long-term field evaluation of the Plantower PMS low-cost particulate matter sensors, *Environmental Pollution*, 2019, **245**, 932–940.
78 D. H. Hagan and J. H. Kroll, Assessing the accuracy of low-cost optical particle sensors using a physics-based approach, *Atmospheric Measurement Techniques*, 2020, **13**, 6343–6355.

79 M.-P. Wan, C.-L. Wu, G.-N. Sze To, T.-C. Chan and C. Y. H. Chao, Ultrafine particles, and $PM_{2.5}$ generated from cooking in homes, *Atmospheric Environment*, 2011, **45**, 6141–6148.
80 S. Patel, S. Sankhyan, E. K. Boedicker, P. F. DeCarlo, D. K. Farmer, A. H. Goldstein, E. F. Katz, W. W. Nazaroff, Y. Tian, J. Vanhanen and M. E. Vance, Indoor Particulate Matter during HOMEChem: Concentrations, Size Distributions, and Exposures, *Environ. Sci. Technol.*, 2020, **54**, 7107–7116.
81 S. Sankhyan, S. Patel, E. F. Katz, P. F. DeCarlo, D. K. Farmer, W. W. Nazaroff and M. E. Vance, Indoor black carbon and brown carbon concentrations from cooking and outdoor penetration: insights from the HOMEChem study, *Environ. Sci.: Processes Impacts*, 2021, **23**, 1476–1487.
82 E. K. Boedicker, E. Emerson, G. McMeeking, S. Patel, M. E. Vance and D. K. Farmer, Fates and spatial variations of accumulation mode particles in a multi-zone indoor environment during the HOMEChem campaign, *Environmental Science: Processes & Impacts*, 2021, **23**, 1029–1039.
83 S. Patel, D. Rim, S. Sankhyan, A. Novoselac and M. E. Vance, Aerosol dynamics modeling of sub-500 nm particles during the HOMEChem study, *Environ. Sci.: Processes Impacts*, 2021, **23**, 1706–1717.
84 K.-H. Kim, S. K. Pandey, E. Kabir, J. Susaya and R. J. C. Brown, The modern paradox of unregulated cooking activities and indoor air quality, *Journal of Hazardous Materials*, 2011, **195**, 1–10.
85 C. Chen, Y. Zhao and B. Zhao, Emission Rates of Multiple Air Pollutants Generated from Chinese Residential Cooking, *Environ. Sci. Technol.*, 2018, **52**, 1081–1087.
86 Q. Zhang, R. H. Gangupomu, D. Ramirez and Y. Zhu, Measurement of Ultrafine Particles and Other Air Pollutants Emitted by Cooking Activities, *International Journal of Environmental Research and Public Health*, 2010, **7**, 1744–1759.
87 J. A. Hoskins, Health Effects due to Indoor Air Pollution, *Indoor and Built Environment*, 2003, **12**, 427–433.
88 Y.-T. Gao, W. J. Blot, W. Zheng, A. G. Ersnow, C. W. Hsu, L. I. Levin, R. Zhang and J. F. Fraumeni Jr., Lung cancer among Chinese women, *International Journal of Cancer*, 1987, **40**, 604–609.
89 K. L. Abdullahi, J. M. Delgado-Saborit and R. M. Harrison, Emissions and indoor concentrations of particulate matter and its specific chemical components from cooking: A review, *Atmospheric Environment*, 2013, **71**, 260–294.
90 L. Lv, L. Zeng, Y. Wu, J. Gao, W. Xie, C. Cao and J. Zhang, The application of an air curtain range hood in reducing human exposure to cooking pollutants, *Building and Environment*, 2021, **205**, 108204.
91 R. U. Shah, E. S. Robinson, P. Gu, J. S. Apte, J. D. Marshall, A. L. Robinson and A. A. Presto, Socio-economic disparities in exposure to urban restaurant emissions are larger than for traffic, *Environ. Res. Lett.*, 2020, **15**, 114039.
92 E. S. Robinson, P. Gu, Q. Ye, H. Z. Li, R. U. Shah, J. S. Apte, A. L. Robinson and A. A. Presto, Restaurant Impacts on Outdoor Air Quality: Elevated Organic

Aerosol Mass from Restaurant Cooking with Neighborhood-Scale Plume Extents, *Environ. Sci. Technol.*, 2018, **52**, 9285–9294.
93 R. Song, A. A. Presto, P. Saha, N. Zimmerman, A. Ellis and R. Subramanian, Spatial variations in urban air pollution: impacts of diesel bus traffic and restaurant cooking at small scales, *Air Qual Atmos Health*, 2021, **14**, 2059–2072.
94 T. Bergman, T. Mielonen, A. Arola and H. Kokkola, Climate and mortality changes due to reductions in household cooking emissions, 2016, EPSC2016-12541.
95 C. Mohr, J. A. Huffman, M. J. Cubison, A. C. Aiken, K. S. Docherty, J. R. Kimmel, I. M. Ulbrich, M. Hannigan and J. L. Jimenez, Characterization of Primary Organic Aerosol Emissions from Meat Cooking, Trash Burning, and Motor Vehicles with High-Resolution Aerosol Mass Spectrometry and Comparison with Ambient and Chamber Observations, *Environ. Sci. Technol.*, 2009, **43**, 2443–2449.
96 L. L. Yeung and W. M. To, Size Distributions of the Aerosols Emitted from Commercial Cooking Processes, *Indoor and Built Environment*, 2008, **17**, 220–229.
97 P. L. Hayes, A. G. Carlton, K. R. Baker, R. Ahmadov, R. A. Washenfelder, S. Alvarez, B. Rappenglück, J. B. Gilman, W. C. Kuster, J. A. de Gouw, P. Zotter, A. S. H. Prévôt, S. Szidat, T. E. Kleindienst, J. H. Offenberg, P. K. Ma and J. L. Jimenez, Modeling the formation and aging of secondary organic aerosols in Los Angeles during CalNex 2010, *Atmospheric Chemistry and Physics*, 2015, **15**, 5773–5801.
98 S. Patel, A. Leavey, S. He, J. Fang, K. O'Malley and P. Biswas, Characterization of gaseous and particulate pollutants from gasification-based improved cookstoves, *Energy for Sustainable Development*, 2016, **32**, 130–139.
99 K. Kang, H. Kim, D. D. Kim, Y. G. Lee and T. Kim, Characteristics of cooking-generated PM_{10} and $PM_{2.5}$ in residential buildings with different cooking and ventilation types, *Science of The Total Environment*, 2019, **668**, 56–66.
100 B. C. Singer, R. Z. Pass, W. W. Delp, D. M. Lorenzetti and R. L. Maddalena, Pollutant concentrations and emission rates from natural gas cooking burners without and with range hood exhaust in nine California homes, *Building and Environment*, 2017, **122**, 215–229.
101 S. Sankhyan, J. K. Witteman, S. Coyan, S. Patel and M. E. Vance, Assessment of $PM_{2.5}$ concentrations, transport, and mitigation in indoor environments using low-cost air quality monitors and a portable air cleaner, *Environ. Sci.: Atmos.*, 2022, **2**, 647-658.
102 D.-C. Zhang, J.-J. Liu, L.-Z. Jia, P. Wang and X. Han, Speciation of VOCs in the cooking fumes from five edible oils and their corresponding health risk assessments, *Atmospheric Environment*, 2019, **211**, 6–17.
103 M. A. Torkmahalleh, S. Gorjinezhad, H. S. Unluevcek and P. K. Hopke, Review of factors impacting emission/concentration of cooking generated particulate matter, *Science of The Total Environment*, 2017, **586**, 1046–1056.

104 W. M. To, L. L. Yeung and C. Y. H. Chao, Characterisation of Gas Phase Organic Emissions from Hot Cooking Oil in Commercial Kitchens, *Indoor and Built Environment*, 2000, **9**, 228–232.
105 C.-Y. Peng, C.-H. Lan, P.-C. Lin and Y.-C. Kuo, Effects of cooking method, cooking oil, and food type on aldehyde emissions in cooking oil fumes, *Journal of Hazardous Materials*, 2017, **324**, 160–167.
106 L. A. Wallace, S. J. Emmerich and C. Howard-Reed, Source Strengths of Ultrafine and Fine Particles Due to Cooking with a Gas Stove, *Environ. Sci. Technol.*, 2004, **38**, 2304–2311.
107 A. Fullana, Á. A. Carbonell-Barrachina and S. Sidhu, Volatile aldehyde emissions from heated cooking oils, *Journal of the Science of Food and Agriculture*, 2004, **84**, 2015–2021.
108 Z. Zhang, W. Zhu, M. Hu, H. Wang, Z. Chen, R. Shen, Y. Yu, R. Tan and S. Guo, Secondary Organic Aerosol from Typical Chinese Domestic Cooking Emissions, *Environ. Sci. Technol. Lett.*, 2021, **8**, 24–31.
109 M. A. Torkmahalleh, I. Goldasteh, Y. Zhao, N. M. Udochu, A. Rossner, P. K. Hopke and A. R. Ferro, $PM_{2.5}$ and ultrafine particles emitted during heating of commercial cooking oils, *Indoor Air*, 2012, **22**, 483–491.
110 F. Lu, B. Shen, S. Li, L. Liu, P. Zhao and M. Si, Exposure characteristics and risk assessment of VOCs from Chinese residential cooking, *Journal of Environmental Management*, 2021, **289**, 112535.
111 T.-A. Chiang, P.-F. Wu and Y.-C. Ko, Prevention of exposure to mutagenic fumes produced by hot cooking oil in Taiwanese kitchens, *Environmental and Molecular Mutagenesis*, 1998, **31**, 92–96.
112 T. Liu, Z. Li, M. Chan and C. K. Chan, Formation of secondary organic aerosols from gas-phase emissions of heated cooking oils, *Atmospheric Chemistry and Physics*, 2017, **17**, 7333–7344.
113 M. Takhar, Y. Li and A. W. H. Chan, Characterization of secondary organic aerosol from heated-cooking-oil emissions: evolution in composition and volatility, *Atmospheric Chemistry and Physics*, 2021, **21**, 5137–5149.
114 T. Liu, Z. Wang, D. D. Huang, X. Wang and C. K. Chan, Significant Production of Secondary Organic Aerosol from Emissions of Heated Cooking Oils, *Environ. Sci. Technol. Lett.*, 2018, **5**, 32–37.
115 R. E. O'Brien, Y. Li, K. J. Kiland, E. F. Katz, V. W. Or, E. Legaard, E. Q. Walhout, C. Thrasher, V. H. Grassian, P. F. DeCarlo, A. K. Bertram and M. Shiraiwa, Emerging investigator series: chemical and physical properties of organic mixtures on indoor surfaces during HOMEChem, *Environ. Sci.: Processes Impacts*, 2021, **23**, 559–568.
116 A. P. Ault, V. H. Grassian, N. Carslaw, D. B. Collins, H. Destaillats, D. J. Donaldson, D. K. Farmer, J. L. Jimenez, V. F. McNeill, G. C. Morrison, R. E. O'Brien, M. Shiraiwa, M. E. Vance, J. R. Wells and W. Xiong, Indoor Surface Chemistry: Developing a Molecular Picture of Reactions on Indoor Interfaces, *Chem*, 2020, **6**, 3203–3218.

117 V. W. Or, M. Wade, S. Patel, M. R. Alves, D. Kim, S. Schwab, H. Przelomski, R. O'Brien, D. Rim, R. L. Corsi, M. E. Vance, D. K. Farmer and V. H. Grassian, Glass surface evolution following gas adsorption and particle deposition from indoor cooking events as probed by microspectroscopic analysis, *Environ. Sci.: Processes Impacts*, 2020, **22**, 1698–1709.
118 W. Chen, P. Wang, D. Zhang, J. Liu and X. Dai, The Impact of Water on Particle Emissions from Heated Cooking Oil, *Aerosol Air Qual. Res.*, 2020, **20**, 533–543.
119 S. W. See and R. Balasubramanian, Physical Characteristics of Ultrafine Particles Emitted from Different Gas Cooking Methods, *Aerosol Air Qual. Res.*, 206AD, **6**, 82–92.
120 T. Kuhn, M. Krudysz, Y. Zhu, P. M. Fine, W. C. Hinds, J. Froines and C. Sioutas, Volatility of indoor and outdoor ultrafine particulate matter near a freeway, *Journal of Aerosol Science*, 2005, **36**, 291–302.
121 J. A. Huffman, P. J. Ziemann, J. T. Jayne, D. R. Worsnop and J. L. Jimenez, Development and Characterization of a Fast-Stepping/Scanning Thermodenuder for Chemically-Resolved Aerosol Volatility Measurements, *Aerosol Science and Technology*, 2008, **42**, 395–407.
122 M. R. Bailey, The New ICRP Model for the Respiratory Tract, *Radiation Protection Dosimetry*, 1994, **53**, 107–114.
123 W. C. Hinds, *Aerosol technology: properties, behavior, and measurement of airborne particles*, Wiley, 1999.
124 L. A. Wallace, S. J. Emmerich and C. Howard-Reed, Source Strengths of Ultrafine and Fine Particles Due to Cooking with a Gas Stove, *Environ. Sci. Technol.*, 2004, **38**, 2304–2311.
125 H. Sakurai, H. J. Tobias, K. Park, D. Zarling, K. S. Docherty, D. B. Kittelson, P. H. McMurry and P. J. Ziemann, On-line measurements of diesel nanoparticle composition and volatility, *Atmospheric Environment*, 2003, **37**, 1199–1210.
126 W. J. An, R. K. Pathak, B.-H. Lee and S. N. Pandis, Aerosol volatility measurement using an improved thermodenuder: Application to secondary organic aerosol, *Journal of Aerosol Science*, 2007, **38**, 305–314.
127 P. K. Saha, A. Khlystov and A. P. Grieshop, Determining Aerosol Volatility Parameters Using a "Dual Thermodenuder" System: Application to Laboratory-Generated Organic Aerosols, *Aerosol Science and Technology*, 2015, **49**, 620–632.
128 C. Kaltsonoudis, E. Kostenidou, E. Louvaris, M. Psichoudaki, E. Tsiligiannis, K. Florou, A. Liangou and S. N. Pandis, Characterization of fresh and aged organic aerosol emissions from meat charbroiling, *Atmospheric Chemistry and Physics*, 2017, **17**, 7143–7155.
129 E. F. Katz, H. Guo, P. Campuzano-Jost, D. A. Day, W. L. Brown, E. Boedicker, M. Pothier, D. M. Lunderberg, S. Patel, K. Patel, P. L. Hayes, A. Avery, L. Hildebrandt Ruiz, A. H. Goldstein, M. E. Vance, D. K. Farmer, J. L. Jimenez and P. F. DeCarlo, Quantification of cooking organic aerosol in the indoor environment using aerodyne aerosol mass spectrometers, *Aerosol Science and Technology*, 2021, **55**, 1099–1114.

130 M. L. Ranney, V. Griffeth and A. K. Jha, Critical Supply Shortages — The Need for Ventilators and Personal Protective Equipment during the Covid-19 Pandemic, *New England Journal of Medicine*, 2020, **382**, e41.
131 S. Rab, M. Javaid, A. Haleem and R. Vaishya, Face masks are new normal after COVID-19 pandemic, *Diabetes & Metabolic Syndrome: Clinical Research & Reviews*, 2020, **14**, 1617–1619.
132 Y. Yan, J. Bayham, A. Richter and E. P. Fenichel, Risk compensation and face mask mandates during the COVID-19 pandemic, *Scientific Reports*, 2021, **11**, 3174.
133 S. L. Miller, W. W. Nazaroff, J. L. Jimenez, A. Boerstra, G. Buonanno, S. J. Dancer, J. Kurnitski, L. C. Marr, L. Morawska and C. Noakes, Transmission of SARS-CoV-2 by inhalation of respiratory aerosol in the Skagit Valley Chorale superspreading event, *Indoor Air*, 2021, **31**, 314–323.
134 T. Günther, M. Czech-Sioli, D. Indenbirken, A. Robitaille, P. Tenhaken, M. Exner, M. Ottinger, N. Fischer, A. Grundhoff and M. M. Brinkmann, SARS-CoV-2 outbreak investigation in a German meat processing plant, *EMBO Molecular Medicine*, 2020, **12**, e13296.
135 J. Lu, J. Gu, K. Li, C. Xu, W. Su, Z. Lai, D. Zhou, C. Yu, B. Xu and Z. Yang, COVID-19 Outbreak Associated with Air Conditioning in Restaurant, Guangzhou, China, 2020, *Emerg Infect Dis*, 2020, **26**, 1628–1631.
136 S. Asadi, C. D. Cappa, S. Barreda, A. S. Wexler, N. M. Bouvier and W. D. Ristenpart, Efficacy of masks and face coverings in controlling outward aerosol particle emission from expiratory activities, *Scientific Reports*, 2020, **10**, 15665.
137 J. Howard, A. Huang, Z. Li, Z. Tufekci, V. Zdimal, H.-M. van der Westhuizen, A. von Delft, A. Price, L. Fridman, L.-H. Tang, V. Tang, G. L. Watson, C. E. Bax, R. Shaikh, F. Questier, D. Hernandez, L. F. Chu, C. M. Ramirez and A. W. Rimoin, An evidence review of face masks against COVID-19, *Proc. Nat. Acad. Sci. U.S.A.*, 2021, **118**, e2014564118.
138 N. H. L. Leung, D. K. W. Chu, E. Y. C. Shiu, K.-H. Chan, J. J. McDevitt, B. J. P. Hau, H.-L. Yen, Y. Li, D. K. M. Ip, J. S. M. Peiris, W.-H. Seto, G. M. Leung, D. K. Milton and B. J. Cowling, Respiratory virus shedding in exhaled breath and efficacy of face masks, *Nature Medicine*, 2020, **26**, 676–680.
139 A. D. Sung, J. A. M. Sung, S. Thomas, T. Hyslop, C. Gasparetto, G. Long, D. Rizzieri, K. M. Sullivan, K. Corbet, G. Broadwater, N. J. Chao and M. E. Horwitz, Universal Mask Usage for Reduction of Respiratory Viral Infections After Stem Cell Transplant: A Prospective Trial, *Clin Infect Dis*, 2016, **63**, 999–1006.
140 L. Zhang, Z. Peng, J. Ou, G. Zeng, R. E. Fontaine, M. Liu, F. Cui, R. Hong, H. Zhou, Y. Huai, S.-K. Chuang, Y.-H. Leung, Y. Feng, Y. Luo, T. Shen, B.-P. Zhu, M.-A. Widdowson and H. Yu, Protection by face masks against influenza A(H1N1)pdm09 virus on trans-Pacific passenger aircraft, 2009, *Emerg Infect Dis*, 2013, **19**, 1403-1410.
141 A. Tcharkhtchi, N. Abbasnezhad, M. Zarbini Seydani, N. Zirak, S. Farzaneh and M. Shirinbayan, An overview of filtration efficiency through the masks: Mechanisms of the aerosols penetration, *Bioactive Materials*, 2021, **6**, 106–122.

142 P. Y. Chia, K. K. Coleman, Y. K. Tan, S. W. X. Ong, M. Gum, S. K. Lau, S. Sutjipto, P. H. Lee, T. T. Son, B. E. Young, D. K. Milton, G. C. Gray, S. Schuster, T. Barkham, P. P. De, S. Vasoo, M. Chan, B. S. P. Ang, B. H. Tan, Y.-S. Leo, O.-T. Ng, M. S. Y. Wong and K. Marimuthu, Detection of Air and Surface Contamination by Severe Acute Respiratory Syndrome Coronavirus 2 (SARS-CoV-2) in Hospital Rooms of Infected Patients, *Nat. Commun.*, 2020, **11**, 2800.

143 J. Pan, C. Harb, W. Leng and L. C. Marr, Inward and outward effectiveness of cloth masks, a surgical mask, and a face shield, *Aerosol Science and Technology*, 2021, **55**, 718–733.

144 F. Santana, S. Fischer, M. Jaeger and G. Wong-Parodi, Responding to simultaneous crises: communications and social norms of mask behavior during wildfires and COVID-19, *Environmental Research Letters*, 2020, **15**, 111002.

145 K. M. Shakya, A. Noyes, R. Kallin and R. E. Peltier, Evaluating the efficacy of cloth facemasks in reducing particulate matter exposure, *J Expo Sci Environ Epidemiol*, 2017, **27**, 352–357.

146 E. O'Kelly, S. Pirog, J. Ward and P. J. Clarkson, Ability of fabric face mask materials to filter ultrafine particles at coughing velocity, *BMJ Open*, 2020, **10**, e039424.

147 S. Rengasamy, B. Eimer and R. E. Shaffer, Simple Respiratory Protection—Evaluation of the Filtration Performance of Cloth Masks and Common Fabric Materials Against 20–1000 nm Size Particles, *The Annals of Occupational Hygiene*, 2010, **54**, 789–798.

148 H. Lu, D. Yao, J. Yip, C.-W. Kan and H. Guo, Addressing COVID-19 Spread: Development of Reliable Testing System for Mask Reuse, *Aerosol Air Qual. Res.*, 2020, **20**, 2309–2317.

149 M. Zhao, L. Liao, W. Xiao, X. Yu, H. Wang, Q. Wang, Y. L. Lin, F. S. Kilinc-Balci, A. Price, L. Chu, M. C. Chu, S. Chu and Y. Cui, Household Materials Selection for Homemade Cloth Face Coverings and Their Filtration Efficiency Enhancement with Triboelectric Charging, *Nano Lett.*, 2020, **20**, 5544–5552.

150 J. T. Brooks, *Maximizing Fit for Cloth and Medical Procedure Masks to Improve Performance and Reduce SARS-CoV-2 Transmission and Exposure, 2021*, Centers for Disease Control and Prevention, 2021.

151 C. H. Park, Y. K. Kang and S. S. Im, Biodegradability of cellulose fabrics, *Journal of Applied Polymer Science*, 2004, **94**, 248–253.

152 S. Salter, Reinventing Cloth Masks in the Face of Pandemics, *Risk Anal*, 2020, **41**, 731-744.

153 C. R. MacIntyre, S. Cauchemez, D. E. Dwyer, H. Seale, P. Cheung, G. Browne, M. Fasher, J. Wood, Z. Gao, R. Booy and N. Ferguson, Face Mask Use and Control of Respiratory Virus Transmission in Households,*Emerg. Infect. Dis.*, 2009, **15**, 233-241.

154 NIOSH, *Determination of particulate filter efficiency level for N95 series filters against solid particulates for non-powered, air-purifying respirators standard testing procedure (STP).*, Pittsburgh, MA, 2019.

155 F. Drewnick, J. Pikmann, F. Fachinger, L. Moormann, F. Sprang and S. Borrmann, Aerosol filtration efficiency of household materials for homemade face masks: Influence of material properties, particle size, particle electrical charge, face velocity, and leaks, *Aerosol Science and Technology*, 2021, **55**, 63–79.
156 U.S. Environmental Protection Agency, Exposure Factors Handbook 2011 Edition (Final Report), Washington, DC, EPA/600/R-09/052F, 2011.
157 R. J. Roberge, E. Bayer, J. B. Powell, A. Coca, M. R. Roberge and S. M. Benson, Effect of Exhaled Moisture on Breathing Resistance of N95 Filtering Facepiece Respirators, *The Annals of Occupational Hygiene*, 2010, **54**, 671–677.
158 ASTM International, Standard Test Method for Determining the Initial Efficiency of Materials Used in Medical Face Masks to Penetration by Particulates Using Latex Spheres. ASTM F2299/F2299M-03; ASTM International, West Conshohocken, PA, 2017, https://doi.org/10.1520/F2299_F2299M-03R17.
159 U.S. Food and Drug Administration (FDA), Surgical masks—Premarket notification [510(k)] submissions. Guidance for Industry and FDA Staff, FDA-2003-D-0305, 2004. (accessed 20 April 2021).
160 A. Konda, A. Prakash, G. A. Moss, M. Schmoldt, G. D. Grant and S. Guha, Aerosol Filtration Efficiency of Common Fabrics Used in Respiratory Cloth Masks, *ACS Nano*, 2020, **14**, 6339–6347.
161 F. G. Morais, V. K. Sakano, L. N. de Lima, M. A. Franco, D. C. Reis, L. M. Zanchetta, F. Jorge, E. Landulfo, L. H. Catalani, H. M. J. Barbosa, V. M. John and P. Artaxo, Filtration efficiency of a large set of COVID-19 face masks commonly used in Brazil, *Aerosol Science and Technology*, 2021, **55**, 1028–1041.
162 NIOSH, *Determination of inhalation resistance test, air-purifying respirators. Standard Testing Procedure (STP).*, Pittsburgh, MA, 2019.
163 A. Podgórski, A. Bałazy and L. Gradoń, Application of nanofibers to improve the filtration efficiency of the most penetrating aerosol particles in fibrous filters, *Chemical Engineering Science*, 2006, **61**, 6804–6815.
164 C. D. Zangmeister, J. G. Radney, E. P. Vicenzi and J. L. Weaver, Filtration Efficiencies of Nanoscale Aerosol by Cloth Mask Materials Used to Slow the Spread of SARS-CoV-2, *ACS Nano*, 2020, **14**, 9188–9200.
165 C.-S. Wang, Electrostatic forces in fibrous filters—a review, *Powder Technology*, 2001, **118**, 166–170.
166 P. N. Ciesielski, W. Wang, X. Chen, T. B. Vinzant, M. P. Tucker, S. R. Decker, M. E. Himmel, D. K. Johnson and B. S. Donohoe, Effect of mechanical disruption on the effectiveness of three reactors used for dilute acid pretreatment of corn stover Part 2: morphological and structural substrate analysis, *Biotechnology for Biofuels*, 2014, **7**, 47.
167 E. M. Karp, M. G. Resch, B. S. Donohoe, P. N. Ciesielski, M. H. O'Brien, J. E. Nill, A. Mittal, M. J. Biddy and G. T. Beckham, Alkaline Pretreatment of Switchgrass, *ACS Sustainable Chem. Eng.*, 2015, **3**, 1479–1491.
168 P. N. Ciesielski, R. Wagner, V. S. Bharadwaj, J. Killgore, A. Mittal, G. T. Beckham, S. R. Decker, M. E. Himmel and M. F. Crowley, Nanomechanics of

cellulose deformation reveal molecular defects that facilitate natural deconstruction, *PNAS*, 2019, **116**, 9825–9830.
169 J. D. Hinkle, P. N. Ciesielski, K. Gruchalla, K. R. Munch and B. S. Donohoe, Biomass accessibility analysis using electron tomography, *Biotechnology for Biofuels*, 2015, **8**, 212.
170 O. Nechyporchuk, M. N. Belgacem and J. Bras, Production of cellulose nanofibrils: A review of recent advances, *Industrial Crops and Products*, 2016, **93**, 2–25.
171 Y. Zhang, T. Nypelö, C. Salas, J. Arboleda, I. C. Hoeger and O. J. Rojas, Cellulose Nanofibrils, *Journal of Renewable Materials*, 2013, **1**, 195–211.
172 M. Schmutz, R. Hischier, T. Batt, P. Wick, B. Nowack, P. Wäger and C. Som, Cotton and Surgical Masks—What Ecological Factors Are Relevant for Their Sustainability?, *Sustainability*, 2020, **12**, 10245.
173 D. H. R. Spennemann, COVID Face Masks: Policy Shift Results in Increased Littering, *Sustainability*, 2021, **13**, 9875.
174 J. C. Prata, A. L. P. Silva, A. C. Duarte and T. Rocha-Santos, Disposable over Reusable Face Masks: Public Safety or Environmental Disaster?, *Environments*, 2021, **8**, 31.
175 N. Boix Rodríguez, G. Formentini, C. Favi and M. Marconi, Engineering Design Process of Face Masks Based on Circularity and Life Cycle Assessment in the Constraint of the COVID-19 Pandemic, *Sustainability*, 2021, **13**, 4948.

APPENDIX A

ASSESSMENT OF $PM_{2.5}$ CONCENTRATIONS, TRANSPORT, AND MITIGATION IN INDOOR ENVIRONMENTS USING LOW-COST AIR QUALITY MONITORS AND A PORTABLE AIR CLEANER

Table A1. Characteristics about the locations used for the study.

Location	**Home 1**	**Home 2**	**Home 3**	**Home 4**
Description	2 bedroom, 1 bath apartment	4 bedroom, 3.5 bath house	2 bedroom, 2 bath apartment	Studio apartment
Floor area	70 m^2	360 m^2	79 m^2	35 m^2
Stove-type	Natural gas	Natural gas	Electric	Electric
Distance between stove and kitchen AQMs	4.2 m	3.5 m	0.9 m	0.7 m
Distance between stove and bedroom AQMs	3 m (around the corner)	9.8 m (around 2 corners)	5 m (in line with the stove)	7 m (diagonally opposite corner)

Table A2. Deployment dates for each phase in all the four homes.

Location	Phase 0A	Phase 1	Phase 2	Phase 3	Phase 0B
Home 1	10/06/2019-10/17/2019	10/18/2019-10/31/2019	11/04/2019-11/09/2019	11/10/2019-11/18/2019	11/19/2019-11/20/2019
Home 2	11/22/2019-11/26/2019	11/27/2019-12/15/2019	12/12/2019-01/05/2020	1/6/2020-1/26/2020	NA
Home 3	NA	02/07/2020-03/05/2020	03/10/2020-03/23/2020	04/06/2020-04/30/2020	04/28/2020-05/01/2020
Home 4	05/22/2020-05/26/2020	05/20/2020-06/15/2020	06/24/2020-07/05/2020	07/06/2020-07/20/2020	NA

Table A3. Correlation parameters for different AQMs with the OPS $PM_{2.5}$ data during cooking periods combined for all the homes. AV, PA and PA(ID) represent AirVisual Pro, PurpleAir and PurpleAir Indoor AQMs.

Sensor	Slope	Intercept	R^2	Root Mean Squared Error ($\mu g\ m^{-3}$)	Mean Normalized Bias
AV1	2.21	3.87	0.61	32	1.54
AV2	1.83	2.83	0.50	33	1.08
PA1	1.57	9.43	0.31	42	1.40
PA2	1.51	11.35	0.33	39	1.50
PA (ID) 1	1.41	9.69	0.35	34	1.26
PA (ID) 2	1.45	10.17	0.38	34	1.34

Table A4. Correlation parameters for different AQMs with the OPS $PM_{2.5}$ data during background periods combined for all the homes. AV, PA and PA(ID) represent AirVisual Pro, PurpleAir and PurpleAir Indoor AQMs.

Sensor	Slope	Intercept	R^2	Root Mean Squared Error ($\mu g\ m^{-3}$)	Mean Normalized Bias
AV1	1.84	0.60	0.88	1.24	1.17
AV2	1.32	0.43	0.88	0.92	0.57
PA1	1.58	0.86	0.80	1.46	1.07
PA2	1.68	0.72	0.82	1.46	1.08
PA (ID) 1	1.40	0.53	0.76	1.45	0.70
PA (ID) 2	1.47	0.63	0.79	1.41	0.82

Table A5. Percentage reduction in mean exposure values in kitchen and bedroom areas during phases of PAC use as compared to Phase 1 data for daytime periods. The absolute values for mean reductions in $\mu g\ m^{-3}$ are also shown in the parentheses.

Reduction (%)	Phase 2 Kitchen	Phase 3 Bedroom
Home 1	67% (47)	53% (39)
Home 2	NA	NA
Home 3	51% (199)	46% (100)
Home 4	31% (18)	85% (41)

Table A6. Percentage reduction in mean exposure values in kitchen and bedroom areas during phases of PAC use as compared to Phase 1 data for nighttime periods. The absolute values for mean reductions in μg m^{-3} are also shown in the parentheses.

Reduction (%)	Phase 2 Kitchen	Phase 3 Bedroom
Home 1	11% (1)	90% (9)
Home 2	NA	33% (4)
Home 3	52% (23)	63% (25)
Home 4	38% (5)	89% (9)

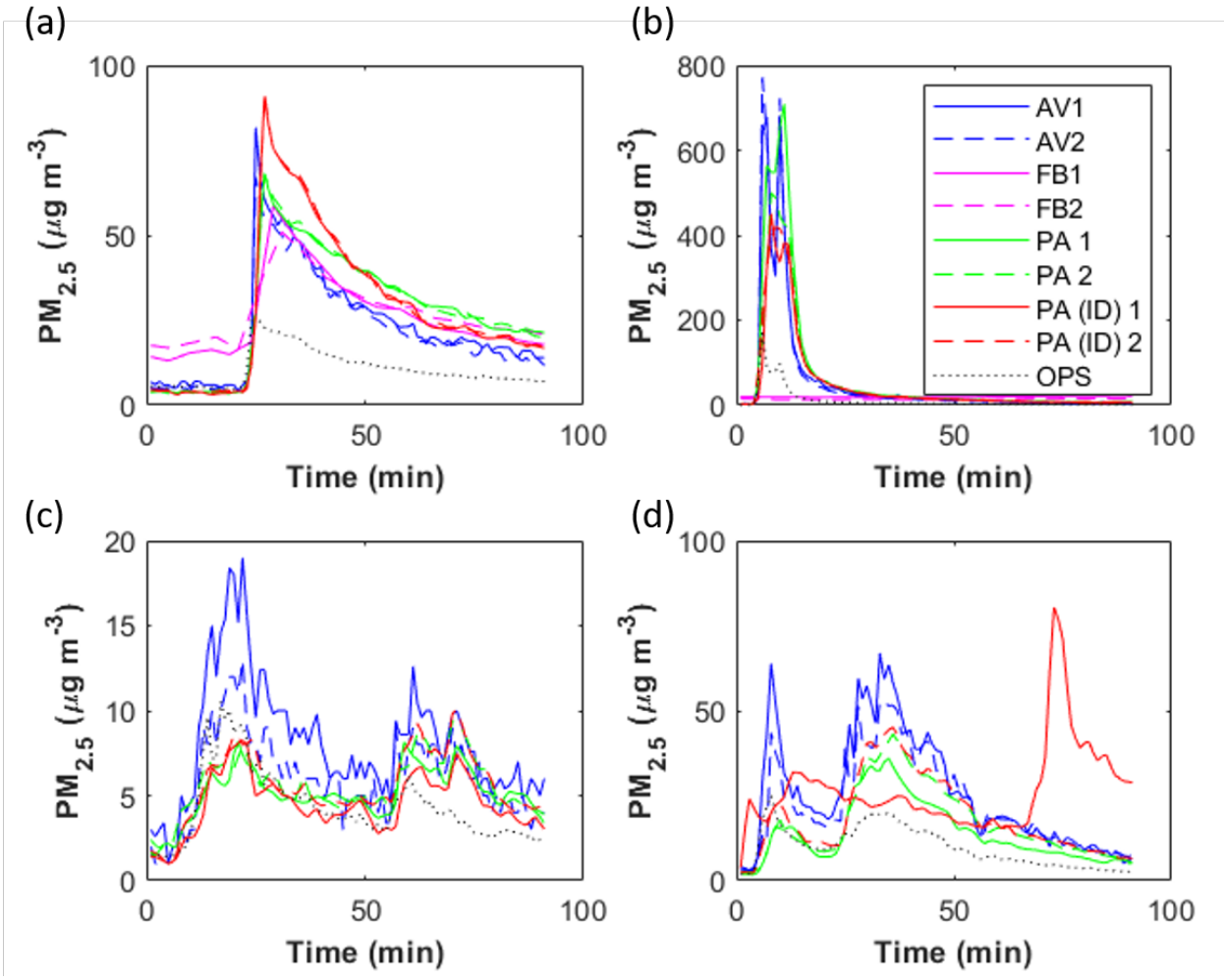

Figure A1. $PM_{2.5}$ time series from OPS and different AQMs used in this study during a given cooking period for Homes 1-4 is shown in panels a, b, c, and d respectively. AV, FB, PA and PA(ID) represent AirVisual Pro, Foobot, PurpleAir and PurpleAir Indoor AQMs.

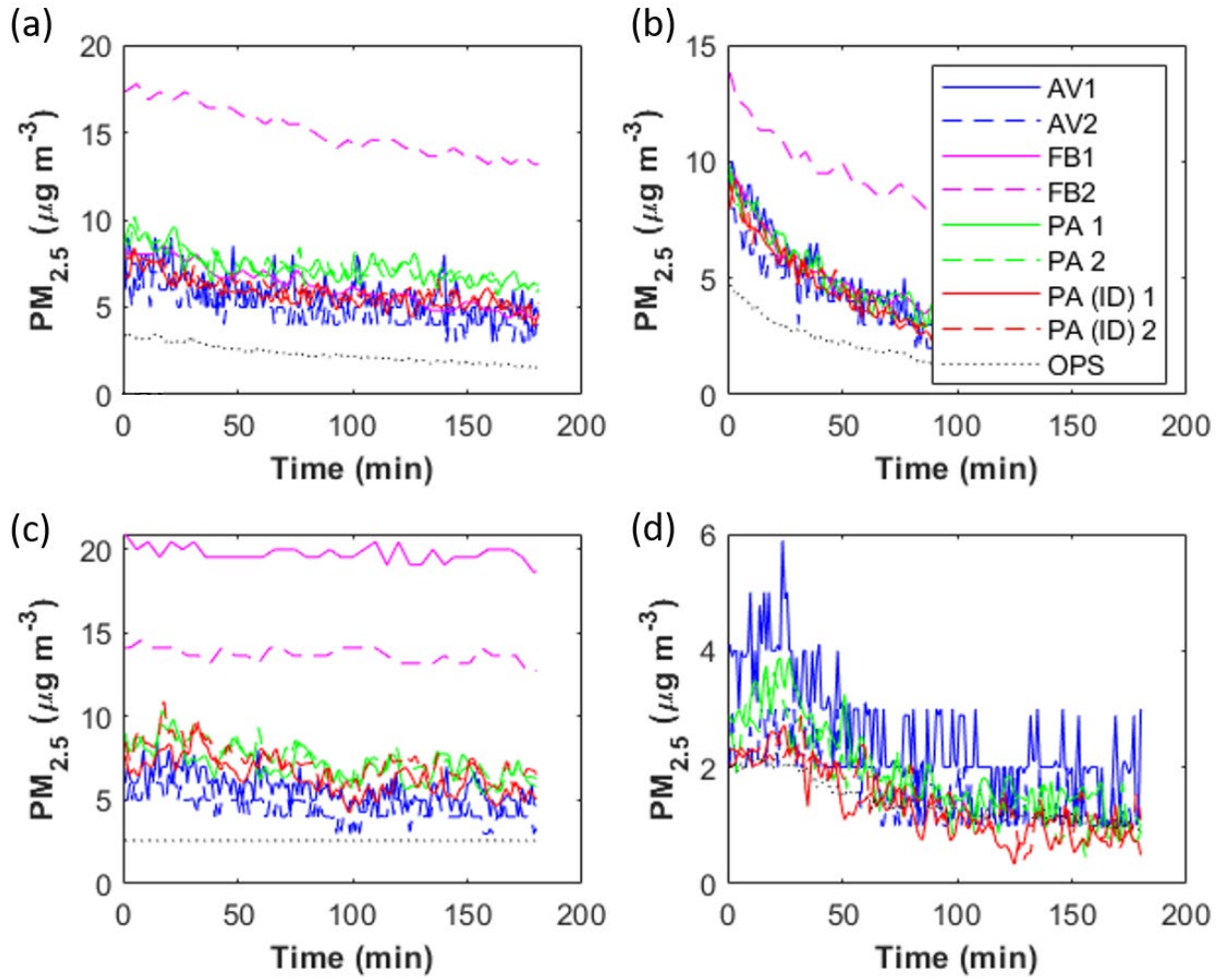

Figure A2. $PM_{2.5}$ time series from OPS and different AQMs used in this study during background periods for Homes 1-4 is shown in panels a, b, c, and d respectively. AV, FB, PA and PA(ID) represent AirVisual Pro, Foobot, PurpleAir and PurpleAir Indoor AQMs.

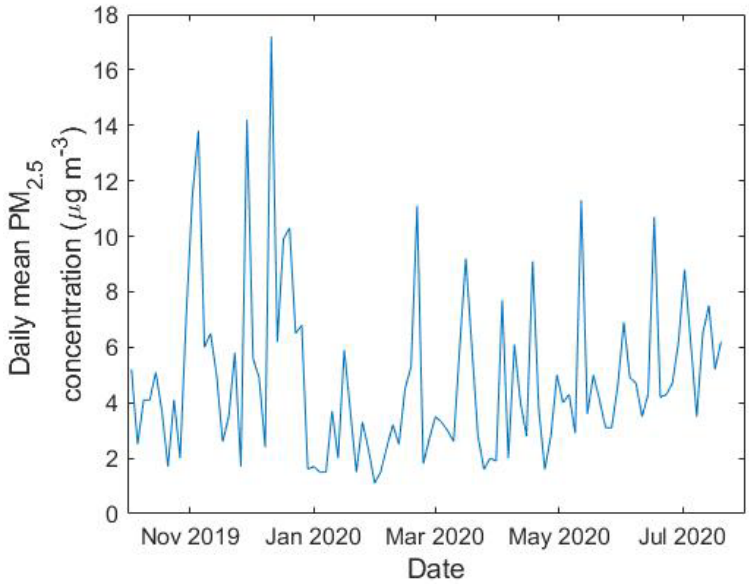

Figure A3. Time series showing daily average ambient $PM_{2.5}$ concentrations reported by EPA monitoring station for Boulder County.

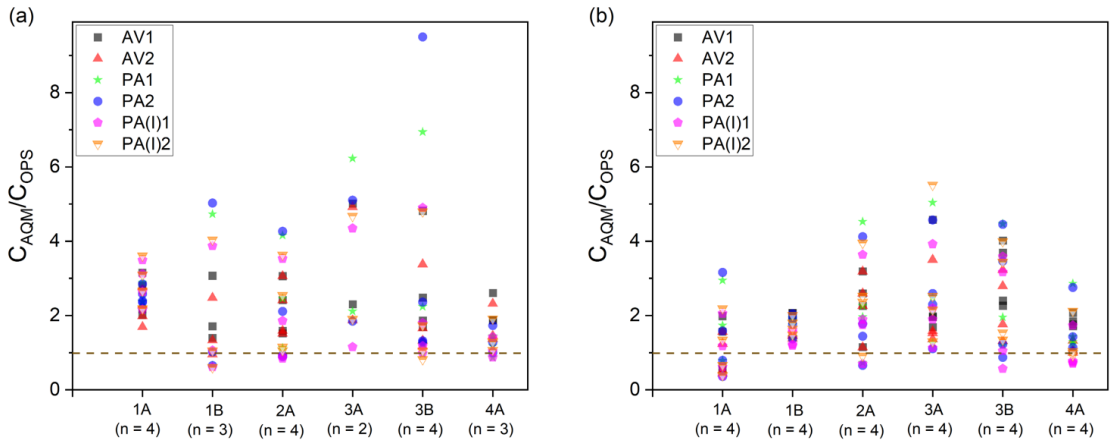

Figure A4. Distributions of C_{AQM}/C_{OPS} values calculated for different AQMs during various collocation phases for (a) cooking periods and (b) background periods. AV, PA and PA(ID) represent AirVisual Pro, PurpleAir and PurpleAir Indoor AQMs.

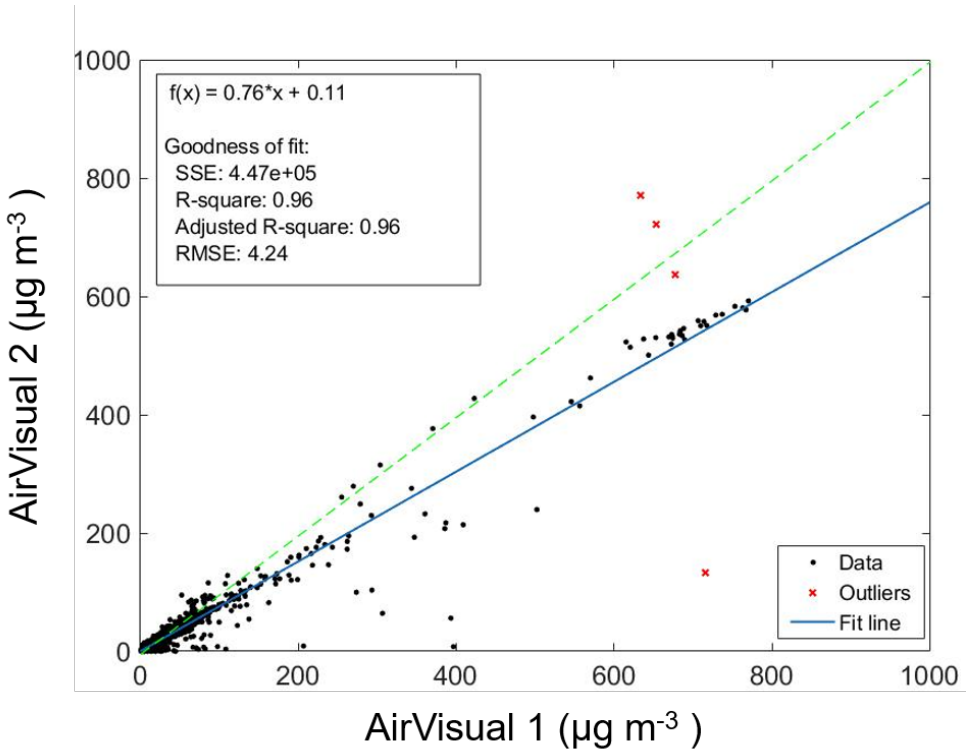

Figure A5. Intercomparison between two identical AirVisual AQMs during the collocation phases for all the homes.

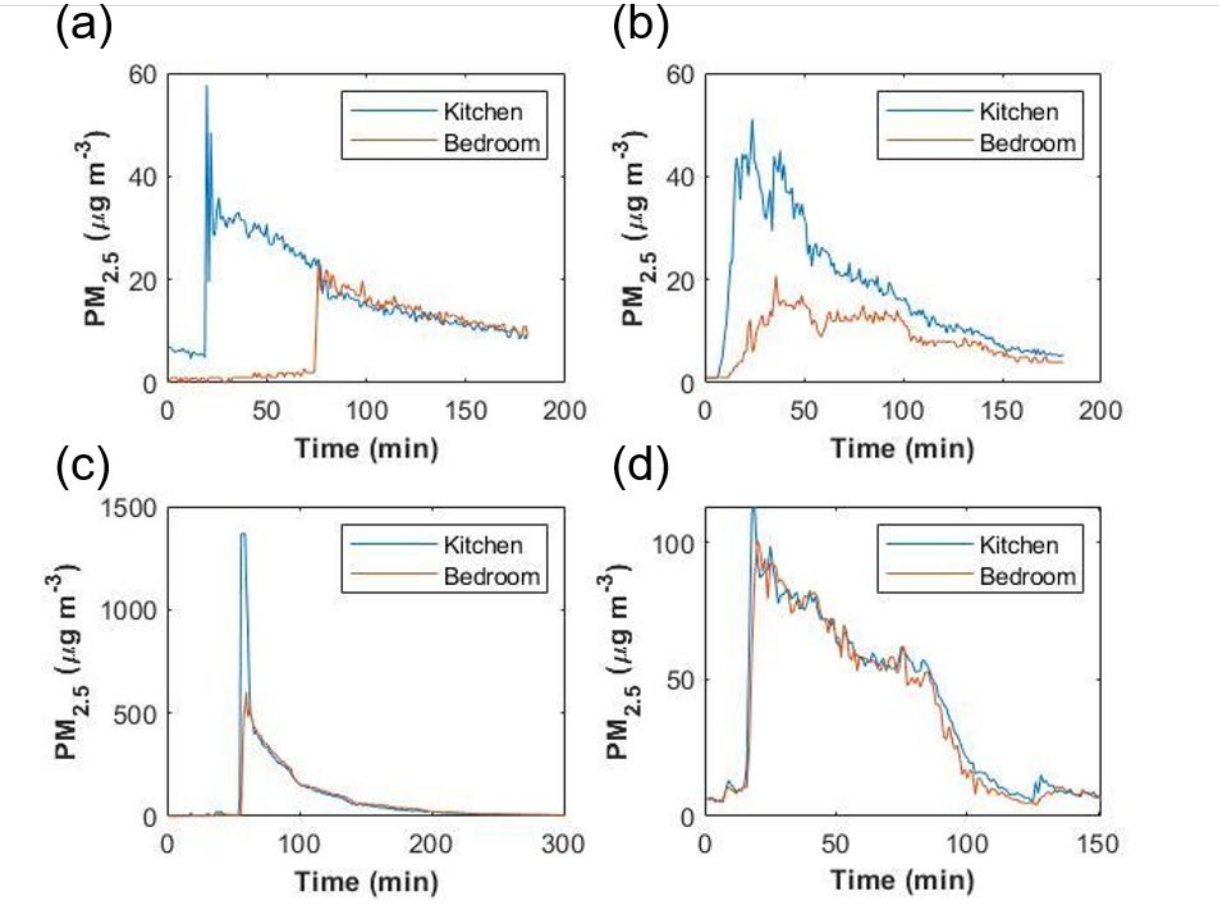

Figure A6. Example $PM_{2.5}$ time series from the bedroom and kitchen AirVisual monitors during Phase 1 for Homes 1-4 are shown in panels a, b, c, and d respectively.

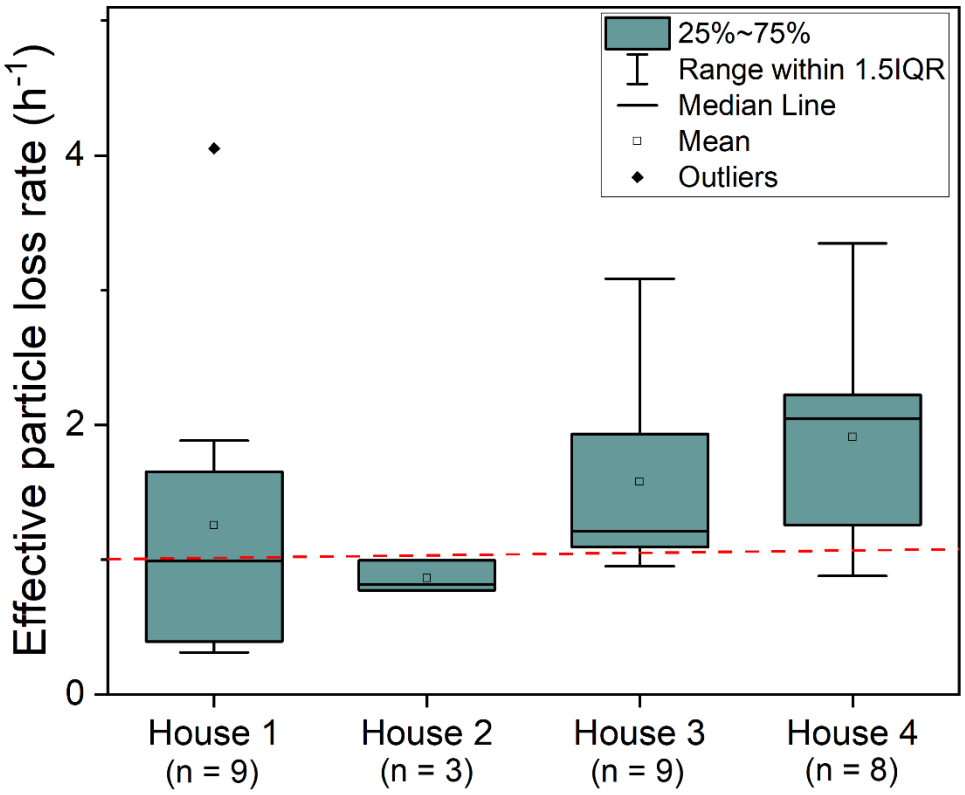

Figure A7. Boxplots showing distribution of effective particle loss rates in the kitchen area for different homes.

APPENDIX B

AEROSOL EMISSIONS AND THEIR VOLATILITY FROM HEATING DIFFERNET COOKING OILS AT MULTIPLE TEMPERATURES

Section B1: Temperature profile for the heating section of the thermodenuder

The temperature inside the center of the heating section of the thermal denuder (TD) was measured using a K-type thermocouple at different distances from the inlet to generate a temperature profile of the heating section is shown below as Figure B1.

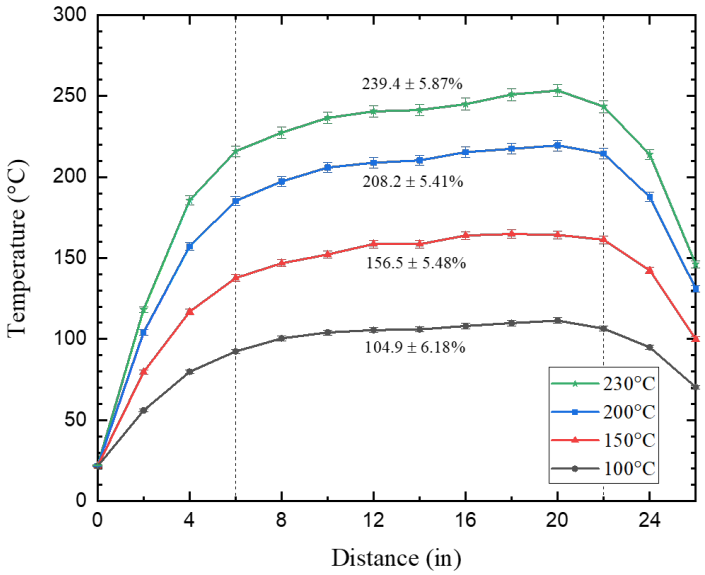

Figure B1. Temperature profile of the heating section as a function of distance from the inlet measured using a thermocouple, for different temperature setpoints.

After an initial increase in recorded temperatures for the first five inches of tube length from inlet, the temperatures started to stabilize for the majority of the tubing section. The average temperatures for lengths between 5-22 inches from the inlet remained within 10% of the set temperature. These results suggest that the TD heating section can provide steady temperatures and therefore can be used for

studying the volatility characteristics of cooking oil generated emissions by observing changes in volume distributions over different TD temperatures.

Section B2: Sampling losses characterization for the sampling line and the thermodenuder system

The diffusion sampling losses for the SMPS line and the TD line for different particle sizes are shown in Figure B2. These losses were calculated using the "AeroCalc" spreadsheet containing equations from Hinds and Wilke and Barron.[1,2]

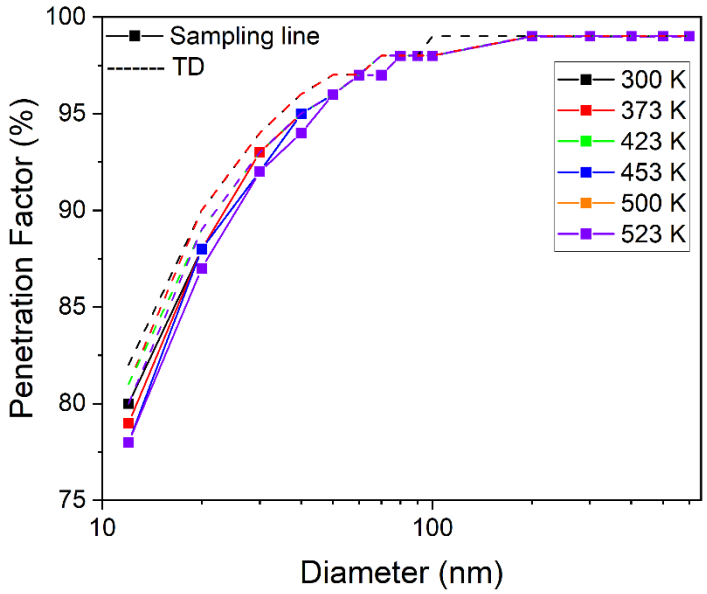

Figure B2. Penetration factor as a function of particle size calculated for the sampling line and the thermodenuder line.

For particle sizes greater than 40 nm, the penetration factor was greater than 95% for all the different temperatures used in the study. We would also like to acknowledge that in previous studies the theoretical models have been shown to overestimate the losses.[3–5] However, in our study since we have compared the aerosol size distributions for different oils using the same setup and the penetration

factor remain largely unchanged with increase in temperature, we did not characterize the sampling loses further.

Table B1. Table showing total concentration and mode values for averaged size distributions obtained for heating a given oil at 180°C.

Frying Oil	**Total Number Concentration ($\times 10^4$ cm^{-3})**	**Aerosol Number Distribution Mode (nm)**	**Total Mass Concentration (μg m^{-3})**	**Aerosol Mass Distribution Mode (nm)**
Lard	4.5	327.8	449.9	406.8
Coconut	6.6	50.5	59.1	283.9
Olive	3.1	128.6	163.8	352.3
Peanut	2.9	62.6	13.9	171.5
Soybean	2.5	89.8	32.8	228.8
Canola	4.9	58.3	29.7	184.3

Table B2. Parameters obtained from the FT-ICR analysis of the smoke sample of a given oil.

Frying Oil	**O/C ratio**	**H/C ratio**	**Number of carbon atoms**	**Average molecular mass (amu)**
Lard	0.15	1.9	38.9	629
Peanut	0.15	1.8	39.5	639
Soybean	0.17	1.9	37.9	620
Canola	0.16	1.8	37.8	619

Table B3. Number of similar chemical compounds containing C, H, and O ions between the smoke samples of different oils used in this study.

Frying Oil	Lard	Peanut	Soybean	Canola
Lard	x			
Peanut	862	x		
Soybean	802	908	x	
Canola	841	961	884	x

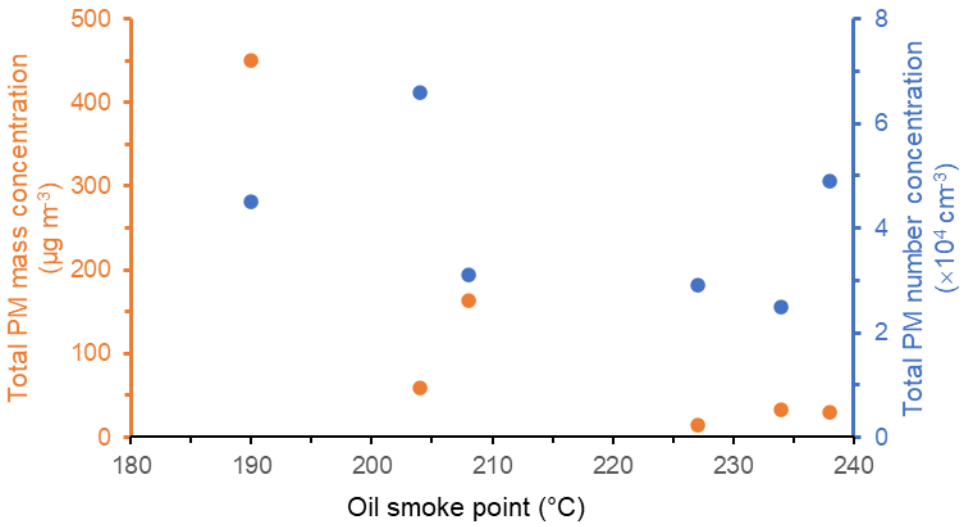

Figure B3. Aerosol mass and number concentrations as a function of oil smoke point.

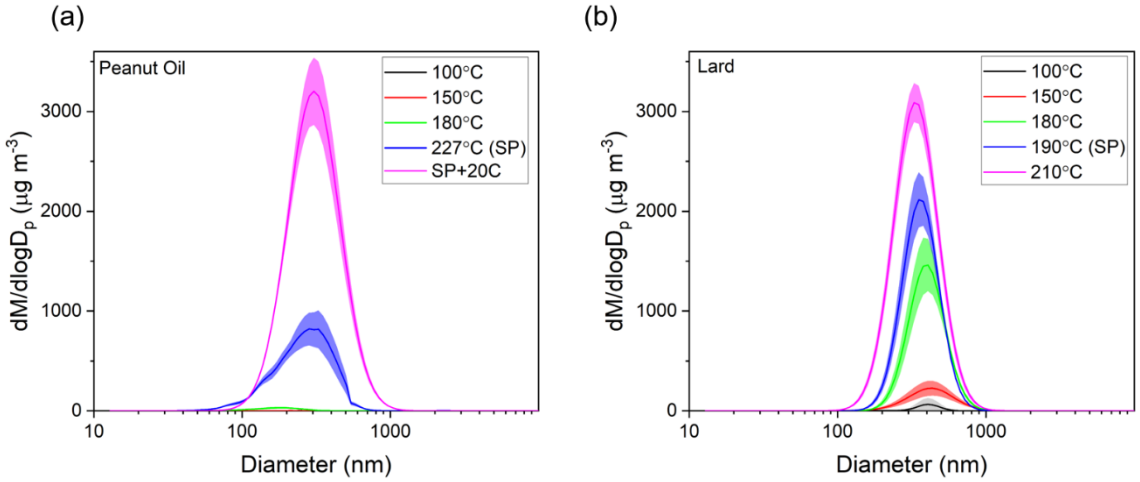

Figure B4. Aerosol mass distributions for peanut oil and lard over different cooking temperatures are shown in panels a and b respectively. The lines represent average values and the shaded region represents the standard error for n = 4.

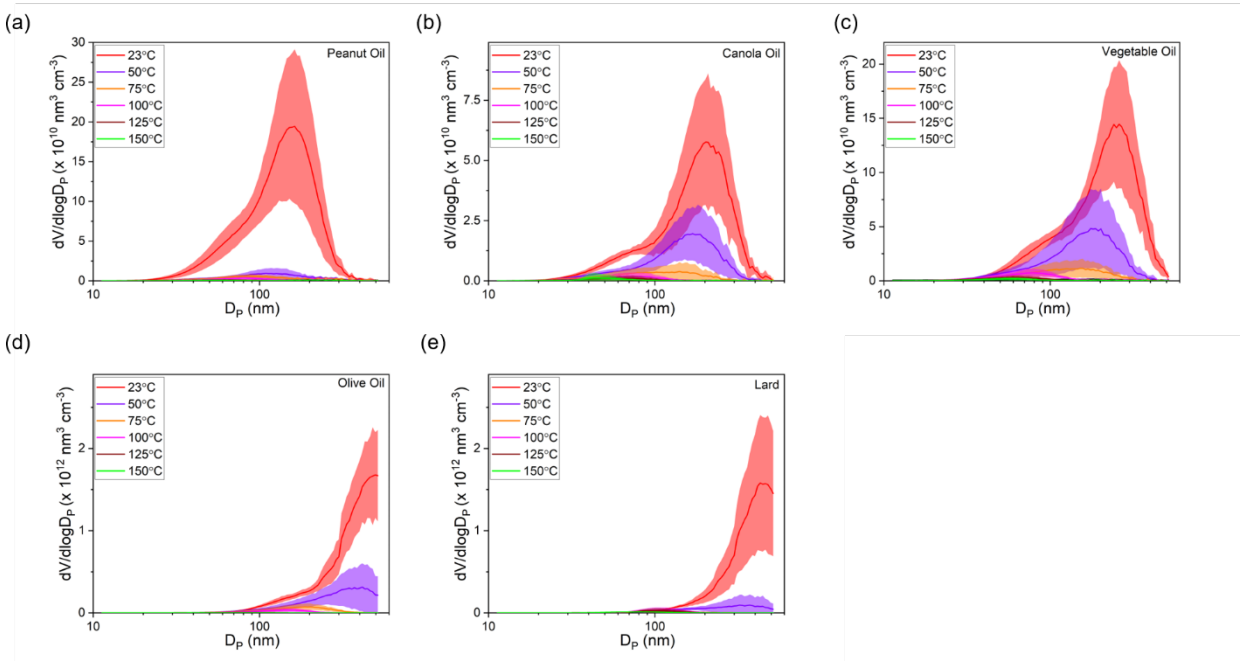

Figure B5. Aerosol volume distributions for different frying oils being heated at 180°C after being thermally conditioned in a TD are shown in panels a-e. The lines represent average and the shaded region represents standard error for n=5. The temperatures of the heated section are also shown in the legend. Note y-axis scale is different for each panel.

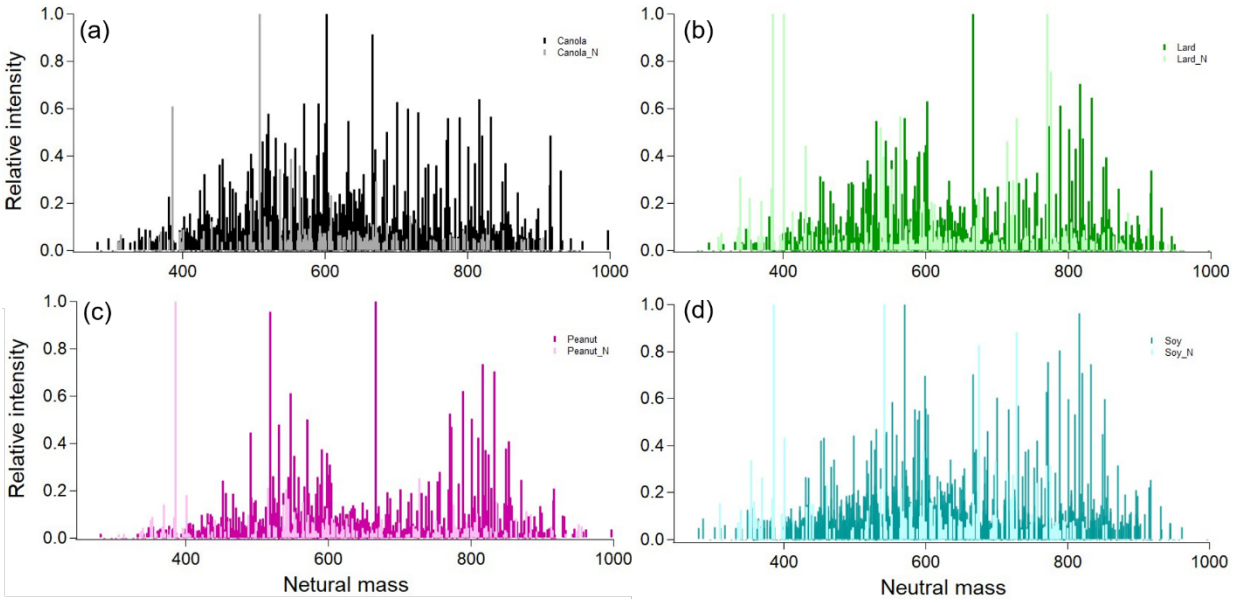

Figure B6. Plot showing the soft ionization mass spectra for the C, H, O, and N containing ions in the extract obtained during the smoking of different frying oils. Panels a-d represent canola, lard, peanut, and soybean oil respectively.

References

(1) W. C. Hinds, Aerosol technology: properties, behavior, and measurement of airborne particles, Wiley, 1999.
(2) P. A. Baron and K. Willeke, Aerosol Measurement: Principles, Techniques, and Applications, Wiley, 2001.
(3) J. A. Huffman, P. J. Ziemann, J. T. Jayne, D. R. Worsnop and J. L. Jimenez, Development and Characterization of a Fast-Stepping/Scanning Thermodenuder for Chemically-Resolved Aerosol Volatility Measurements, Aerosol Science and Technology, 2008, 42, 395–407.
(4) P. K. Saha, A. Khlystov and A. P. Grieshop, Determining Aerosol Volatility Parameters Using a "Dual Thermodenuder" System: Application to Laboratory-Generated Organic Aerosols, Aerosol Science and Technology, 2015, 49, 620–632.
(5) L. Mendes, K. Eleftheriadis and G. Biskos, Performance comparison of two thermodenuders in Volatility Tandem DMA measurements, Journal of Aerosol Science, 2016, 92, 38–52.

APPENDIX C

FILTRATION PERFORMANCE OF LAYERING MASKS AND FACE COVERINGS AND THE REUSABILITY OF COTTON CLOTH MASKS AFTER REPEATED WASHING AND DRYING

Table C1: Filtration efficiency results (average ± standard deviation) in terms of total $PM_{2.5}$ number and mass, and in terms of PM mass at 300 nm for all samples evaluated in this study along with the pressure drop results. These filtration efficiency results were obtained using Experimental Setup 1.

Mask	**$PM_{2.5}$ number efficiency**	**$PM_{2.5}$ mass efficiency**	**Efficiency at 300 nm (mass)**	**Pressure drop (Pa)[a]**
N95 A	96% ± 1%	95% ± 1%	95% ± 1%	182 ± 2
N95 B	98% ± 0%	97% ± 1%	98% ± 1%	169 ± 1
N95 C	99% ± 0%	99% ± 0%	99% ± 0%	127 ± 3
KN95 A	92% ± 2%	93% ± 3%	93% ± 3%	166 ± 5
KN95 B	92% ± 1%	92% ± 2%	92% ± 2%	182 ± 2
KN95 C	93% ± 1%	93% ± 1%	93% ± 2%	189 ± 5
KN95 D	89% ± 2%	85% ± 2%	83% ± 3%	176 ± 1
KN95 E	97% ± 0%	98% ± 0%	98% ± 0%	168 ± 6
KN95 F	93% ± 1%	94% ± 1%	93% ± 1%	178 ± 5
SM A	87% ± 0%	89% ± 0%	88% ± 0%	45 ± 3
SM B	79% ± 1%	49% ± 0%	62% ± 2%	49 ± 6
SM C	71% ± 1%	49% ± 0%	50% ± 2%	55 ± 6
SM D	71% ± 1%	44% ± 1%	42% ± 6%	39 ± 7
CM A	42% ± 3%	16% ± 1%	18% ± 4%	11 ± 6
CM B	36% ± 2%	14% ± 1%	16% ± 2%	52 ± 3
CM C	53% ± 2%	23% ± 1%	23% ± 4%	19 ± 6
2-ply bandana	27% ± 2%	9% ± 1%	9% ± 4%	33 ± 6
SM A(x2)	88% ± 0%	87% ± 0%	86% ± 1%	93 ± 6
SM B(x2)	86% ± 0%	80% ± 0%	81% ± 2%	100 ± 9
SM C(x2)	83% ± 0%	72% ± 1%	70% ± 2%	95 ± 3
CM A + SM A	91% ± 0%	90% ± 0%	91% ± 2%	68 ± 8
CM A + SM B	85% ± 1%	72% ± 1%	68% ± 2%	72 ± 2
CM A + SM C	82% ± 1%	61% ± 1%	64% ± 2%	66 ± 4

***a*: NIOSH threshold limit for N95 respirators is 343 Pa.**

Figure C1. Different samples that were used in this study are shown from top right to bottom in clockwise direction: N95 respirator, KN95 respirator, Surgical mask (SM), wash/dry sample coupon, 2-ply bandana and Cloth mask (CM).

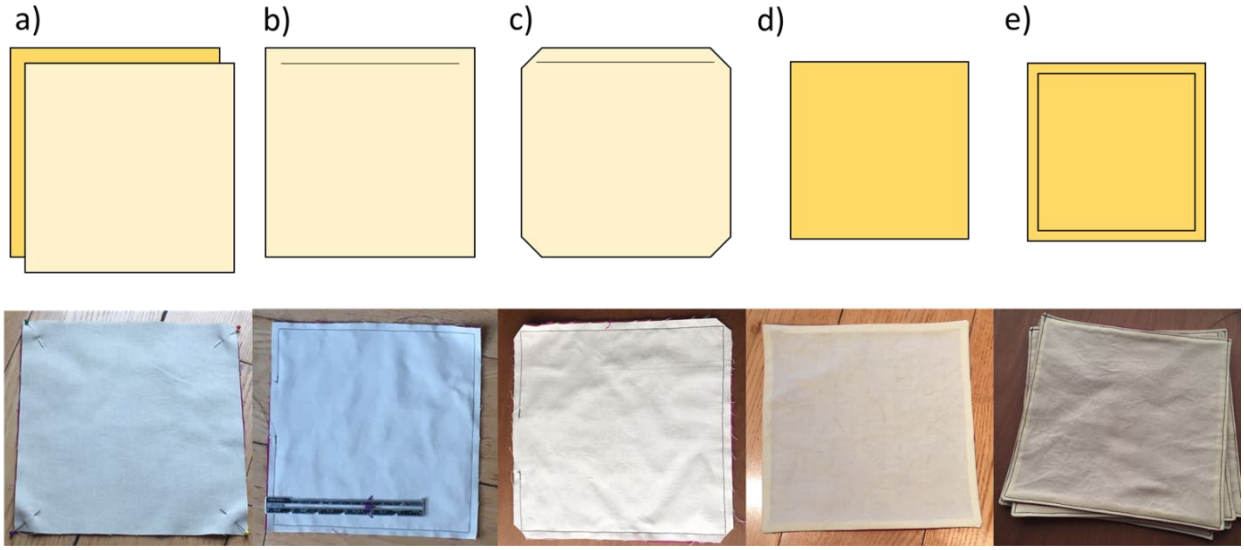

Figure C2. Wash/dry sample coupon fabrication steps. (a) 8" squares are cut from the two different fabrics, and one of each color are placed right sides together (b) a ¼" seam is stitched around the edges, leaving a ~2" gap for flipping inside out (c) corners are clipped to remove bulk (d) sample coupon is flipped inside out and pressed into shape (e) topstitching around the outside edge to enclose raw edges and reinforce seams.

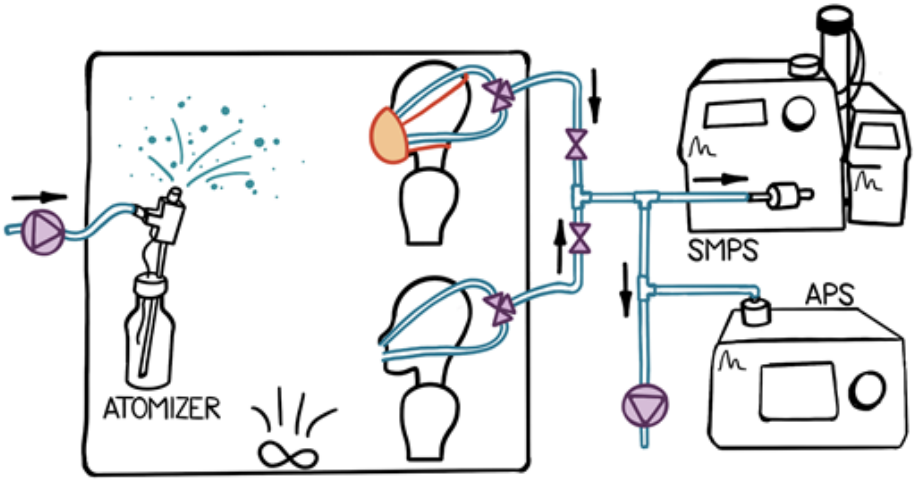

Figure C3. Schematic of Setup 1 used for characterizing the filtration efficiency in the 60- 450 nm particle size range. The figure is not to scale with the actual setup. Not shown in schematic: The aerosol stream passed through a diffusion dryer and an X-ray neutralizer before being injected into the testing chamber.

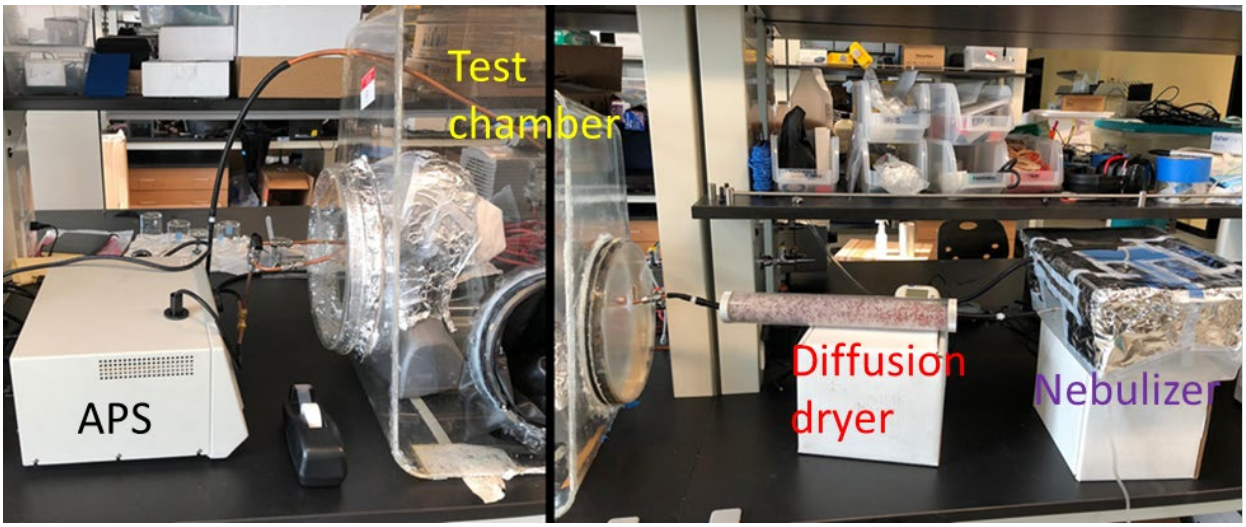

Figure C4. Setup 2 used for characterizing the filtration efficiency in the 542 nm- 4 µm particle size range.

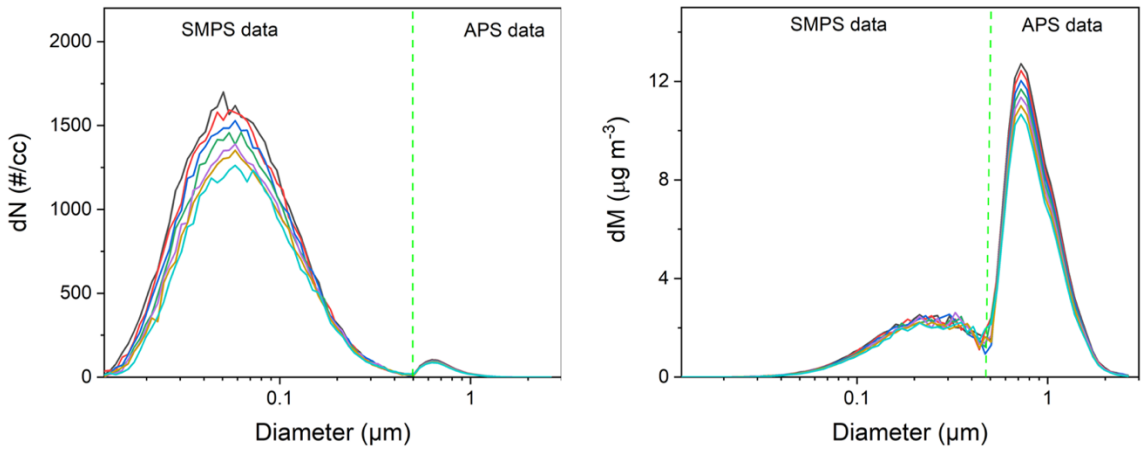

Figure C5. Temporal evolution of aerosol size distributions inside the chamber (shown via series of different colored lines) during the testing duration for Setup 1.

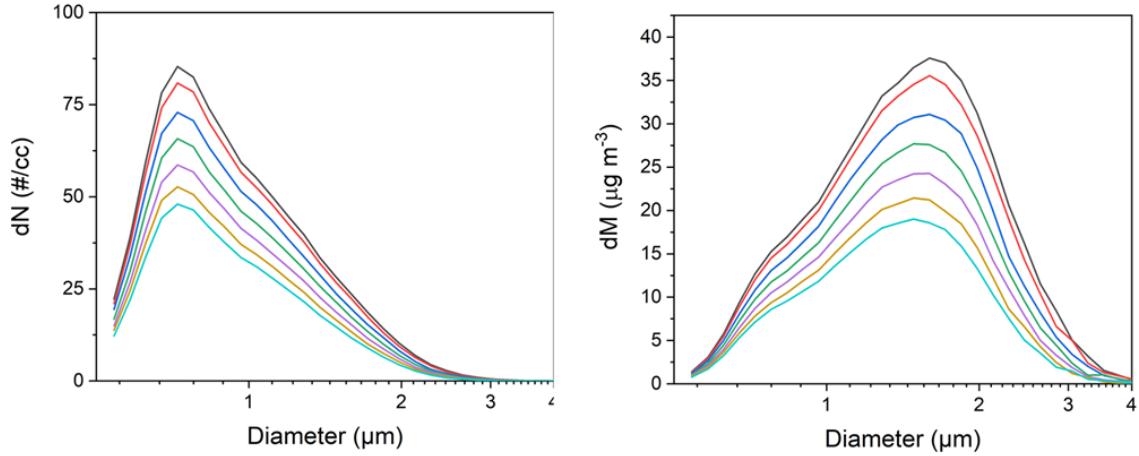

Figure C6. Temporal evolution of aerosol size distributions inside the chamber (shown via series of different colored lines) during the testing duration for Setup 2.

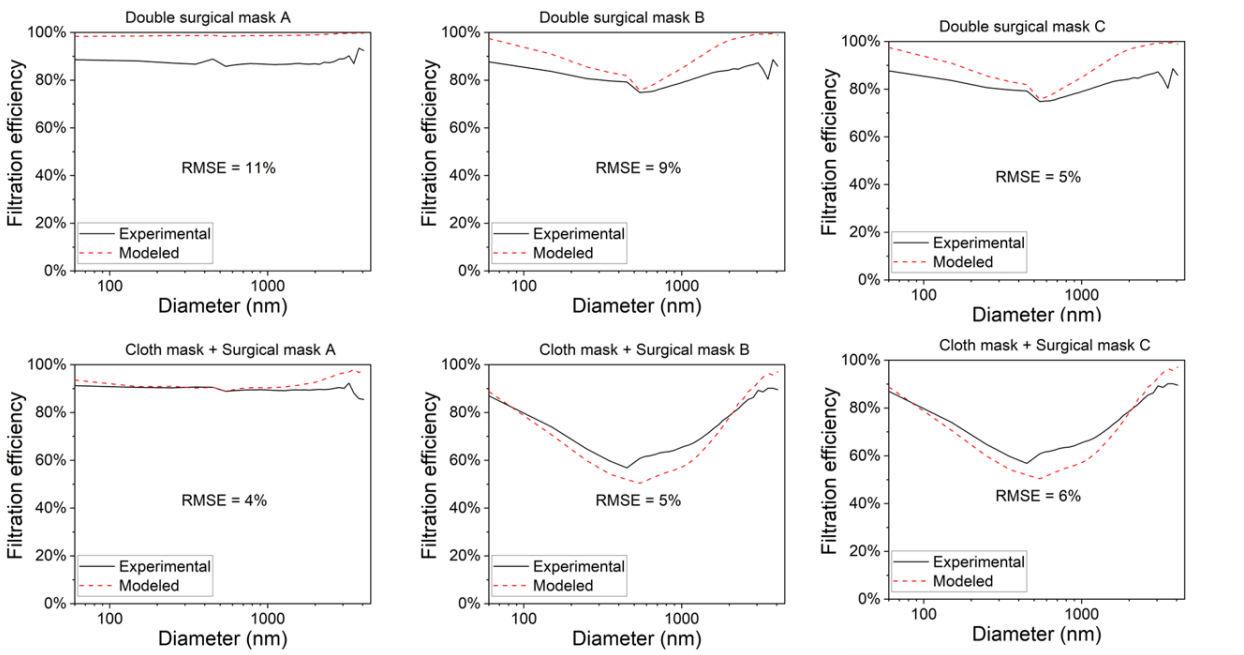

Figure C7. Comparison between the experimental results and the results from a particle transmission model based on classical filtration theory for all six mask combinations. Root mean squared error (RMSE) between experimental and theoretical curves is also shown for each mask combination.

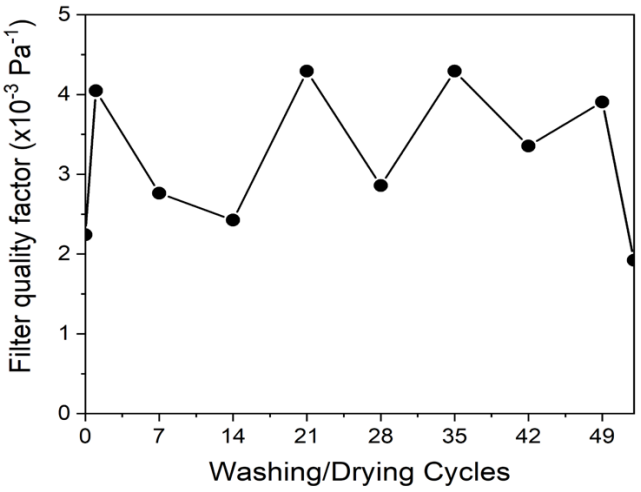

Figure C8. Filter quality factor values (QF) as a function of different wash/dry cycles.

APPENDIX D

USE OF CELLULOSE NANOBFIBRIL AS COATING MATERIAL FOR IMPROVING FILTRATION EFFICIENCY OF COTTON FABRIC

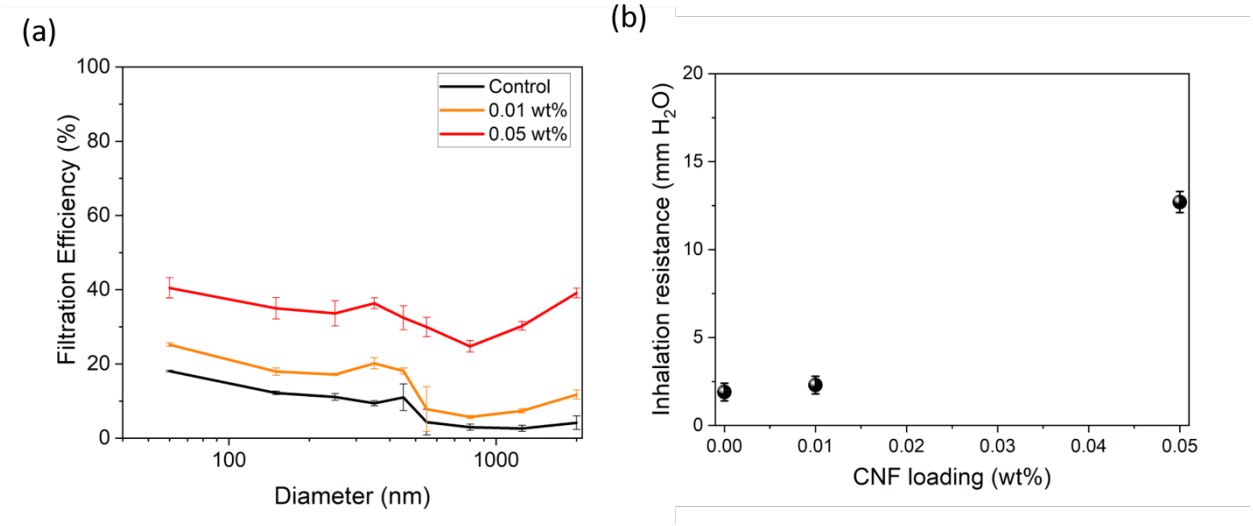

Figure D1. Size-resolved filtration efficiency results for different CNF coated fabric samples are shown in panel (a). The corresponding inhalation resistance trends are shown in panel (b).